HELSINGIN YLIOPISTO
HELSINGFORS UNIVERSITET
UNIVERSITY OF HELSINKI

THE EFFECT OF METFORMIN ON DNA DAMAGE, PROLIFERATION AND APOPTOSIS IN HIGH-GRADE SEROUS OVARIAN CANCER CELLS

Auguste Ciparyte
Genetics and Molecular Biosciences
Faculty of Biological and Environmental Sciences
University of Helsinki
2020

HELSINGIN YLIOPISTO
HELSINGFORS UNIVERSITET
UNIVERSITY OF HELSINKI

Tiedekunta – Fakultet – Faculty	Koulutusohjelma – Utbildningsprogram – Degree Programme
Faculty of Biological and Environmental Sciences	Genetics and Molecular Biosciences

Tekijä – Författare – Author

Auguste Ciparyte

Työn nimi – Arbetets titel – Title

The Effect of Metformin on DNA Damage, Proliferation and Apoptosis in High-Grade Serous Ovarian Cancer Cells

Oppiaine/Opintosuunta – Läroämne/Studieinriktning – Subject/Study track

Genetics and Genomics

Työn laji – Arbetets art – Level	Aika – Datum – Month and year	Sivumäärä – Sidoantal – Number of pages
Master's Thesis	September, 2020	71+33

Tiivistelmä – Referat – Abstract

Diabetic ovarian cancer patients who take metformin as part of their anti-diabetic medication generally respond better to DNA-damaging cancer treatment. The molecular mechanisms of the anti-cancer effects of metformin are currently being investigated, but they remain poorly elucidated. Not much is understood about the metformin effect on DNA damage in ovarian cancer cells, where it is of particular importance. When chemotherapy-induced double-stranded DNA breaks are unrepaired, cells reach a point when they cannot tolerate the accumulated DNA damage and die. However, some ovarian cancer cells efficiently employ DNA repair mechanisms, the most prominent being homologous recombination (HR), to overcome DNA damage. Efficient HR causes chemoresistance. An important question is whether metformin has the ability to induce the HR-deficient state in cancer cells, thereby sensitizing them to treatment. This study did not examine HR directly, but it assessed HR indirectly by observing the effect of metformin on recovery from DNA damage in two ovarian cancer cell lines: OVCAR4 (HR-proficient) and Kuramochi (HR-deficient). Additionally, this study evaluated the metformin effect on cell proliferation and apoptosis. OVCAR4 and Kuramochi cells were exposed to varying metformin concentrations (0,5 mM, 5 mM, 10 mM, 15 mM, 20 mM and 25 mM) and for varying durations (24 hours and 48 hours). This study also tested how metformin pretreatment affected the cells' ability to repair externally (ionizing irradiation) induced DNA damage. The cells were imaged with a high-content imaging system, and percentages of nuclei that were positive for markers for different cellular processes (i.e., DNA damage, proliferation, and apoptosis) were calculated. The study found that only high metformin concentrations, such as 20 mM were able to increase DNA damage and reduce cell proliferation in HR-proficient OVCAR4 cells, both non-irradiated and irradiated. The HR-deficient Kuramochi cell line was generally more sensitive to metformin, particularly with regards to DNA damage, which increased using metformin concentrations < 20 mM. However, 20 mM concentration resulted in the most significant effects. Similarly, only high metformin concentration (25 mM) increased apoptosis, although data were obtained only for a limited number of Kuramochi cells. More experiments on apoptosis would be beneficial. Also, more extensive experiments for the irradiation part are needed to validate these preliminary findings, as well as examining whether high metformin concentrations (> 20 mM) affect specifically the HR-mediated DNA repair pathway.

Avainsanat – Nyckelord – Keywords

High-grade serous ovarian cancer, epithelial ovarian cancer, OVCAR4, Kuramochi, metformin, DNA damage, proliferation, apoptosis, ionizing radiation

Ohjaaja tai ohjaajat – Handledare – Supervisor or supervisors

Liisa Kauppi, PhD, Associate Professor, University of Helsinki
Manuela Tumiati, Postdoctoral Researcher, University of Helsinki
Taina Turunen, M.Sc., University of Helsinki

Säilytyspaikka – Förvaringställe – Where deposited

Ethesis
HELDA - Helsingin yliopiston digitaalinen arkisto / HELDA - Helsingfors universitets digitala publikationsarkiv / HELDA - Digital Repository of the University of Helsinki

Muita tietoja – Övriga uppgifter – Additional information

HELSINGIN YLIOPISTO
HELSINGFORS UNIVERSITET
UNIVERSITY OF HELSINKI

TABLE OF CONTENTS

ABBREVIATIONS

AMPK	Adenosine monophosphate-activated protein kinase
Bcl-2	B-cell lymphoma 2
Bcl-xL	B-cell lymphoma-extra large
BSA	Bovine serum albumin
cCasp3	Cleaved caspase-3
CI	Confidence interval
CSV	Comma-separated values
DMSO	Dimethyl sulfoxide
DSB	Double-stranded break
EOC	Epithelial ovarian cancer
FBS	Fetal bovine serum
HGSOC	High-grade serous ovarian cancer
HR	Homologous recombination
HRD	Homologous recombination deficiency
IR	Ionizing radiation
LKB1	Liver kinase B1
Macro	Macroinstruction
NF-κB	Nuclear factor kappa-light-chain-enhancer of activated B cells
PARP	Poly (ADP-ribose) polymerase
PBS	Phosphate-buffered saline
PBS++	Phosphate-buffered saline containing calcium and magnesium
PFA	Paraformaldehyde
P/S	Penicillin-streptomycin
SET	Solid, pseudo-endometrioid and/or transitional cell carcinoma-like
SSB	Single-stranded break

1. INTRODUCTION

1. 1. Ovarian cancer

1. 1. 1. Ovarian cancer prevalence, prognosis, and mortality

Ovarian cancer is typically a late-life disease, usually occurring after menopause, the median age at diagnosis being 63 (Ozols et al., 2004). Despite constituting just three percent of cancers in women (Bodmer et al., 2011), it is the most fatal cancer of the female reproductive system as well as the eighth cause of cancer-related deaths in females worldwide (Ozols et al., 2004; Ferlay et al., 2015). Early detection is often impeded by a sustained clinically silent onset, the lack of specific symptoms as well as proper screening programs, and even though the initial treatments involving cytoreductive surgery and chemotherapy are often successful, the disease recurs, metastasizes, and becomes drug-resistant for most patients, ultimately resulting in their death (Chien et al., 2007). According to the latest publication of cancer statistics, the overall five-year survival rate of patients with ovarian cancer is 48 % (Siegel et al., 2020).

1. 1. 2. Ovarian cancer classification

Epithelial ovarian cancer (EOC) constitutes the majority of ovarian cancers, around ninety percent (Aletti et al., 2007). The other types are ovarian stromal tumors and ovarian germ cell tumors (Aletti et al., 2007).

According to the newest dualistic model of ovarian carcinogenesis, EOC can be categorized into Type 1 and Type 2 (Kurman et al., 2016). Tumors belonging to the Type 1 category that often has a better prognosis originate from benign lesions embedded on the ovary followed by a slow malignant metamorphosis (Kurman et al., 2016). In contrast, more aggressive Type II tumors usually arise from intraepithelial carcinomas in the fallopian tube, followed by rapid dissemination to the inside and the outside of the ovary, resulting in a worse prognosis (Kurman et al., 2016).

In addition, EOC can be divided into the following histologically different classes based on tissue architecture resemblance: serous, mucinous, endometrioid, clear cell, transitional (Brenner), squamous, mixed, and undifferentiated, each with specific morphologic and genetic variations (Bell, 2005; Desai et al., 2014). Approximately three-quarters of EOCs belong to the serous category, which based on the level

of cellular aberration can be further classified into low-grade and high-grade subtypes, the latter being more common (Berns et al., 2012; Desai et al., 2014).

High-grade serous ovarian cancer (HGSOC) falls into the Type II category of EOCs (Kurman et al., 2016). Being the most prevalent and aggressive subtype, it constitutes 70-80 % of deaths from ovarian cancer (Bowtell et al., 2015).

1. 1. 3. Risk and protection factors of HGSOC

Familial history of HGSOC is one of the risk factors for developing the disease (Webb et al., 2017). The most common hereditary predisposition is germline mutations in BRCA1 or BRCA2 genes, contributing up to 50 % lifetime risk of the disease, compared to 1,4 % risk in the general population (Boyd, 2003; Webb et al., 2017). Since BRCA1 and BRCA2 mutations are also associated with breast cancer, familial and personal history of breast cancer also increases HGSOC risk (Webb et al., 2017; Stewart et al., 2018). In addition, HGSOC risk can be elevated by various low-penetrance mutations in other genes, for example, BRIP1, RAD1C, RAD1D, PALB2, and BARD1 (Lisio et al., 2019). The connection between these genes is that they participate in homologous recombination (HR)-mediated DNA repair, which is an important pathway in HGSOC pathophysiology (Lisio et al., 2019). Furthermore, three additional loci have been associated with HGSOC susceptibility: at 2q13, 8q24.1, and 12q24.31 (Phelan et al., 2017). Finally, numerous factors have been associated with the decreased risk of HGSOC, including a smaller number of ovulatory events, (multi)parity, breastfeeding, tubal ligation, and the use of oral contraceptives (estrogen and progestin), whereas the use of hormone (estrogen) replacement therapy during menopause as well as having certain other medical conditions like Lynch syndrome, pelvic inflammatory disease, and endometriosis increase the risk of the disease (Stewart et al., 2018; Lisio et al., 2019).

1. 1. 4. HGSOC properties

Cytological features of HGSOC include extreme nuclear atypia, big, pleomorphic, and hyperchromatic nuclei, multinucleation, pronounced nucleoli, and high mitotic index (Lisio et al., 2019). Morphologically HGSOCs can be divided into two groups: the usual type and a SET variant (also known as “solid, pseudo-endometrioid and/or transitional cell carcinoma-like”), whereas molecularly they can be divided into immunoreactive, differentiated, proliferative, and mesenchymal types, based on gene expression signatures (Kurman et al., 2016). The morphologically usual type of HGSOC often presents

as a solid cell mass with slit-like gaps and necrotic areas, and is arranged in a papillary, glandular, or cribriform fashion, while the SET variant presents as a solid cell mass resembling endometrioid or transitional cell carcinomas, and is characterized by a higher mitotic index and larger numbers of tumor-infiltrating lymphocytes (Kurman et al., 2016). The molecular types of HGSOC have not been revealed to correlate in any way with the morphological types, but associations between molecular types and clinical outcomes have been made, the immunoreactive type providing survival advantage, while proliferative and mesenchymal types having worse prognosis (Konecny et al., 2014; Kurman et al., 2016).

Moving on to the genetic features of HGSOC, methylation in the promoters of 168 genes has been observed, as well as 113 focal DNA copy number alterations due to profound genomic instability of HGSOC (Cancer Genome Atlas Research Network, 2011). The most prevalent are CCNE1, MYC, and MECOM gene amplifications (Cancer Genome Atlas Research Network, 2011). However, the single most prominent feature of HGSOC is TP53 mutation (Kurman et al., 2016). Somatic mutations in other genes are infrequent, but may occasionally occur in NF1, CDK12, and RB1 genes (Cancer Genome Atlas Research Network, 2011). Also, BECN1 and LC3 genes associated with autophagy can be mono-allelically deleted in HGSOC (Delaney et al., 2017). Of particular interest are germline and sometimes somatic mutations of BRCA1 and/or BRCA2 genes, occurring in up to 23 % of HGSOCs (Hennessy et al., 2010; Cancer Genome Atlas Research Network, 2011). In addition, BRCA1 promoter methylation is common, making up 10-20 % of HGSOCs (Konstantinopoulos et al., 2015). As a result, BRCA1/2, which is a tumor suppressor gene, is often either genetically or epigenetically inactivated in HGSOC. Alterations in BRCA1 and BRCA2 genes have been associated with the defective HR pathway of DNA repair, which is present in approximately half of HGSOCs (Cancer Genome Atlas Research Network, 2011). An important observation is that BRCA-mutant patients have better five-year survival compared to the non-mutant ones (Bolton et al., 2012), demonstrating that defective HR is an important element to consider when studying HGSOC. Other pathways that can also be altered in HGSOC include RB1, PI3K/RAS, PIK3/AKT pathways, as well as FOXM1 transcription factor pathway (it is often activated), and less frequently – NOTCH signaling pathway (Cancer Genome Atlas Research Network, 2011).

1. 1. 5. Homologous recombination

Many chemotherapeutic agents used in cancer treatment such as platinum and platinum analogs bind to purine DNA bases and cause intra- and inter-strand crosslinks that can then create double-stranded

breaks (DSBs) in the DNA (Kelland, 2007; Zhang et al., 2007). DSBs can also be produced by ionizing radiation (IR) and other external DNA damaging agents or they can be formed from accumulated unrepaired single-stranded breaks (SSBs) (Haince et al., 2005). DSBs are detrimental to cells and lead to cell cycle arrest, which in turn result in programmed cell death (Kelland, 2007). The mechanism of action in DNA-damaging cancer treatment is precisely based on this idea that the accumulation of DNA damage will destroy cancer cells (Haince et al., 2005). However, DSBs also activate DNA damage recognition and repair pathways, limiting the treatment effectiveness (Kelland, 2007). In HGSOC, the prominent DNA repair pathway that influences chemotherapy outcome is HR (Konstantinopoulos et al., 2015).

During HR which occurs in late S and G2 phases of the cell cycle, DSBs are repaired by aligning the break with homologous DNA sequence, present on the newly replicated sister chromatid (Kennedy et al., 2006; Damia et al., 2007). First, the 3′ ends on both flanks of a DSB are resected, then the sequence from the undamaged sister chromatid is accessed by the complementary 3′ advancing strand from the damaged homologous chromosome and is used as a template by a DNA polymerase (Khanna et al., 2001). When the strand extension is long enough to cover the area of the DSB, the 3′ end of the advancing strand reverts to the initial chromosome followed by a continuation of replication (Khanna et al., 2001). HR is a very accurate way of repairing DSBs (Hoeijmakers, 2007). In case it is not available, cells can use another DSB repair pathway, non-homologous end joining, which is error-prone, because the break ends are simply processed and directly ligated without using a complementary template (Kennedy et al., 2006; Hoeijmakers, 2007).

Paradoxically, cancer cells initially benefit from genomic instability, because it fuels tumor progression, but disrupted DNA repair pathways, the main cause for genomic instability, results in heightened sensitivity to DNA-damaging chemotherapeutic agents (Kennedy et al., 2006). Defects in HR-mediated DNA repair causing homologous recombination deficiency (HRD) are a major reason for the initially successful response to chemotherapy in HGSOC treatment (Konstantinopoulos et al., 2015; Testa et al., 2018). The aforementioned case of germline BRCA-mutated patients is the most distinct example. Patients with BRCA-mutated, that is, HR-deficient tumors also benefit from the use of poly (ADP-ribose) polymerase (PARP) inhibitors (Fong et al., 2009; Moore et al., 2018). The PARP superfamily of proteins participate in repairing SSBs, so when PARP proteins are inhibited, unrepaired SSBs accumulate and cause DSBs, which cannot be repaired due to HR deficiency (Fong et al., 2009). When used in combination with DNA-damaging agents, PARP inhibitors make the treatment more efficient and selective, sparing normal healthy cells where HR is intact (Haince et al., 2005; Fong et al.,

2009). However, genetic and epigenetic alterations in HR-related genes are present in roughly half of HGSOCs (Konstantinopoulos et al., 2015). This group of patients benefits from existing drug treatments, while clinical outcomes for the remainder of patients remain poor, as there are no alternative treatment options at the moment.

1. 2. Metformin

1. 2. 1. Repurposing metformin

Considering the poor prognosis and high mortality of HGSOC, there is a need to determine novel targeted therapeutic approaches to improve treatment and patients' survival. One therapeutic strategy involves the development of an entirely new drug, but this approach has a high probability of failure, and it may take 10-17 years and cost over USD 800 million to achieve this goal (Tobinick, 2009). An alternative approach is drug repositioning, in which drugs that are already available for the treatment of some other disease(s) are put into use for the improved treatment of cancer (Tobinick, 2009).

Metformin hydrochloride, or simply metformin, derived from the *Galega officinalis* plant, is a biguanide class of hypoglycemic drug that is widely prescribed to people with type-2 diabetes (Kumar et al., 2013; Sanchez-Rangel et al., 2017). Interestingly, an association has been made between metformin intake as part of anti-diabetic medication and improved survival in ovarian cancer (Kumar et al., 2013). In fact, after the initial epidemiologic findings that metformin taken by diabetic patients is associated with a lower cancer risk as well as lower cancer-related mortality (Evans et al., 2005; Bowker et al., 2006), many studies have been conducted with various types of tumors. These studies have shown that metformin can inhibit the growth of cancer cells *in vitro*, namely, lung (Ashinuma et al., 2012), pancreatic (Kisfalvi et al., 2009), colon (Zakikhani et al., 2008), rectal (Park et al., 2019), renal (Liu et al., 2013), prostate (Ben Sahra et al., 2008), breast (Zakikhani et al., 2006), as well as ovarian (Gotlieb et al., 2008). For many of these cancer types, the initial findings from cell culture experiments are since supported by evidence from *in vivo* studies as well, usually using mouse models.

For ovarian cancer specifically, it has been demonstrated that metformin suppresses cancer growth and enhances sensitivity to chemotherapeutic agents both *in vitro* and *in vivo* in mice (Lengyel et al., 2015). In addition, ovarian cancer cells have been shown to even overcome resistance to chemotherapeutic agents as evidenced by the induced apoptosis and augmented autophagy after metformin treatment *in vitro* (Yang et al., 2019). Furthermore, it has been discovered that metformin is

able to limit the development and expansion of ovarian cancer stem cells *in vitro* and in mice *in vivo* (Shank et al., 2012).

1. 2. 2. Anti-neoplastic mechanisms of metformin in ovarian cancer

Metformin is thought to suppress carcinogenesis indirectly by obstructing the insulin / insulin-like growth factor 1 pathway leading to reduced insulin levels (Hijaz et al., 2016). Possible direct mechanisms of anti-cancer effects of metformin are currently being investigated, but they remain poorly understood.

Among the studied molecular pathways in ovarian cancer, metformin has first been shown to restrict cell growth by increasing 5′ adenosine monophosphate-activated protein kinase (AMPK) activity (Gotlieb et al., 2008). In addition, liver kinase B1 (LKB1) has been found to be necessary for activating AMPK (Rattan et al., 2011a/b). Upon the activation of the LKB1-AMPK pathway, the signaling through the mammalian target of rapamycin pathway is suppressed, resulting in reduced cell proliferation (Rattan et al., 2011a/b).

It has also been revealed that metformin can induce apoptosis in ovarian cancer cells by reducing mitochondria-associated B-cell lymphoma 2 (also known as Bcl-2) and B-cell lymphoma-extra large (also known as Bcl-xL) protein expression and increasing Bax and Cytochrome c expression (Patel et al., 2015). Furthermore, metformin has been found to generate anti-cancer effects in chemoresistant ovarian cancer cells by diminishing protein kinase B, or Akt, expression via the regulation of mitochondrial E3 ubiquitin protein ligase 1 expression (Lee et al., 2019).

Moreover, metformin inhibits cell proliferation of chemoresistant ovarian cancer cells by decreasing the mRNA expression of inflammatory cytokines and nuclear factor kappa-light-chain-enhancer of activated B cells (NF-κB) signaling pathway, which are typically activated by chemotherapy and associated with chemoresistance (Dos Santos Guimarães et al., 2018). Repressed interleukin 6 secretion via the inhibition of NF-κB signaling by metformin was also found to inactivate ovarian cancer stromal fibroblasts, resulting in constrained tumor development in mice (Xu et al., 2018). Additionally, *in vitro* experiments revealed that metformin represses platelet-mediated ovarian cancer angiogenesis and growth (Erices et al., 2017) as well as adipocyte-mediated adipogenesis and tumor expansion and progression (Tebbe et al., 2014).

1. 2. 3. Metformin and DNA damage

Currently, there is controversy over the metformin effect on DNA damage.

One proposed concept is that the reason behind the general anti-tumorigenic effect of metformin is its ability to prevent DNA damage and boost DNA damage repair, including the HR pathway, this way protecting against genomic instability which is a common characteristic of cancer cells (Najafi et al., 2018). For instance, one study has shown that metformin diminishes DNA damage due to the suppression of mitochondrial complex I followed by the disruption of mitochondrial respiration and cellular metabolism, which decreases reactive oxygen species and oxidative stress (Algire et al., 2012). Another study has presented decreased DNA damage owing to metformin treatment in human lung carcinoma, epidermoid carcinoma, and normal lymphoblastoid cells (Halicka et al., 2011). There is also a study that has demonstrated that metformin protects against ultraviolet C-induced DNA damage and increases DNA repair in lung cancer cells (Lee et al., 2016).

On the other hand, there are studies indicating a different side of metformin effects. Metformin has been found to increase oxidative DNA damage under oxidative conditions (Ohnishi et al., 2016), to enhance DNA damage in Chinese hamster ovary cell line CHO-K1 (Amador et al., 2012), and to intensify IR-induced DNA damage in pancreatic cancer cells via AMPK thus improving the efficiency of radiation treatment (Fasih et al., 2014). Also, it has been shown that metformin reduces DNA repair in human hepatoma cells exposed to IR via abatement of adenosine triphosphate production (Liu et al., 2012) as well as in human lung cancer cells by suppressing the expression of a p38 mitogen-activated protein kinase-dependent set of DNA repair proteins, excision repair cross-complementing 1 (Tseng et al., 2013). A study of colorectal cancer cells has even revealed that metformin impedes repair of IR-induced DNA damage by decreasing the expression of several HR-related DNA repair proteins *in vitro* and *in vivo*, improving radiosensitivity even in radioresistant cells and tumors (Jeong et al., 2015).

Nevertheless, there are also studies that have not found any effect of metformin on DNA damage. For example, metformin was not able to protect against the induced oxidative DNA damage in cultured human peripheral blood lymphocytes (Onaran et al., 2006) or induce DNA damage in SKOV3 and A2780 ovarian cancer cell lines (Hijaz et al., 2016). However, it is worth noting that the latter are not HGSOC cell lines.

It could be that the metformin effect depends on cell type. For ovarian cancer cells specifically, the data on this matter is very scarce. Ovarian cancers (and thus ovarian cancer cell lines) display high intra- and especially inter-patient genomic heterogeneity. Different *in vitro* studies have often used different cell lines, and conceivably the metformin effect on DNA damage could differ between cell lines. Because

of the varying results from metformin and DNA damage studies and the limited data from them on ovarian cancer, there is a need to examine this area further.

In ovarian cancer, the aspect of DNA damage in relation to HR is of particular importance. Even those patient tumors that initially have been declared as HR-deficient still have a sub-population of cells that are HR-proficient. These HR-proficient cells survive chemotherapy, eventually continue their expansion, the patient relapses, and after a certain number of chemotherapy treatments, the patient becomes chemoresistant. This is called acquired resistance to chemotherapy (Chien et al., 2007; Konstantinopoulos et al., 2015). The situation is even worse for those patients whose cancer is identified as HR-proficient from the very beginning. They can be considered to have intrinsic resistance to chemotherapy. The existing chemotherapeutic treatment has no beneficial effect at all on roughly 20 % of HGSOCs (Chien et al., 2007).

Since metformin has been associated with improved survival rate in diabetic ovarian cancer patients, and HR status is of significant importance for chemotherapeutic outcome in this disease, one can hypothesize that metformin may have the ability to induce an HR-deficient state in cancer cells, sensitizing them to treatment. While this study did not examine HR directly, it investigated HR indirectly by observing the effect of metformin on: *(i)* DNA damage, *(ii)* cell proliferation, and *(iii)* apoptosis. These read-outs were obtained for two commercially available HGSOC cell lines with known HR status: OVCAR4 (HR-proficient) and Kuramochi (HR-deficient) (Domcke et al., 2013; Tumiati et al., 2018; Tumiati, in preparation).

2. AIMS

A) To inspect the effects of metformin on DNA damage, proliferation, and apoptosis in two HGSOC cell lines *in vitro* using metformin at varying concentrations and treatment times.

B) To test whether metformin pre-treatment (with selected concentrations and treatment times) changes the capacity of HGSOC cells *in vitro* to respond to irradiation-induced DNA damage.

3. MATERIALS AND METHODS

Three experiments were performed in total. The workflow consisted of: 1) cell culture, 2) irradiation (only in the third experiment), 3) cell fixing and staining by indirect immunofluorescence, 4) high-content analysis, and 5) computational data processing and analysis. Reagents, equipment, and other resources are listed in Appendix A.

3.1. Cell Culture

Cell culture was performed in a laminar flow cabinet in a near-sterile environment. Two commercial HGSOC cell lines were used: Kuramochi as HR-deficient, and OVCAR4 as HR-proficient cell line. Both types of cells were initially frozen in cryogenic vials. One vial per cell line was thawn to initiate cell culture. Cells were cultured in RPMI 1640 growth medium supplemented with 10 % fetal bovine serum (FBS), 2 mM glutamine, and 1 % penicillin-streptomycin (P/S), and split and frozen as needed throughout the experimental part of the study.

3.1.1. Culturing the cells from cryogenic vials

Each of the two cryogenic vials (one for each cell line) contained 1 ml of cells and growth medium mixture with 10 % dimethyl sulfoxide (DMSO). The vials were first incubated in a 37 ºC water bath for about 1 minute until their contents thawed. Their whole contents were transferred to 50-ml centrifuge tubes that each contained 10 ml of warm (37 ºC) growth medium. The tubes were centrifuged at 1250 rpm and 22 ºC for 5 minutes, and after discarding the supernatant, 10 ml of fresh warm medium was poured onto the cell pellets. The cells were resuspended in the medium and transferred to two 100-mm culture dishes per cell line. The dishes were placed in an incubator (37 ºC, 5 % CO_2) and cells were left to grow for ~72 hours.

3.1.2. Passaging and freezing the cells

When the cells reached ~80-90 % confluence, they were either passaged into more dishes or frozen. For both purposes, first, the old medium from each dish was discarded, then, the cells were washed with 5 ml of phosphate-buffered saline (PBS). The PBS was discarded, 1 ml of 0,25 % trypsin/EDTA was added to each dish, and dishes were placed in an incubator at 37 ºC for 7-8 minutes. After that, the dishes

were slapped on the side a few times and checked under a microscope to see whether the cells had detached from the bottom. If necessary, dishes were returned to the incubator for a few more minutes. When most of the cells had detached, 5 ml of warm medium was poured onto each dish, and after pipetting a few times, the content of each dish was transferred to 50-ml centrifuge tubes. All tubes were centrifuged at 1250 rpm and 22 ºC for 5 minutes, discarding the supernatant afterward.

For the passaging procedure, 20-30 ml of warm medium was poured to each tube. Then, the cell pellets were mixed with the media, and the content of each tube was transferred to two-three 100-mm culture dishes. Finally, the dishes were placed in an incubator, leaving the cells to grow there for ~72 hours.

For the freezing procedure, 2 ml of medium with 10 % DMSO was transferred to each tube with a cell pellet, and the pellet was resuspended. Finally, this mixture was transferred to cryogenic vials (1 ml per vial), the vials were snap-frozen in a freezing container at -80 ºC, and transferred to -150 ºC for long-term storage.

3.1.3. Seeding the cells

One dish per cell line was used for seeding into 96-well plates after the cells reached ~80-90 % confluence. In the first experiment, cells were thawed from cryogenic vials approximately 72 hours earlier. In the second and third experiments, cells were kept in long-term culture and regularly passaged.

The procedure began with removing the old medium from the dishes, rinsing with 5 ml of PBS, dissociating the cells with 1 ml of 0,25 % trypsin/EDTA, and incubating for 7-8 minutes. When the cells were freely floating in the dishes, they were mixed with 9 ml of warm media and then moved to 50-ml centrifuge tubes.

After that, cells were counted as follows. 10 µl of the cell suspension from each tube was mixed with 10 µl of trypan blue. 10 µl of this mixture was transferred into a chamber in a cell counting slide to be counted in a cell counter. In the first experiment, there were $4{,}68 \times 10^5$ Kuramochi cells and $9{,}41 \times 10^5$ OVCAR4 cells, in the second experiment, $3{,}65 \times 10^5$ and $6{,}61 \times 10^5$, and in the third experiment, $3{,}98 \times 10^5$ and $4{,}72 \times 10^5$ cells per 1 ml respectively. The volume of medium after centrifugation was adjusted such that 3000 cells were seeded per well in the first experiment, and 5000 cells in the second and the third experiments, in a total volume of 100 µl per well.

Cells were dispensed into 96-well plates (according to the pattern shown in figure 1), and then plates were placed in an incubator for 24 hours to allow the cells to adhere to the bottom of the wells (figure 2).

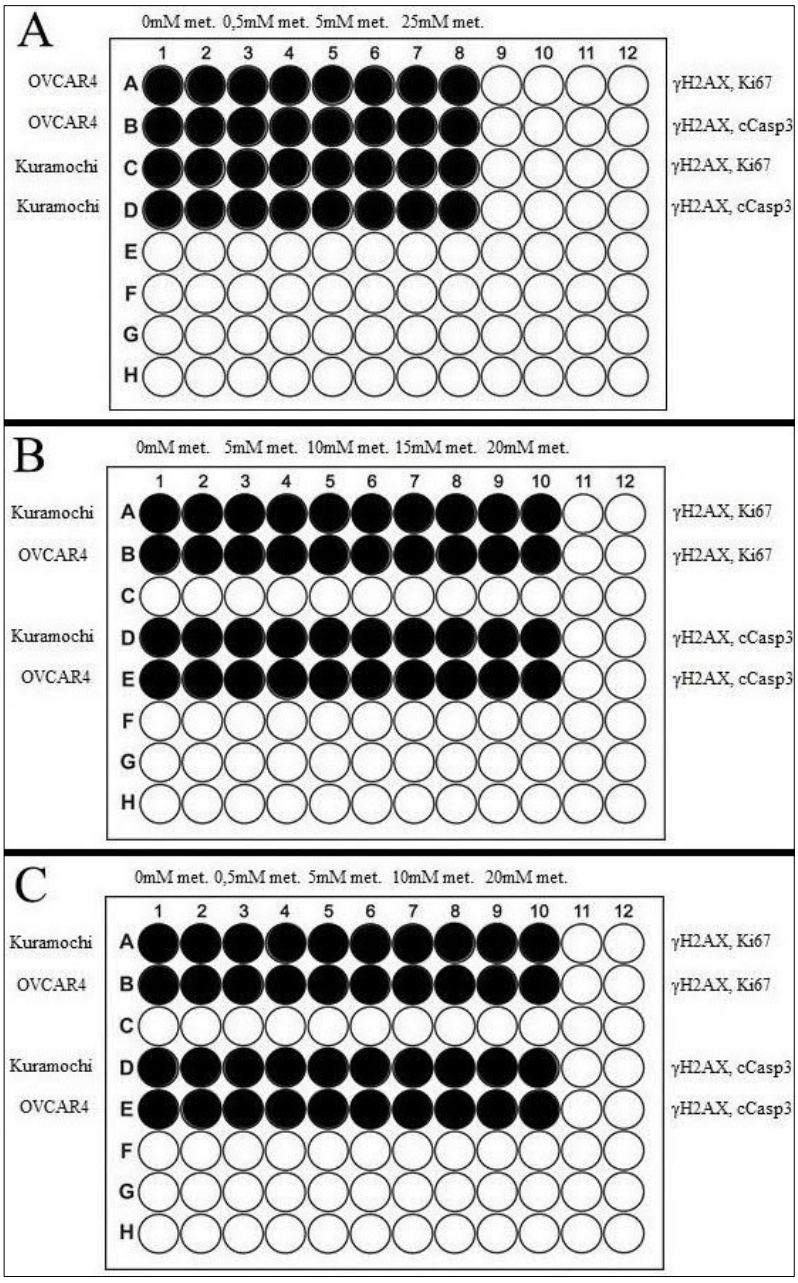

Figure 1. Schematic views of the 96-well plates throughout the experimental part.

Each well had a replicate well. Black wells mark the occupied wells in the plates. Lines "Kuramochi" and "OVCAR4" on the left next to the rows marked by letters indicate which cell line was seeded in that row. Above the numerical values of the columns, the numbers indicate the metformin (met.) concentrations (mM) used in the columns below them (one concentration for two columns due to the duplicate wells); columns 1-2 did not include any metformin, the media from the seeding part was left untouched there, i.e., these are control wells. The linear text fields on the right indicate the primary antibody combinations used in the rows next to them.

A – The pattern used for all of the plates in the first experiment; B – The pattern used for all of the plates in the second experiment; C – The pattern used for all of the plates in the third experiment.

3.1.4 Testing different metformin concentrations

In all three experiments, the cells were exposed to varying concentrations of metformin (figures 1-2). Metformin solution of the highest concentration was always made first by dissolving the weighted metformin powder amount in the appropriate volume of warm growth medium, and then filtering the solution. From this solution, serial dilutions were prepared to obtain the desired lower concentrations. The first experiment tested the effect of metformin solutions of 0,5 mM, 5 mM, and 25 mM

concentrations. The second experiment included 5 mM, 10 mM, 15 mM, and 20 mM metformin concentrations. In the third and last experiment, 0,5 mM, 5 mM, 10 mM, and 20 mM metformin concentrations were used.

After removing the old media from the wells (with the exception of the no-metformin control wells in columns 1 and 2), 100 µl of the prepared metformin solutions were put to the appropriate wells (according to the patterns shown in figure 1). After adding the metformin solutions, the plates were placed in an incubator.

Figure 2. Schematic visualization of the set-up of each experiment.

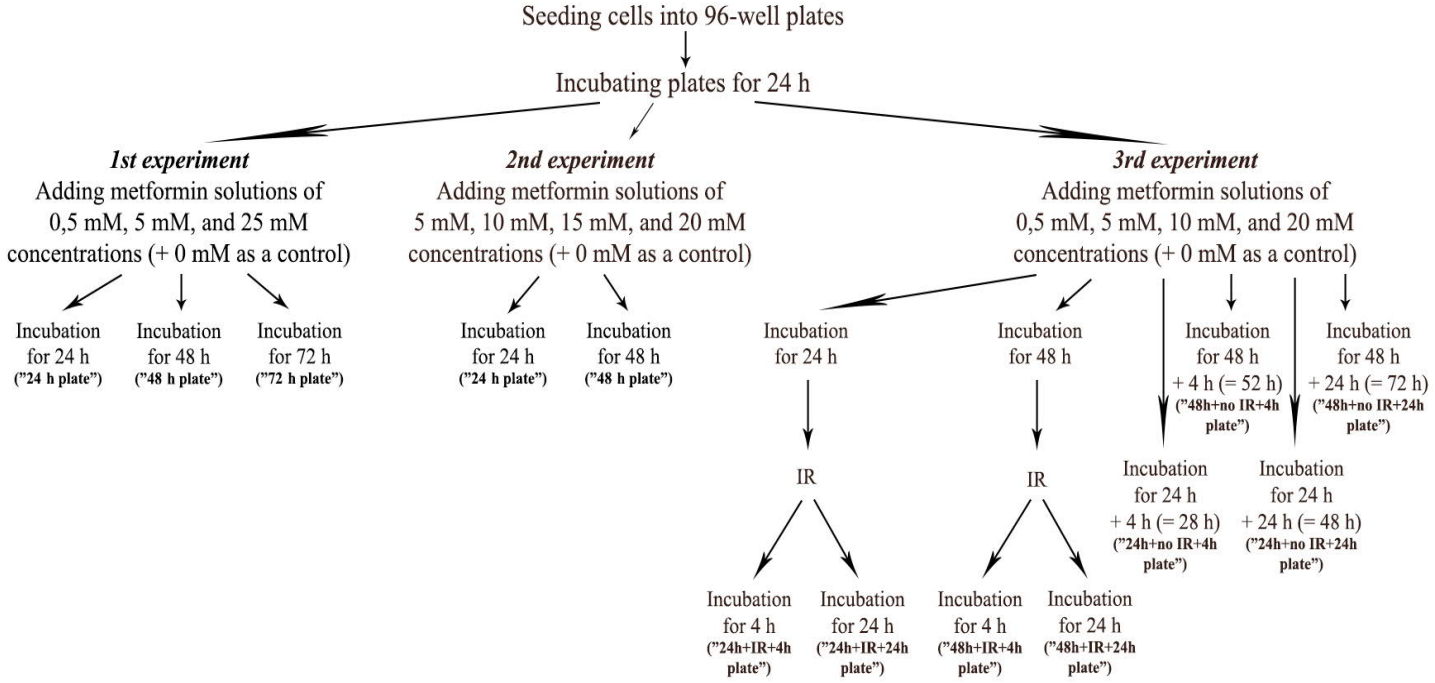

3.1.5. Testing different metformin treatment lengths

In addition to testing the effect of different metformin concentrations, I also tested different treatment lengths (figure 2). In the first experiment, one plate was kept in the incubator for 24 hours, another plate for 48 hours, and the last one remained for 72 hours. These plates are referred to as the "24h plate", the "48h plate", and the "72h plate". The second experiment included only 24h and 48h treatments; the plates are called the "24h plate" and the "48h plate" respectively. The third experiment had more variations due to the irradiation part, described next (section 3.2). In the third experiment, the duration of in-plate metformin treatment prior to irradiation was either 24 hours or 48 hours, and the subsequent incubation

was either for 4 hours or 24 hours. The non-irradiated counterpart plates were consequently incubated while affected with metformin either for 28 hours, 48 hours, 52 hours, or 72 hours. The next paragraph gives a more detailed explanation of this rationale, at the same time indicating the names of the plates used in this experiment.

3.2. Irradiation

The third experiment additionally included DNA damage induction *via* irradiation after metformin treatment (figure 2). The cells in half of the plates (4 out of 8) were exposed to 5 Gy of IR. Two plates were irradiated after 24 hours of metformin treatment. Afterward, both were returned to the incubator and one remained there for 4 hours (from now one referred to as the "24h+IR+4h plate"), and the other one for 24 hours (named as the "24h+IR+24h plate"). That is, the cellular properties were checked at two time points: 4 hours and 24 hours after irradiation. The other two plates were irradiated after 48 hours of metformin treatment. Likewise, one of these two plates stayed in the incubator afterward for 4 hours (called the "48h+IR+4h plate"), and the other one for 24 hours (referred to as the "48h+IR+24h plate").

The other half of the plates (the remaining 4) were not irradiated and served as a non-irradiated control. Their time spent in the incubator matched each one of the irradiated plates. This thus created the variability in the incubation hours described in the earlier section. The non-irradiated plates were marked as the "24h+no IR+4h plate", the "24h+no IR+24h plate", the "48h+no IR+4h plate" and the "48h+no IR+24h plate".

3.3. Cell fixing and staining

These procedures were performed in a normal laboratory environment (i.e., no extra sterility measures were taken).

3.3.1. Rinsing and fixing the cells

The procedure was performed for every plate in all three experiments after the desired metformin treatment durations, and in the case of the third experiment, at the above-specified time points after irradiation.

First, the media was discarded from the wells, and the cells were washed with 100 µl of PBS. Then, the cells were fixed using 100 µl of 2 % paraformaldehyde (PFA) diluted in phosphate-buffered saline containing calcium and magnesium (PBS++) at 4 ºC for 10 minutes. After discarding the fixative, the cells were rinsed with 100 µl of PBS. Afterward, the wells were replenished with 100 µl of PBS, the plates were sealed with laboratory film and stored in 4 ºC until the staining procedure.

3.3.2. Staining the cells

PBS was removed from the wells, and the cells were permeabilized with permeabilization buffer (consisting of PBS++ with 0,2 % Triton X-100) for 20 minutes. After discarding the permeabilization buffer, the cells were washed three times with 100 µl of staining buffer (consisting of PBS with 0,5 % bovine serum albumin (BSA), 0,15 % glycine, and 0,1 % Triton X-100) on a see-saw rocker for 5 minutes each time, followed by blocking with 100 µl of staining buffer for 30 minutes, again on a rocker.

In the meantime, primary antibodies were diluted in staining buffer. Details on primary antibodies, the function of the proteins they detect, and dilution ratios can be found in table 1. Due to the identical host species in which some primary antibodies were raised, it was necessary to perform two double stainings in order to differentiate the signals. One row of each cell line received the combination of γH2AX and Ki67, while the other row, γH2AX and cleaved caspase-3 (cCasp3) antibodies appropriately diluted in staining buffer (figure 1). Each well was filled with 50 µl of the appropriate compound, then the plates were sealed with laboratory film and left for overnight incubation at 4 ºC in order for the primary antibodies to recognize and bind to their epitopes in the cells.

The next day, primary antibodies were discarded from the wells, and the cells were washed three times with 100 µl of staining buffer on a rocker at room temperature for 5 minutes each time. Meanwhile, two secondary Alexa-conjugated antibodies were diluted in staining buffer (table 1). These secondary antibodies bind to the primary antibodies and have a fluorescent tail which is detectable by epifluorescence microscopy. Every occupied well was filled with 50 µl of the secondary antibodies and staining buffer mixture, and then the plates were left for 1 hour at room temperature in the dark, as secondary antibodies need to be protected from light. After incubation, secondary antibodies were discarded from the wells, and the cells were washed three times with 100 µl of staining buffer on a rocker for 5 minutes each time while protecting from light. Then, the cells were counterstained with 100 µl of 2 µg/ml Hoechst dye diluted in PBS. Hoechst was used to visualize nuclei. After approximately 7-8 minutes in the dark, the Hoechst stain was discarded, the cells were rinsed with 100 µl of PBS, and the

wells were replenished with 100 µl of PBS for imaging. Finally, the plates were sealed with laboratory film, wrapped in foil to protect from light, and stored in 4 ºC until imaging.

Table 1. Primary and secondary antibodies used in the experiments.

Antibody	Dilution Ratio	The Process that the Antibody Allows to Visualize
Primary Antibodies		
Mouse anti-γH2AX (abcam, 22551)	1:1000	DNA damage
Rabbit anti-Ki67 (abcam, 15580)	1:1000	Proliferation
Rabbit anti-cCasp3 (Cell Signaling Technology, 9664)	1:300	Apoptosis
Secondary Antibodies		
Goat anti-Mouse Alexa 488 (Molecular Probes, A 11029)	1:1000	DNA damage
Goat anti-Rabbit Alexa 647 (Molecular Probes, A 21245)	1:1000	Either proliferation or apoptosis

3.4. Automated fluorescence image acquisition with a high-content screening system

The plates from the first experiment were imaged with a high-content screening system Thermo Cellinsight. Separate protocols were created for each of the three plates. The main parameter that required adjusting between the protocols was exposure time. Firstly, different exposure times were needed for different channels: channel 1, which visualizes nuclei (Hoechst dye); channel 2, which displays DNA damage (γH2AX); and channel 3, which shows either proliferation (Ki67) or apoptosis (cCasp3). Once the appropriate values for exposure time were determined for the 24h plate, 5 fields of every well were arbitrarily chosen to be scanned. After scanning the first plate, the starting protocol was applied to the second plate (i.e., 48h plate), and exposure times were slightly adjusted according to the preview on the screen, following the scanning of 5 random fields. Finally, the same procedure was carried out for the third, 72h plate.

Due to changes in instrumentation in the Biomedicum bioimaging facility during the course of this thesis project, the plates from the second and third experiments were imaged with a different high-content

screening system, ImageXpress Pico. Two protocols were created for the two double stainings. Similarly to Thermo Cellinsight, exposure times were separately determined for each channel. For every well, one large image was obtained that covered most of the well, excluding the edges, because focusing there proved difficult due to the color of the plate plastic.

3.5. Computational data processing and analysis

From the first experiment, images of the scanned fields were exported in an 8-bit TTF format and analyzed with the open-source image processing program ImageJ with the Fiji package. Six highest-quality images were chosen for each condition for analysis. When needed, visible particles that were not cells (e.g., dust particles, fibers) were manually deleted from the images. Macroinstructions, or macros, were used for automated analysis (the commands can be found in Appendix B). Firstly, a macro for the channel 1 image was used to identify all the nuclei in an image. This created a mask that was then applied to the channel 2 and channel 3 images. After running the first macro, a macro for the channel 2 image was used to determine how many nuclei from the ones identified in channel 1 displayed DNA damage. Then, macros for the channel 3 images (separate macros for Ki67 and cCasp3) were applied in order to determine how many nuclei from channel 1 were positive for markers of proliferation and apoptosis, respectively. After using the macros for each channel, the software reported the number of the identified objects in each channel in the form of a pop-up table. The data from the table were copied onto a Microsoft Excel spreadsheet.

From data entered into the Excel spreadsheet, the following calculations were performed. First, the percentage of nuclei marked with γH2AX, Ki67, or cCasp3 out of all nuclei (as identified by Hoechst) was calculated. Then, averages and confidence intervals (CIs) for all four markers were calculated for each set of six images that were included for each condition using Excel functions, “AVERAGE” and “CONFIDENCE”, respectively, while standard deviation necessary for CI calculation was found using Excel function “STEDV.S”.

From the second and third experiments, images were analyzed with the analysis module installed in ImageXpress Pico. Two protocols were created for the two double stainings. The variable settings included segmentation parameters, namely, intensity, minimum width and maximum width values in all three channels. Additionally, channels 2 and 3 had scoring parameters, namely the cellular part that had been stained, and the minimum stained area value. The program then counted the nuclei present in the

scanned area for every channel, and also calculated their percentage, like when processing the data from the first experiment. Since every well had a replicate well, the wells that happened to have large trash objects like fibers or dust particles mistakenly recognized as nuclei were excluded from the analysis. When both duplicate wells had issues and neither could be used, the scoring was done manually with ImageJ+Fiji using only high-quality areas of the wells and analyzing at least close to 200 nuclei per condition. In addition, manual scoring was performed for all γH2AX images in the third experiment, because the Pico analysis module did not work equally well in both γH2AX staining combinations.

The data collected with the Pico analysis module were downloaded as comma-separated values (CSV) files which were then converted to XLSX format using an online tool and processed with Microsoft Excel. When both replicate wells were used in the analysis, averages and CIs were calculated using Excel functions, “AVERAGE” and “CONFIDENCE”, respectively. In the cases when only one well could be used, no average and CI calculations could be performed. In the manual scoring, both duplicate wells were used, so it was possible to perform average and CI calculations.

The data from all experiments were transformed into bar charts that illustrated how the numbers of nuclei with DNA damage (γH2AX), the numbers of proliferating nuclei (Ki67), and the numbers of apoptotic nuclei (cCasp3) were affected by increasing metformin concentrations, treatment duration, and in the case of the third experiment, exposure to irradiation. The data was also pooled when possible and turned into bar charts as well. When pooling the data, even though the treatment durations slightly varied between the experiments, for simplification and convenience purposes, three major treatment duration groups were created: *i)* the first group contained 24h treatment and 24h+no IR+4h treatment; *ii)* the second group included 48h treatment, 48h+no IR+4h treatment, and 24h+no IR+24h treatment; *iii)* the third group consisted of 72h treatment and 48h+no IR+24h treatment. Finally, statistical significance was evaluated with Fisher’s exact two-tailed test using an online calculator: results at each lower metformin concentration were compared with results at every higher metformin concentration, and results of shorter metformin treatments at specific metformin concentration were compared with results of longer metformin treatments at the same metformin concentration.

4. RESULTS

This section briefly describes the main results from the three separate experiments and gives an overview of the pooled data. The pooled data presented in this section is comprised of only the most common metformin concentrations used throughout the experimental part in order to provide more comparable and informative data, considering that not all experiments were performed under the same conditions (e.g., short-term / long-term culture differences, different image acquisition and processing methods). For reviewing full pooled data, please refer to Appendix D. Also note that the first experiment has only data from Kuramochi cells, because not enough of OVCAR4 cells survived the experiment.

The purpose of the first and second experiments was to test a range of various metformin concentrations and metformin treatment durations in order to examine whether metformin alone can cause DNA damage and apoptosis in Kuramochi and OVCAR4 cells and influence their proliferation, as well as to find the most suitable metformin conditions for the third experiment involving IR. These initial metformin concentrations and treatment lengths were chosen based on previously published articles related to metformin, ovarian cancer, and observed proliferation-inhibitory, apoptosis-inducing, cell viability-decreasing, and similar metformin effects (Gotlieb et al., 2008; Rattan et al., 2011a; Shank et al., 2012; Wu et al., 2012; Lengyel et al., 2015; Patel et al., 2015; Dos Santos Guimarães et al., 2018; Yang et al., 2019). The purpose of the third experiment was to test whether any of the refined metformin pre-treatment conditions prior to IR has an effect on recovery from IR-induced DNA damage in Kuramochi and OVCAR4 cells. For this final experiment, it was decided to include a few higher as well as lower metformin concentrations from the tested range, in order to have both harsher conditions and milder ones that would better resemble physiological conditions.

4.1. γH2AX results

Upon DNA damage, namely DSBs, the histone variant H2AX is phosphorylated (Kuo et al., 2008). Thus, the phosphorylated form, γH2AX, can be exploited as a marker for DSB detection by using an antibody against it. Throughout the experiments, the antibody against γH2AX was used in two separate staining combinations: γH2AX+Ki67 and γH2AX+cCasp3. γH2AX results were consistent between the two stainings (see Appendix C) and for this reason, γH2AX data (in a form of means as percentages) from these separately performed stainings were combined.

In the first experiment (figure 4), among the untreated control Kuramochi cells (i.e., 0 mM metformin), 35 ± 7 % of analyzed nuclei displayed DNA damage 24 hours, 50 ± 4 % 48 hours, and 34 ± 4 % 72 hours after seeding (figure 3, A). Overall, the lower metformin concentrations, i.e., 0,5 mM and 5 mM did not have a meaningful effect in the quantities of the γH2AX-marked Kuramochi nuclei. Changes were visible using only the highest metformin concentration, i.e., 25 mM, in the 24h and 72h treatments, but statistical significance was not reached in the 48h treatment (62 ± 11 %; p = 0,0829,

Figure 3. Immunofluorescence images of Kuramochi cells in the first experiment: left – all nuclei in a part of a field as identified with Hoechst; right – γH2AX-positive nuclei in the same part of the field. A: 72h plate, 0 mM metformin. B: 72h plate, 25 mM metformin. Green arrows mark γH2AX-positive nuclei.

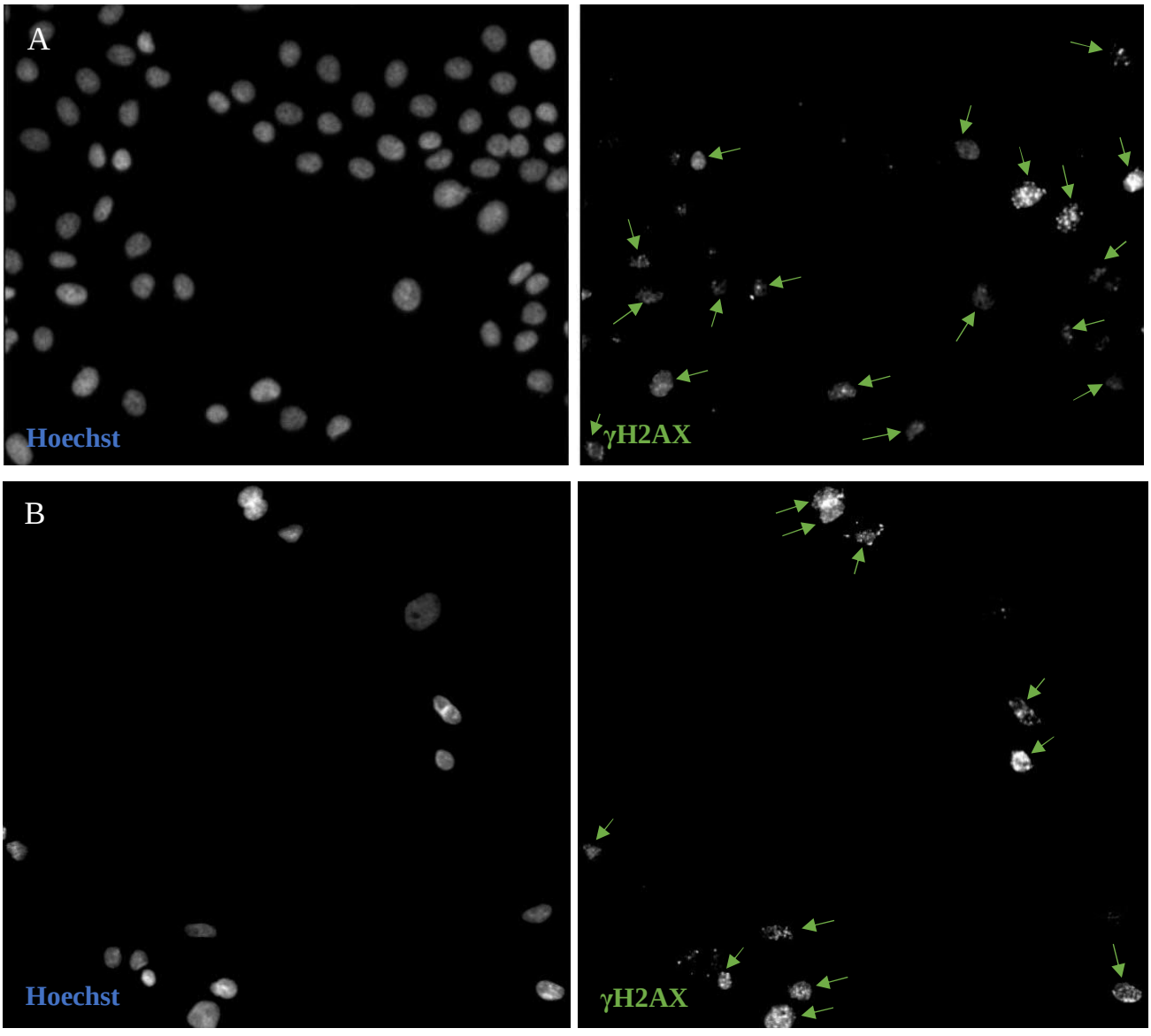

compared to controls). In the 24h treatment, this 25 mM metformin concentration resulted in 57 ± 12 % of nuclei exhibiting DNA damage ($p = 0{,}0079$, compared to controls), and 62 ± 14 % in the 72h treatment ($p < 0{,}0001$, compared to controls) (figure 3, B).

Figure 4. γH2AX results combined from γH2AX+Ki67 and γH2AX+cCasp3 staining combinations from Kuramochi cells in the first experiment. 24 h refers to 24h metformin treatment, 48 h refers to 48h metformin treatment, 72 h refers to 72h metformin treatment. Horizontal gray brackets mark statistically significant changes in DNA damage ($p < 0{,}05$).

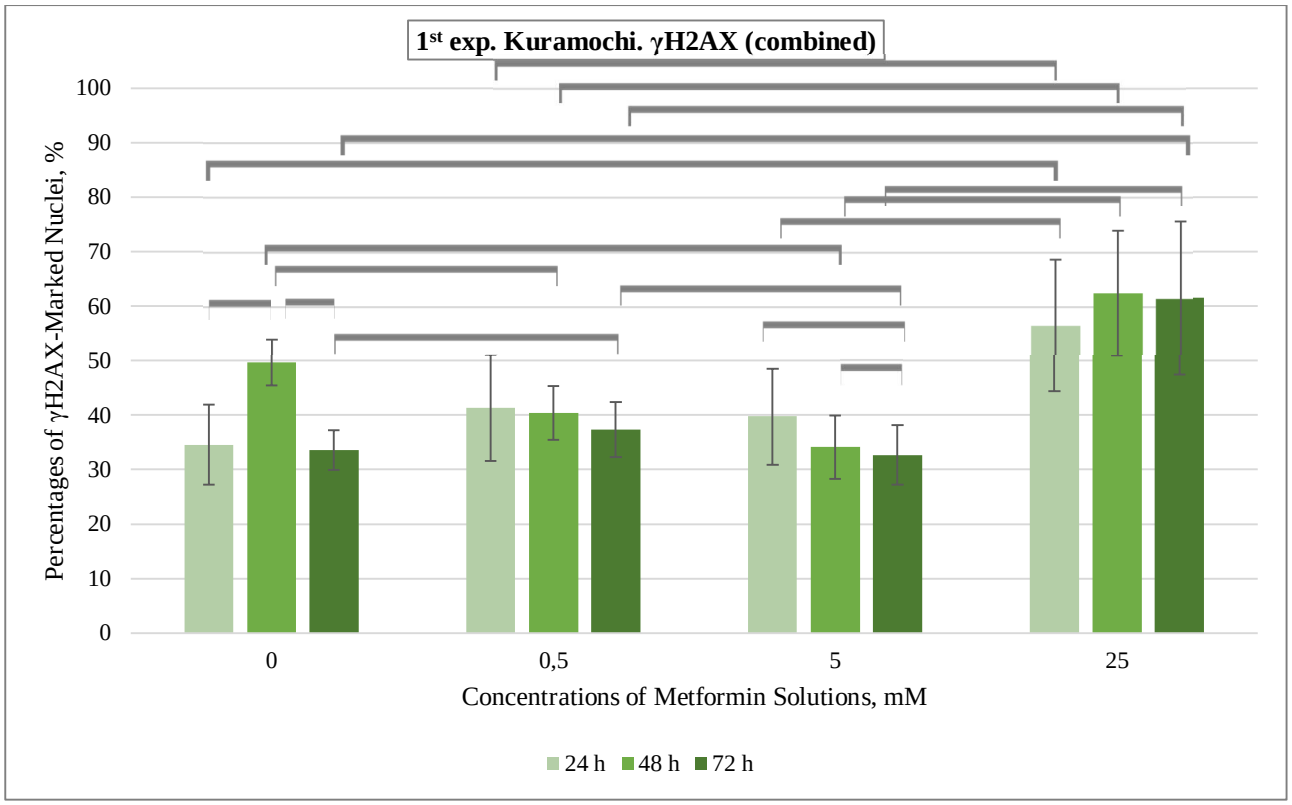

Results from the second experiment (figure 7) showed a general tendency of Kuramochi cells to slightly increasingly accumulate DNA damage with increasing metformin concentrations in both treatment durations, especially with 48h treatment (24h treatment: $p < 0{,}0001$ for 0 mM vs. 5 mM, and 10 mM vs. 15 mM; 48h treatment: $p < 0{,}0001$ for 0 mM vs. 5 mM, 5 mM vs. 10 mM, 10 mM vs. 15 mM, and 15 mM vs. 20 mM). Only 5 mM vs. 10 mM and 15 mM vs. 20 mM in the 24h treatment did not follow this tendency. Using the highest (i.e., 20 mM) metformin concentration, the difference between accumulated DNA damage compared to controls was 69 ± 7 % of nuclei versus 51 ± 6 % of nuclei in the

24h treatment, and 69 ± 4 % versus 38 ± 2 % in the 48h treatment (figure 5) ($p < 0,0001$ for both). OVCAR4 cells, on the other hand, were more resistant to metformin. Only the higher metformin concentrations, i.e., 15 mM and 20 mM, increased DNA damage (24h and 48h treatment: $p < 0,0001$ for 0 mM vs. 15 mM, and 0 mM vs. 20 mM). With 20 mM metformin, 74 ± 9 % of nuclei exhibited DNA damage compared to 63 ± 2 % of nuclei in the control group in the 24h treatment, and respectively, 55 ± 5 % compared to 39 ± 4 % in the 48h treatment (figure 6). Also, generally, more DNA damage was visible in the 24h treatment compared to the 48h treatment, particularly in OVCAR4 cells. Since it was also visible in controls (no metformin), it is possible that the reason for this was adverse cell reaction to plating (i.e., being moved from one growth condition to another). Cells had more time to recover from this procedure in the 48h treatment, and this could be why they displayed less DNA damage.

Figure 5. Immunofluorescence images of Kuramochi cells in the second experiment: left side – all nuclei in a part of a field as identified with Hoechst; right side – γH2AX-positive nuclei in the same part of the field. A: 48h plate, 0 mM metformin. B: 48h plate, 20 mM metformin. Green arrows mark γH2AX-positive nuclei.

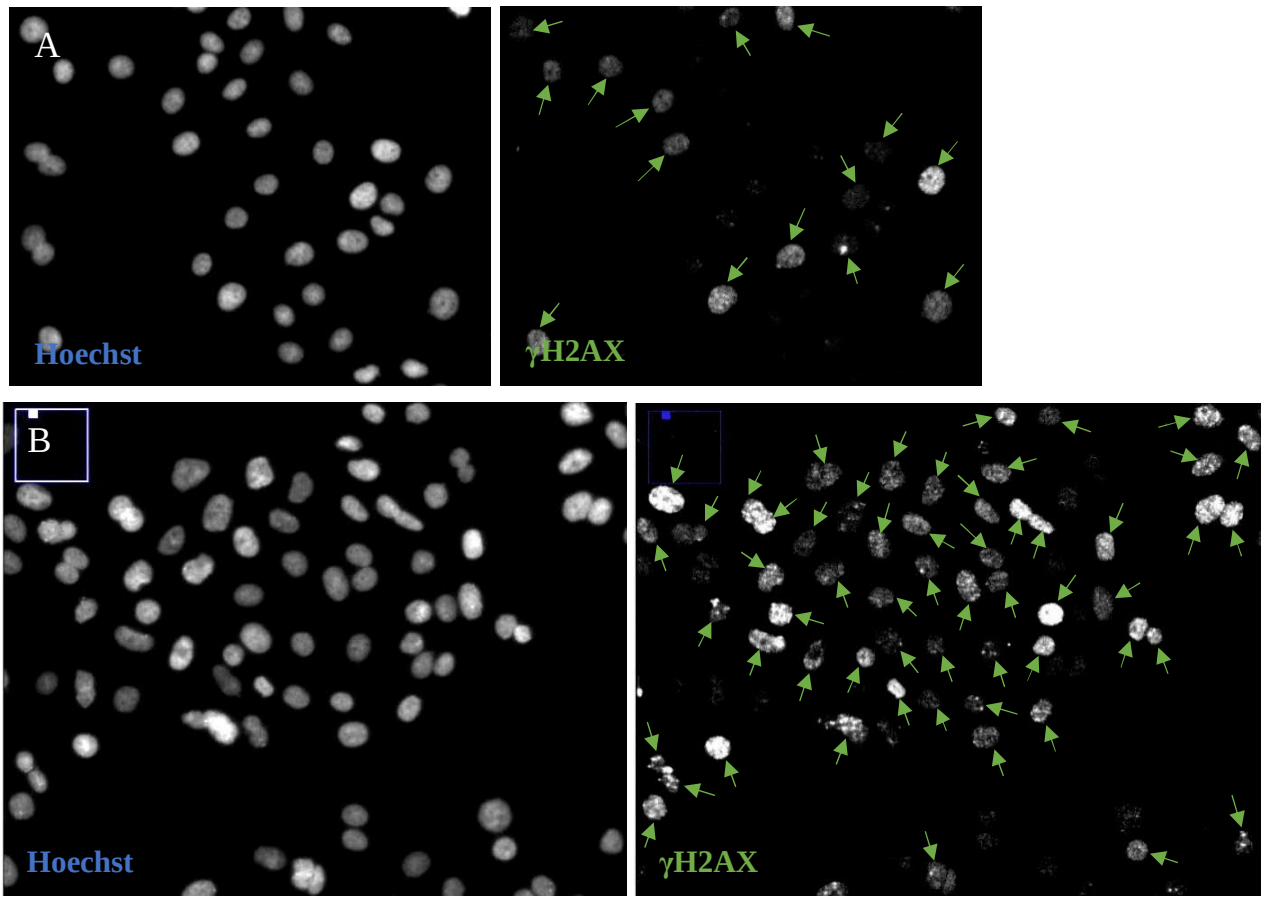

Figure 6. Immunofluorescence images of OVCAR4 cells in the second experiment: left side – all nuclei in a part of a field as identified with Hoechst; right side – γH2AX-positive nuclei in the same part of the field. A: 48h plate, 0 mM metformin. B: 48h plate, 20 mM metformin. Green arrows mark γH2AX-positive nuclei.

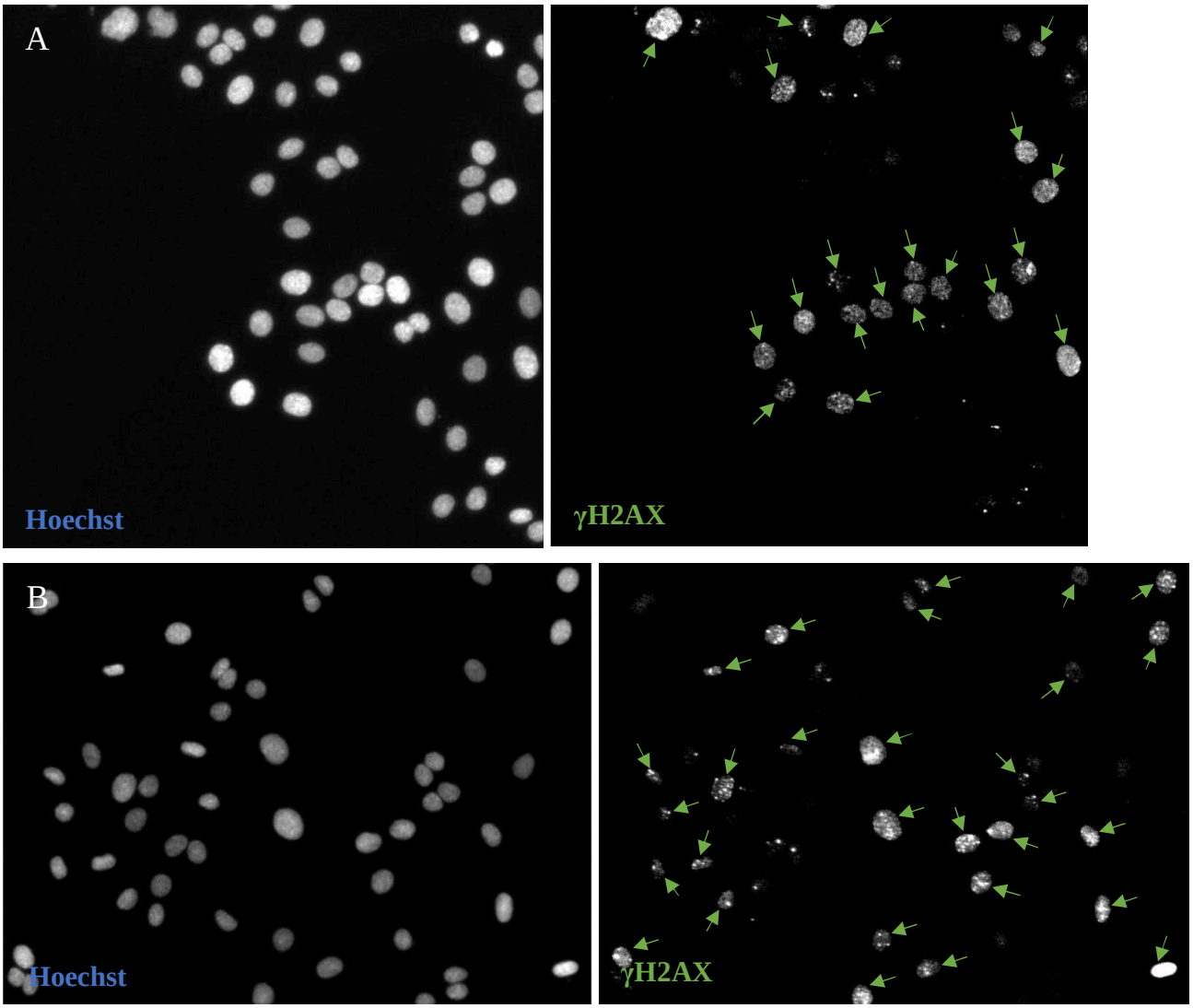

Figure 7. γH2AX results combined from γH2AX+Ki67 and γH2AX+cCasp3 staining combinations from Kuramochi cells (A) and OVCAR4 cells (B) in the second experiment. 24 h refers to 24h metformin treatment, 48 h refers to 48h metformin treatment. Gray text fields indicate statistically significant changes in DNA damage ($p < 0,05$).

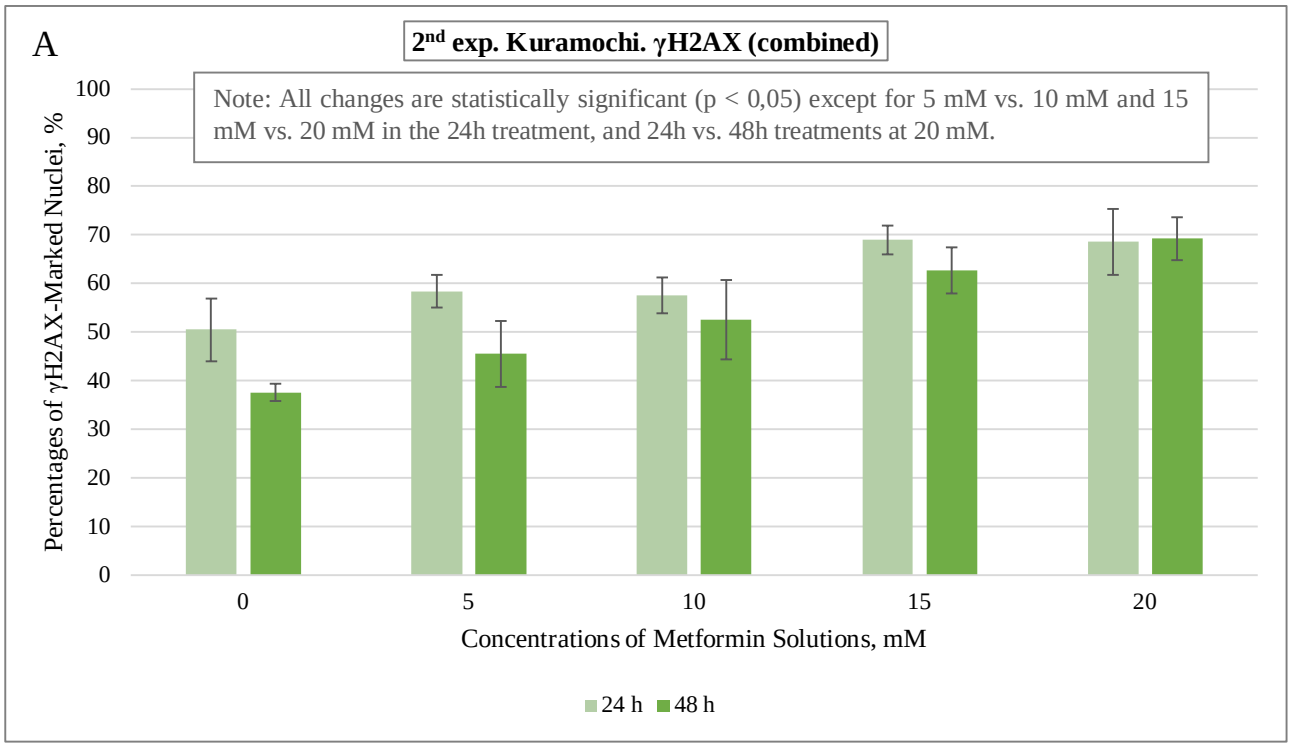

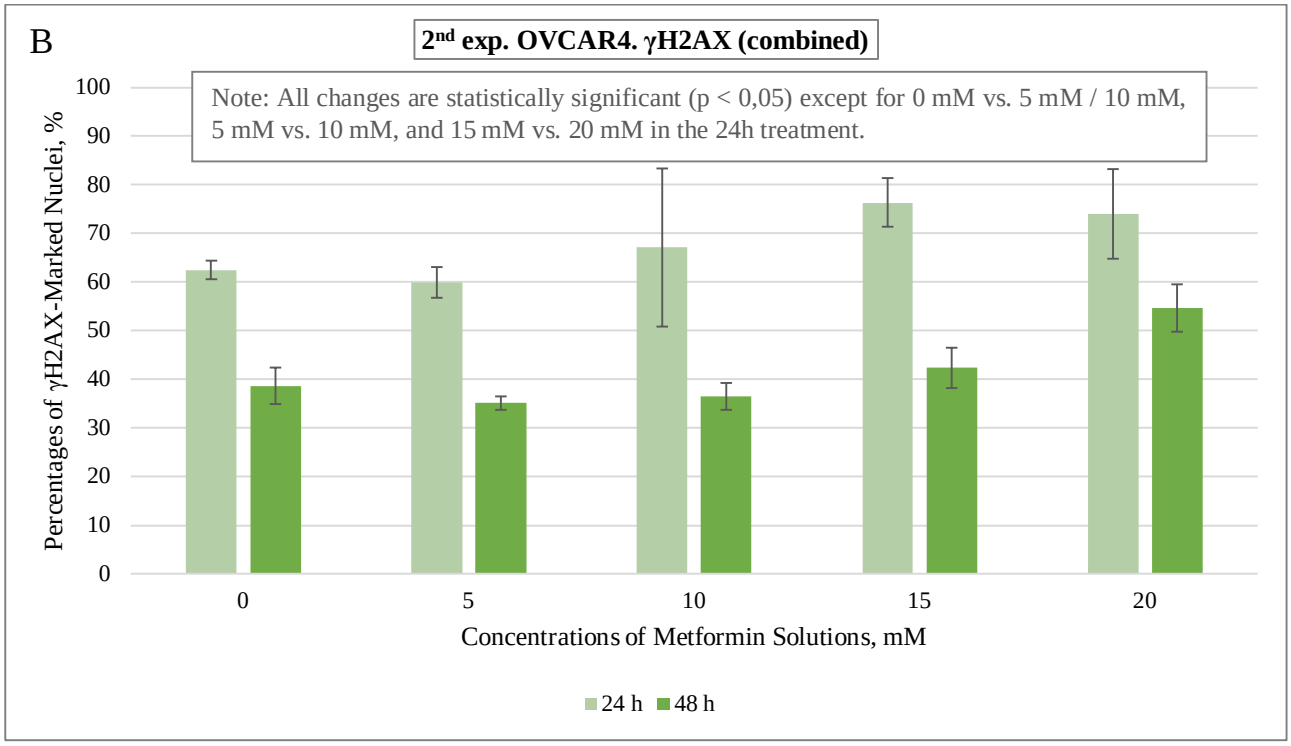

The third experiment had a different setup than the other two experiments: it started with metformin pre-treatment (for either 24 hours or 48 hours), followed by IR and subsequent incubation (for either 4 hours or 24 hours), in order to examine whether metformin impedes the recovery from DNA damage caused by IR; half of the plates, however, were not affected with IR for comparison (figure 2). The 4h post-IR incubation time point was selected, because γH2AX then is at its highest point, which is useful for assessing whether IR was successful in inducing DNA damage, as well as for having the starting point at its maximum value for comparison purposes (i.e., with the other time point). The 24h post-IR incubation time point was chosen in order to examine if cells can recover from the IR-induced DNA damage under the influence of metformin when given a substantial amount of time.

In this third experiment, non-irradiated cells produced similar DNA damage results in 24h+no IR+4h vs. 24h+no IR+24h and 48h+no IR+4h vs. 48h+no IR+24h treatments (figure 10). Generally, Kuramochi cells very slightly and almost gradually accumulated more DNA damage with increasing metformin concentrations in the 48h treatments. However, in the 24h treatments, statistical significance was reached only between 20 mM and 0 mM / 0,5 mM / 5 mM / 10 mM (24h+no IR+4h treatment), or only between 20 mM and 0 mM, as well as 10 mM and 0 mM (24h+no IR+24h treatment). In all cases, the highest metformin concentration, i.e., 20 mM, was the most effective in inducing DNA damage: 61 ± 3 % of nuclei were marked with γH2AX at 20 mM compared to 46 ± 5 % of nuclei at 0 mM in the 24h+no IR+4h treatment ($p < 0,0001$), and respectively, 59 ± 3 % compared to 42 ± 6 % in the 48h+no IR+4h treatment ($p < 0,0001$), 53 ± 4 % compared to 43 ± 5 % in the 24h+no IR+24h treatment ($p = 0,0034$), and 58 ± 2 % compared to 38 ± 2 % in the 48h+no IR+24h treatment ($p < 0,0001$) (figure 8). In comparison, γH2AX positivity in OVCAR4 cells was mostly unaffected by metformin. There was only a slight increase in DNA damage with the highest metformin concentration (20 mM) in the longest treatment duration (48h+no IR+24h) going from 42 ± 6 % of nuclei with DNA damage at 0 mM to 47 ± 2 % at 20 mM ($p = 0,0190$) (figure 9).

Figure 8. Immunofluorescence images of Kuramochi cells in the no IR part of the third experiment: left side – all nuclei in a part of a field as identified with Hoechst; right side – γH2AX-positive nuclei in the same part of the field. A: 48h+no IR+24h plate, 0 mM metformin. B: 48h+no IR+24h plate, 20 mM. Green arrows mark γH2AX-positive nuclei.

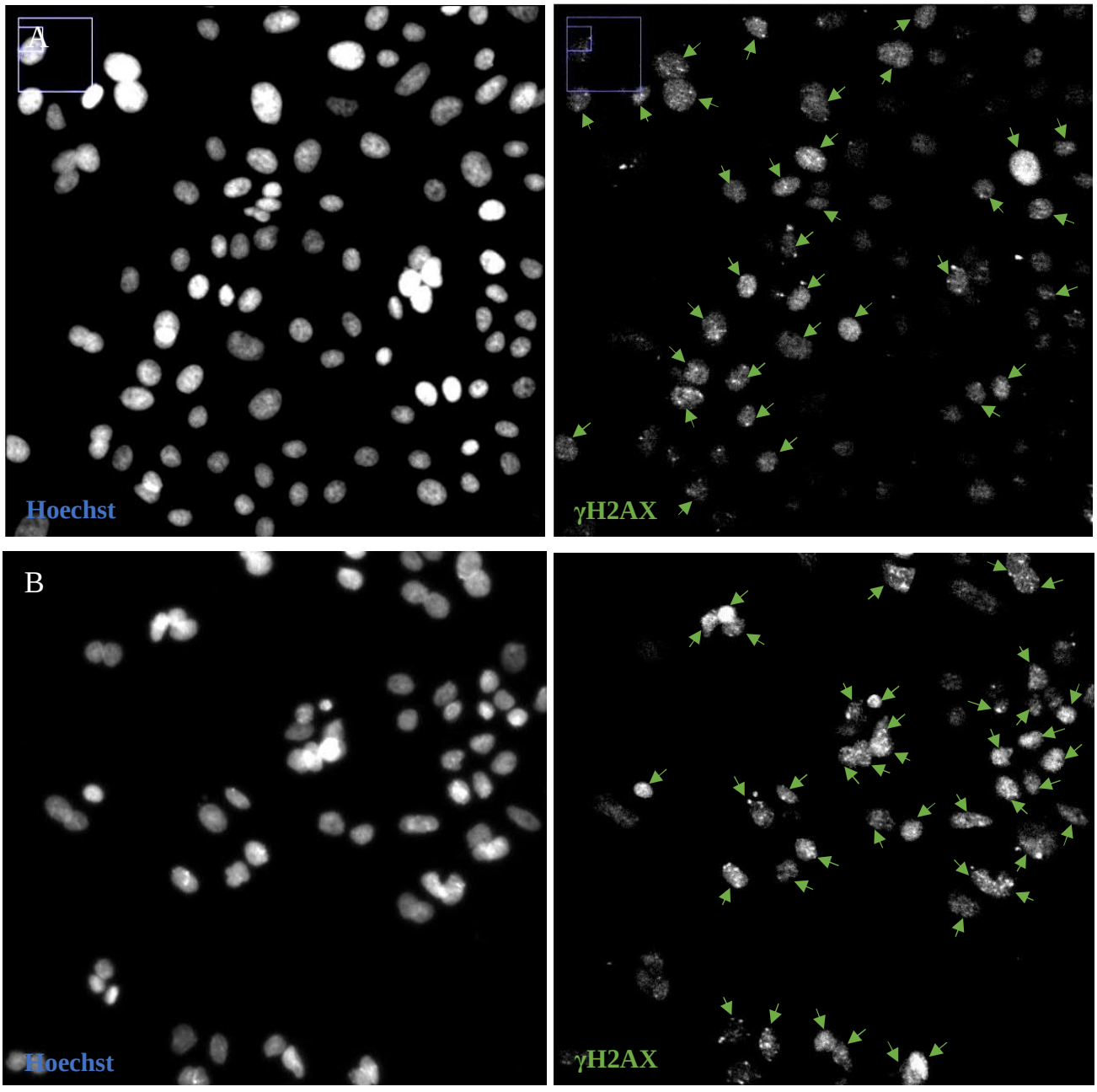

Figure 9. Immunofluorescence images of OVCAR4 cells in the no IR part of the third experiment: left side – all nuclei in a part of a field as identified with Hoechst; right side – γH2AX-positive nuclei in the same part of the field. A: 48h+no IR+24h plate, 0 mM metformin. B: 48h+no IR+24h plate, 20 mM. Green arrows mark γH2AX-positive nuclei.

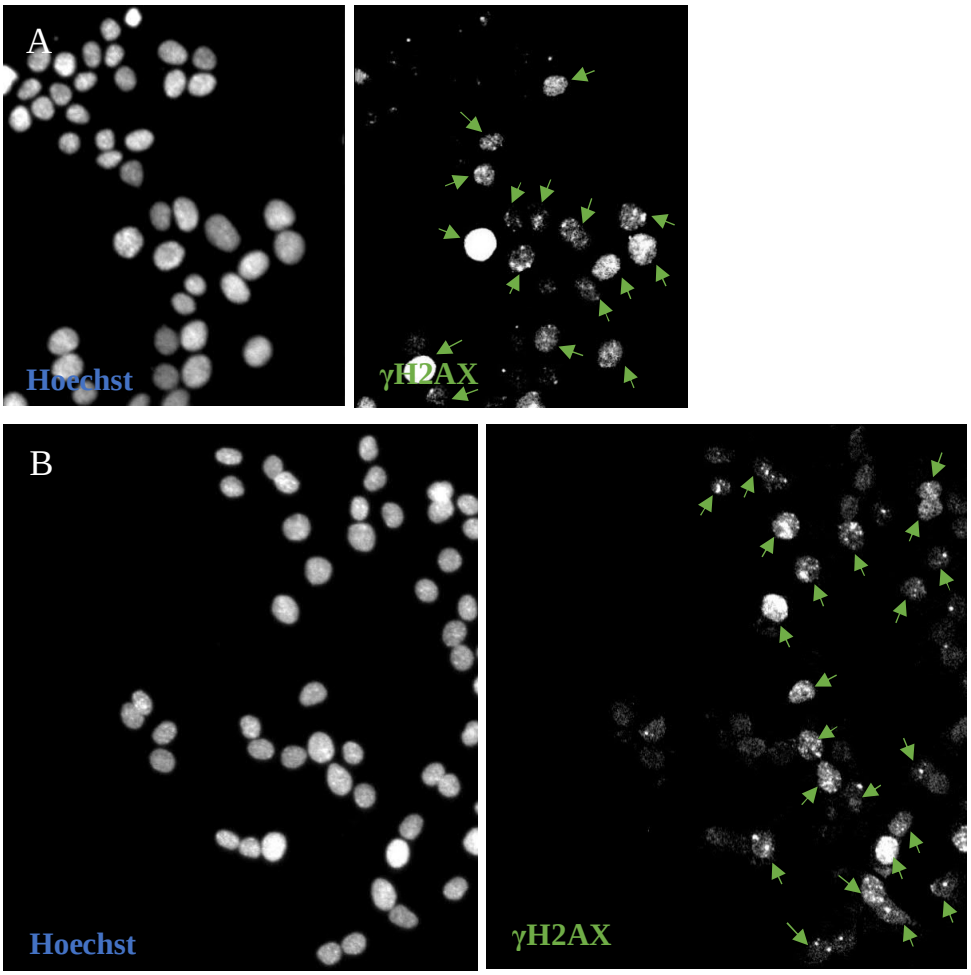

Figure 10. γH2AX results combined from γH2AX+Ki67 and γH2AX+cCasp3 staining combinations from Kuramochi cells in the no IR+4h (A) and the no IR+24h (C) parts of the third experiment, and from OVCAR4 cells in the no IR+4h (B) and the no IR+24h (D) parts of the third experiment. Legends indicate metformin treatment durations. Horizontal gray brackets mark statistically significant changes in DNA damage ($p < 0,05$).

A

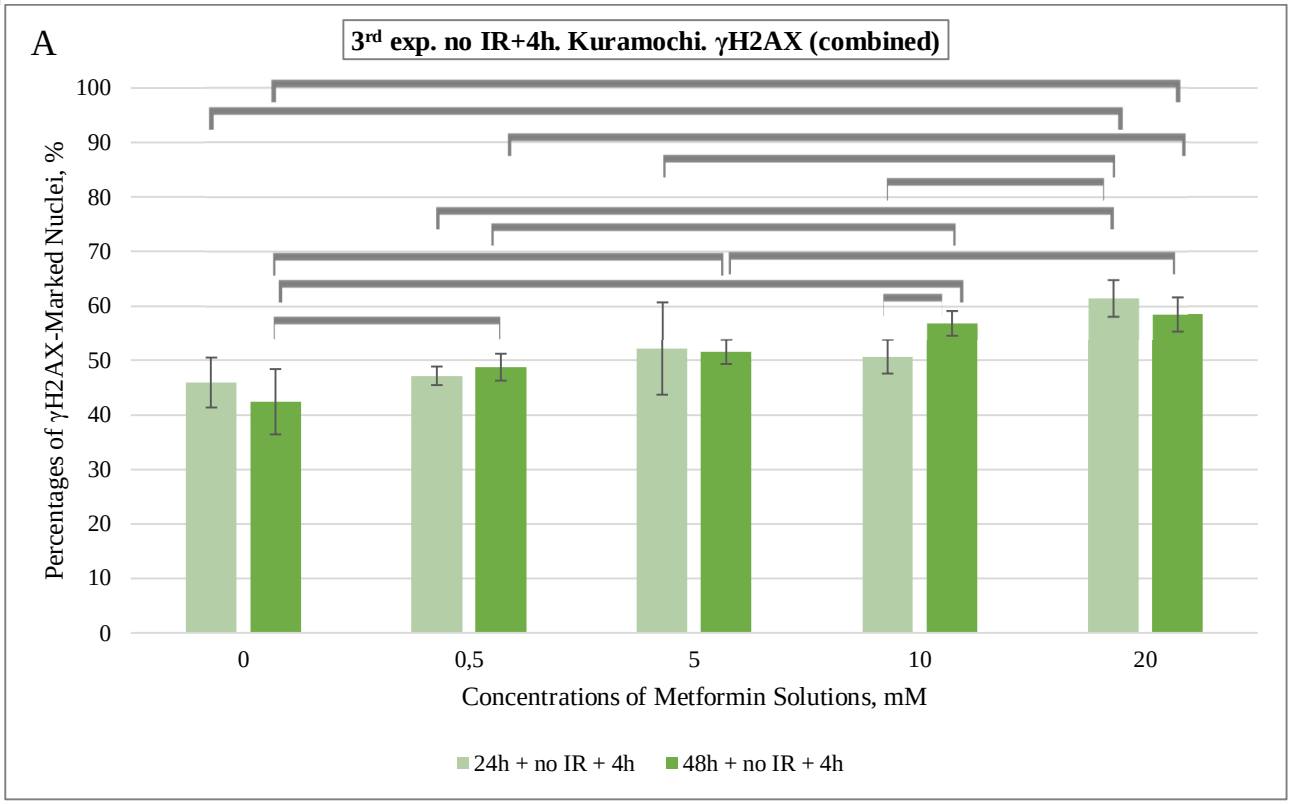
3rd exp. no IR+4h. Kuramochi. γH2AX (combined)
Percentages of γH2AX-Marked Nuclei, %
100
90
80
70
60
50
40
30
20
10
0
0
0,5
5
10
20
Concentrations of Metformin Solutions, mM
24h + no IR + 4h
48h + no IR + 4h

B

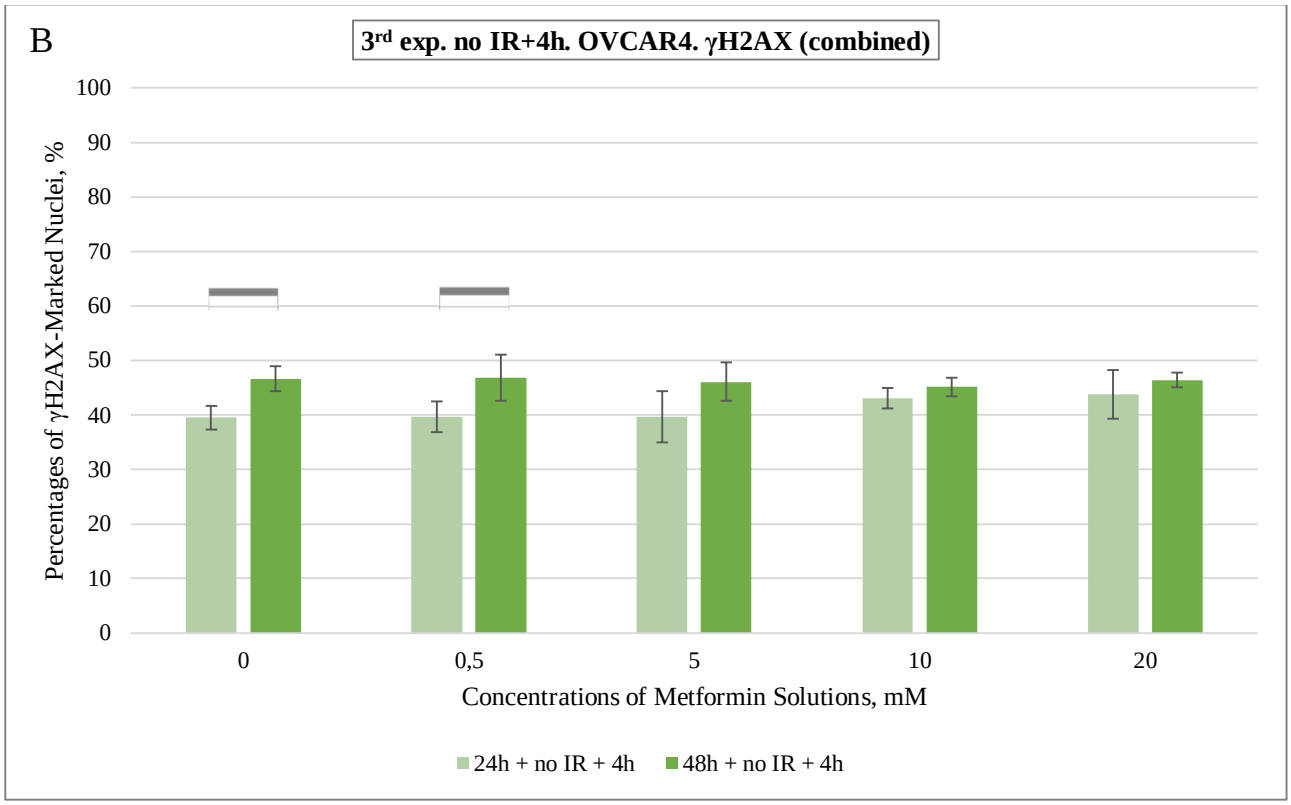
3rd exp. no IR+4h. OVCAR4. γH2AX (combined)
Percentages of γH2AX-Marked Nuclei, %
100
90
80
70
60
50
40
30
20
10
0
0
0,5
5
10
20
Concentrations of Metformin Solutions, mM
24h + no IR + 4h
48h + no IR + 4h

C

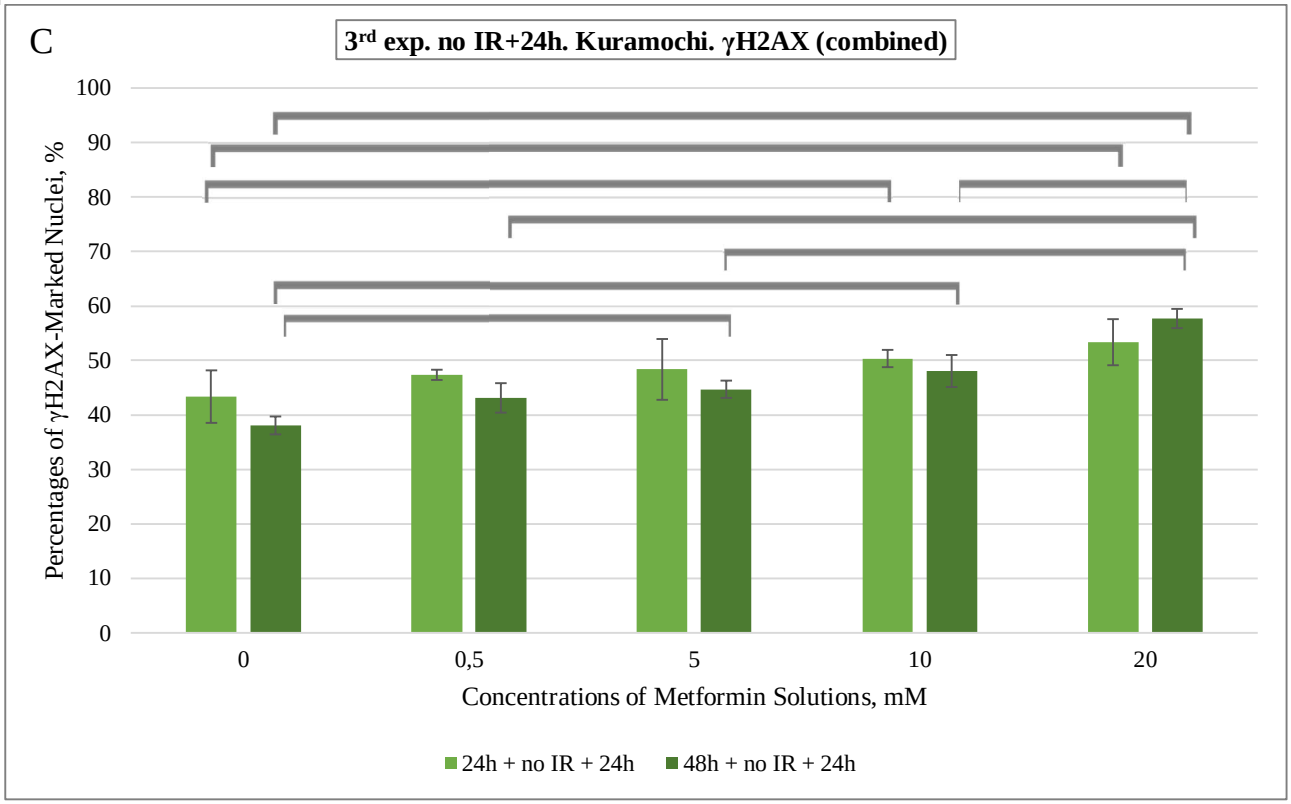
3rd exp. no IR+24h. Kuramochi. γH2AX (combined)
Percentages of γH2AX-Marked Nuclei, %
100
90
80
70
60
50
40
30
20
10
0
0
0,5
5
10
20
Concentrations of Metformin Solutions, mM
24h + no IR + 24h
48h + no IR + 24h

D

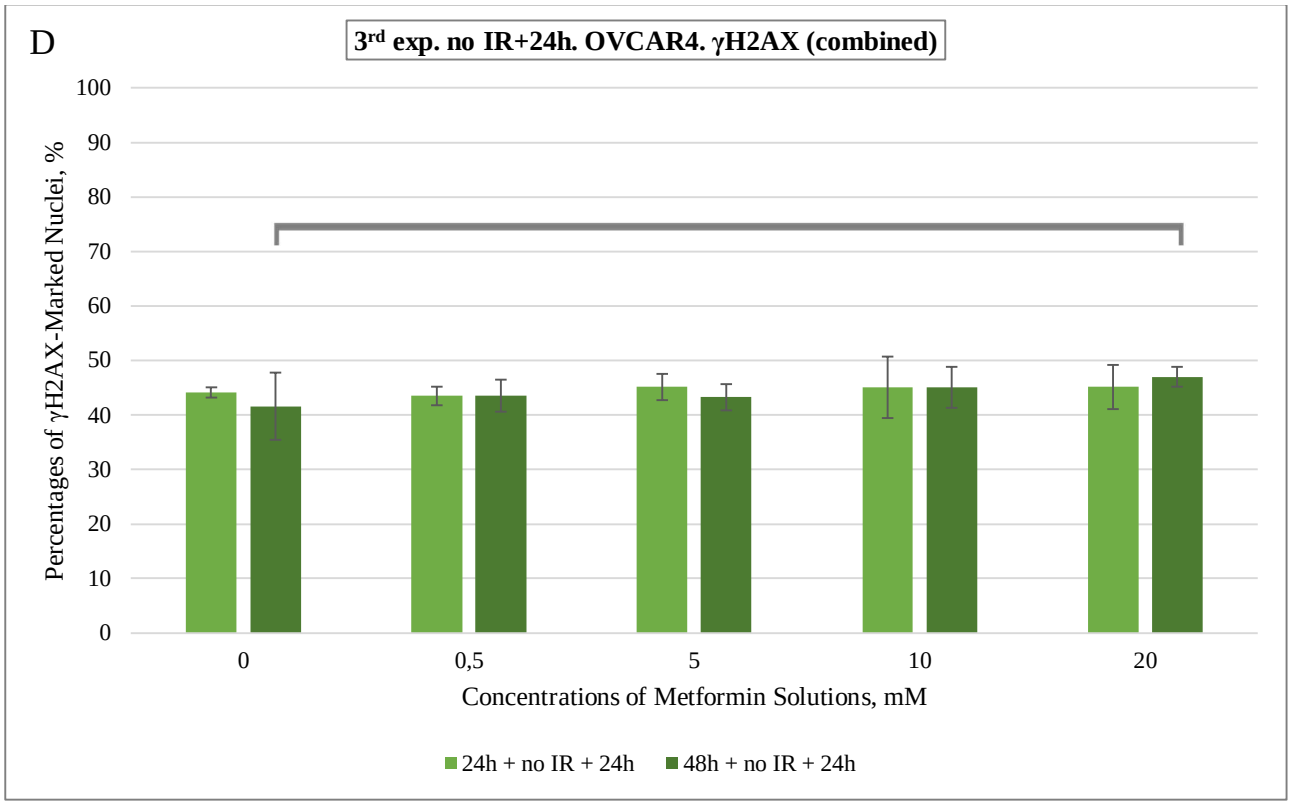
3rd exp. no IR+24h. OVCAR4. γH2AX (combined)
Percentages of γH2AX-Marked Nuclei, %
100
90
80
70
60
50
40
30
20
10
0
0
0,5
5
10
20
Concentrations of Metformin Solutions, mM
24h + no IR + 24h
48h + no IR + 24h

After pooling the data from all experimental parts that did not include irradiation (figure 11), it is visible that tested metformin treatment durations overall did not have much an effect on DNA damage, but concentrations mattered. Kuramochi cells experienced a substantial increase in DNA damage with ≥ 10 mM metformin solutions in all treatment lengths ($p < 0{,}0001$), whereas OVCAR4 responded to as high as 20 mM concentration of metformin ($p \leq 0{,}0190$) and only marginally. Metformin concentration of 20 mM increased the percentage of Kuramochi nuclei with DNA damage from 39 ± 6 % at 0 mM to 65 ± 4 % at 20 mM in the 24h treatment group, and respectively, from 45 ± 3 % to 60 ± 4 % in the 48h treatment group, and from 35 ± 3 % to 58 ± 2 % in the 72h treatment group. The same metformin concentration raised the percentage of OVCAR4 nuclei with DNA damage from 49 ± 9 % at 0 mM to 59 ± 12 % at 20 mM in the 24h treatment group, and respectively, from 44 ± 2 % to 49 ± 3 % in the 48h treatment group, and from 42 ± 6 % to 47 ± 2 % in the 72h treatment group.

Figure 11. Pooled γH2AX results from all non-irradiated Kuramochi (A) and OVCAR4 (B) cells. Legends indicate metformin treatment duration groups. Gray text fields indicate statistically significant changes in DNA damage ($p < 0{,}05$).

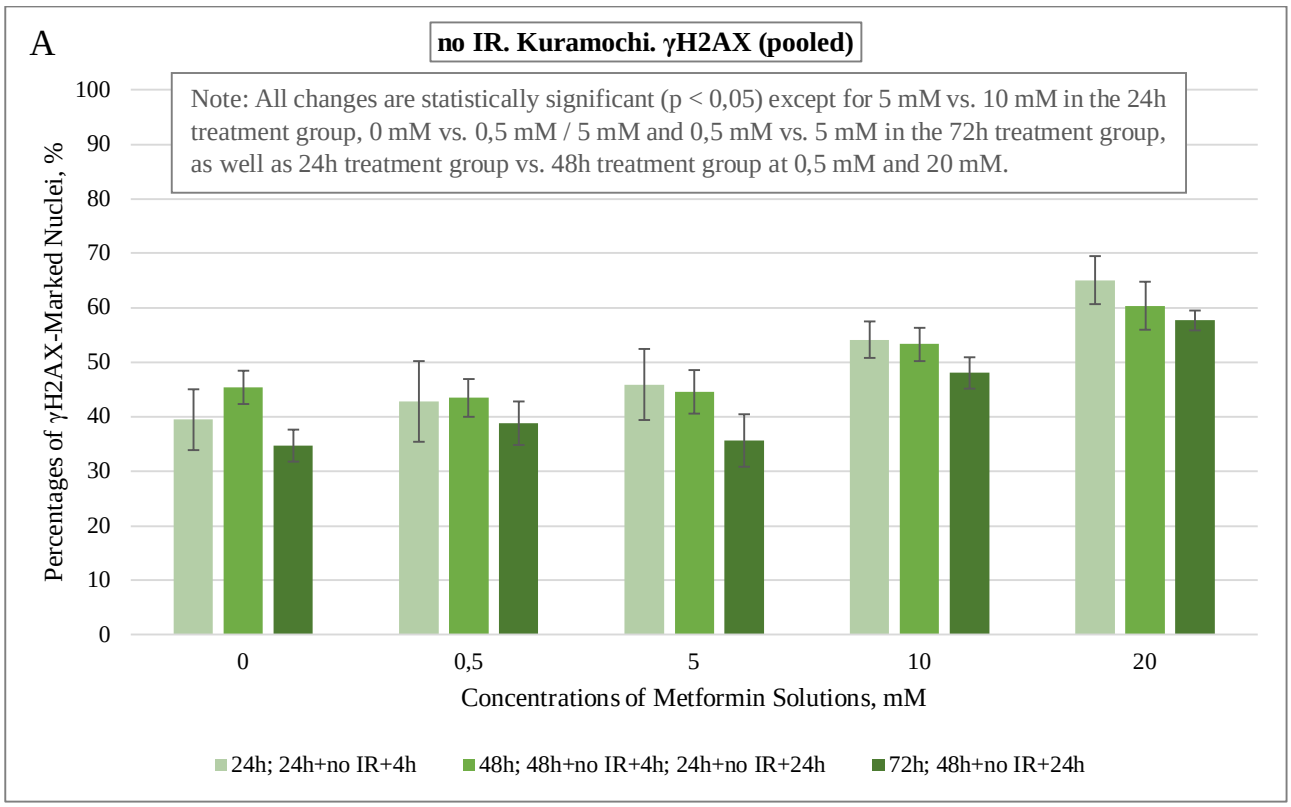

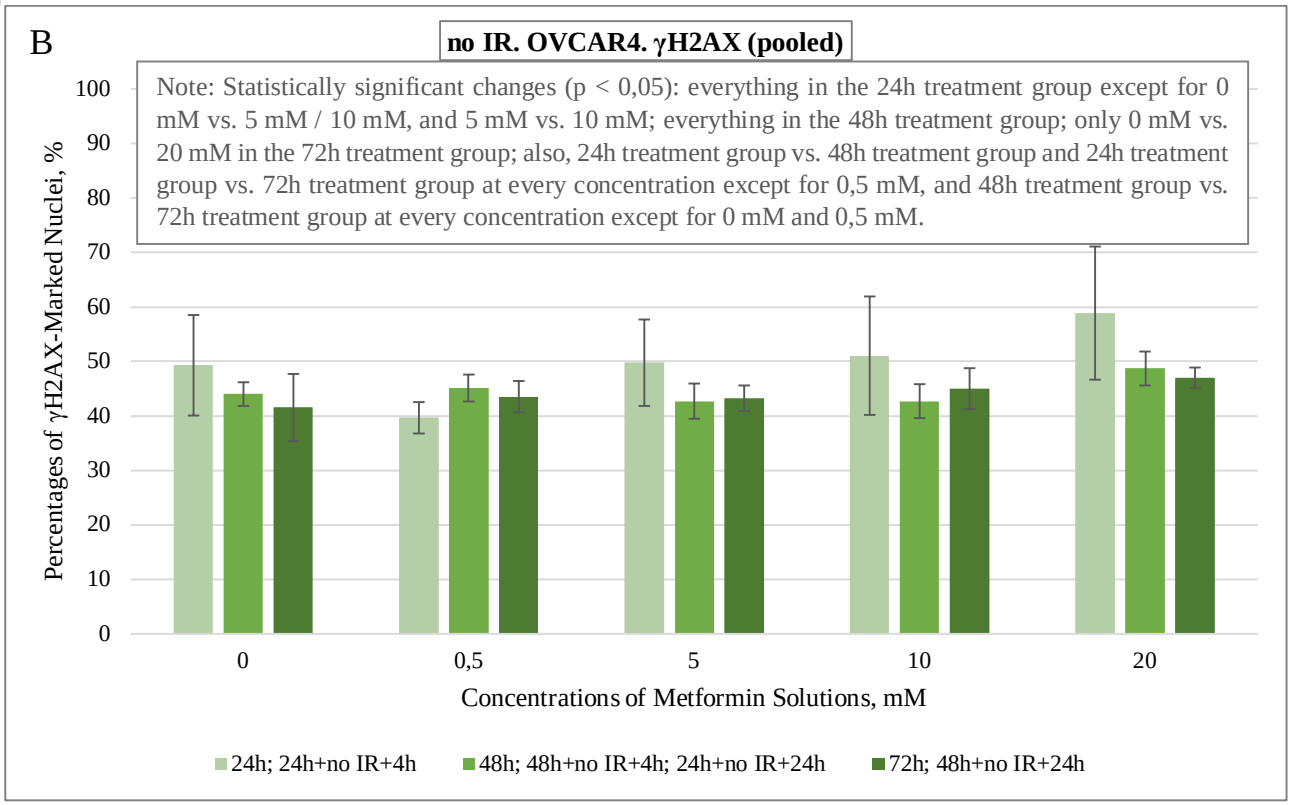

Irradiated cells in the third experiment displayed high amounts of DNA damage when 4 hours had passed since irradiation (figure 14), as expected, because repair was still ongoing at this time point. Nearly 100% of nuclei exhibited DNA damage in both cell lines and all metformin treatment conditions including controls (figures 12-13), indicating that irradiation successfully induced DNA damage in effectively all cells.

Figure 12. Immunofluorescence images of Kuramochi cells in the IR+4h part of the third experiment: left side – all nuclei in a part of a field as identified with Hoechst; right side – γH2AX-positive nuclei in the same part of the field. A: 48h+IR+4h plate, 0 mM metformin. B: 48h+IR+4h plate, 20 mM metformin. All nuclei on the right-side panels can be considered as γH2AX-positive.

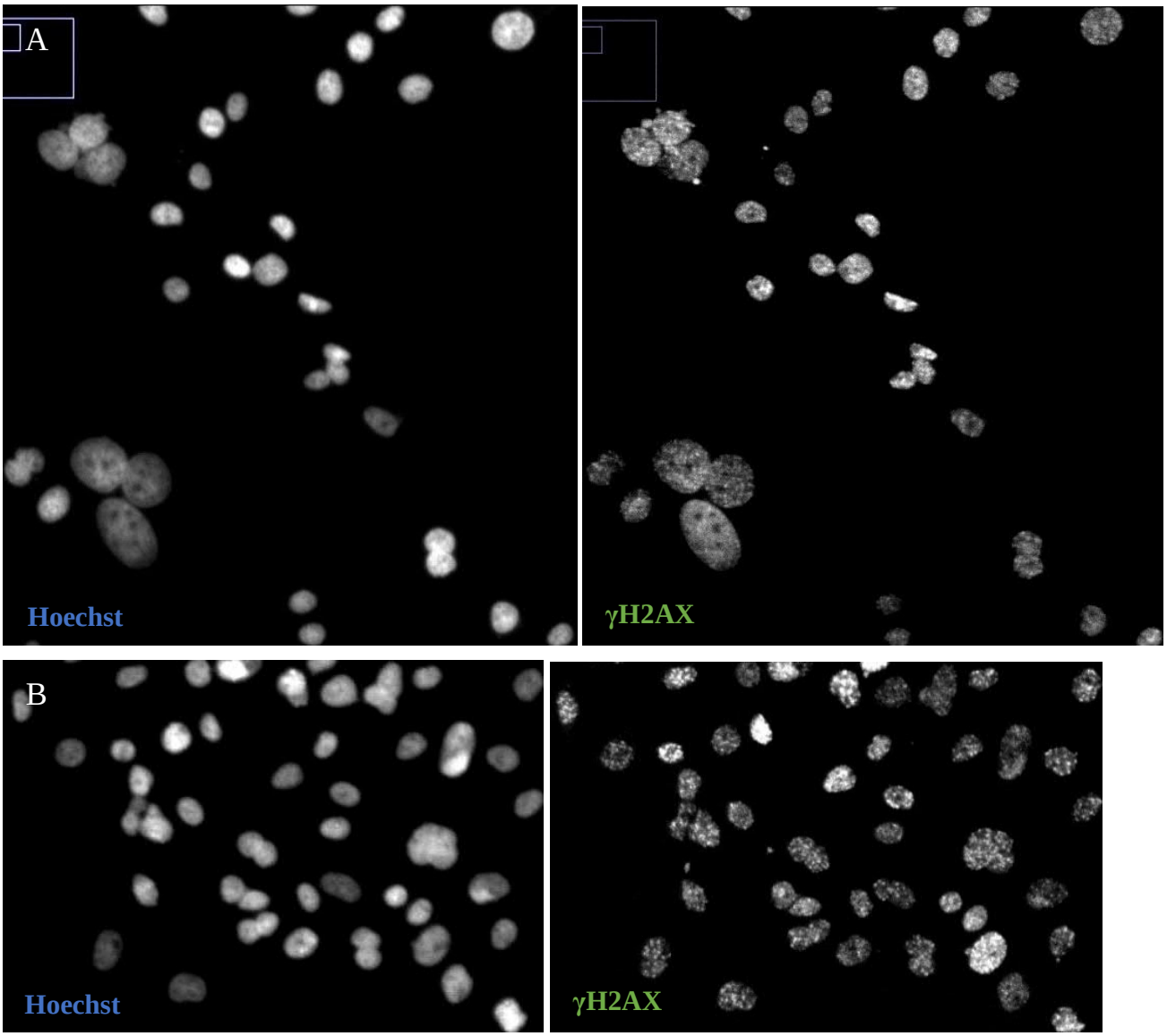

Figure 13. Immunofluorescence images of OVCAR4 cells in the IR+4h part of the third experiment: left side – all nuclei in a part of a field as identified with Hoechst; right side – γH2AX-positive nuclei in the same part of the field. A: 48h+IR+4h plate, 0 mM metformin. B: 48h+IR+4h plate, 20 mM metformin. All nuclei on the right-side panels can be considered as γH2AX-positive.

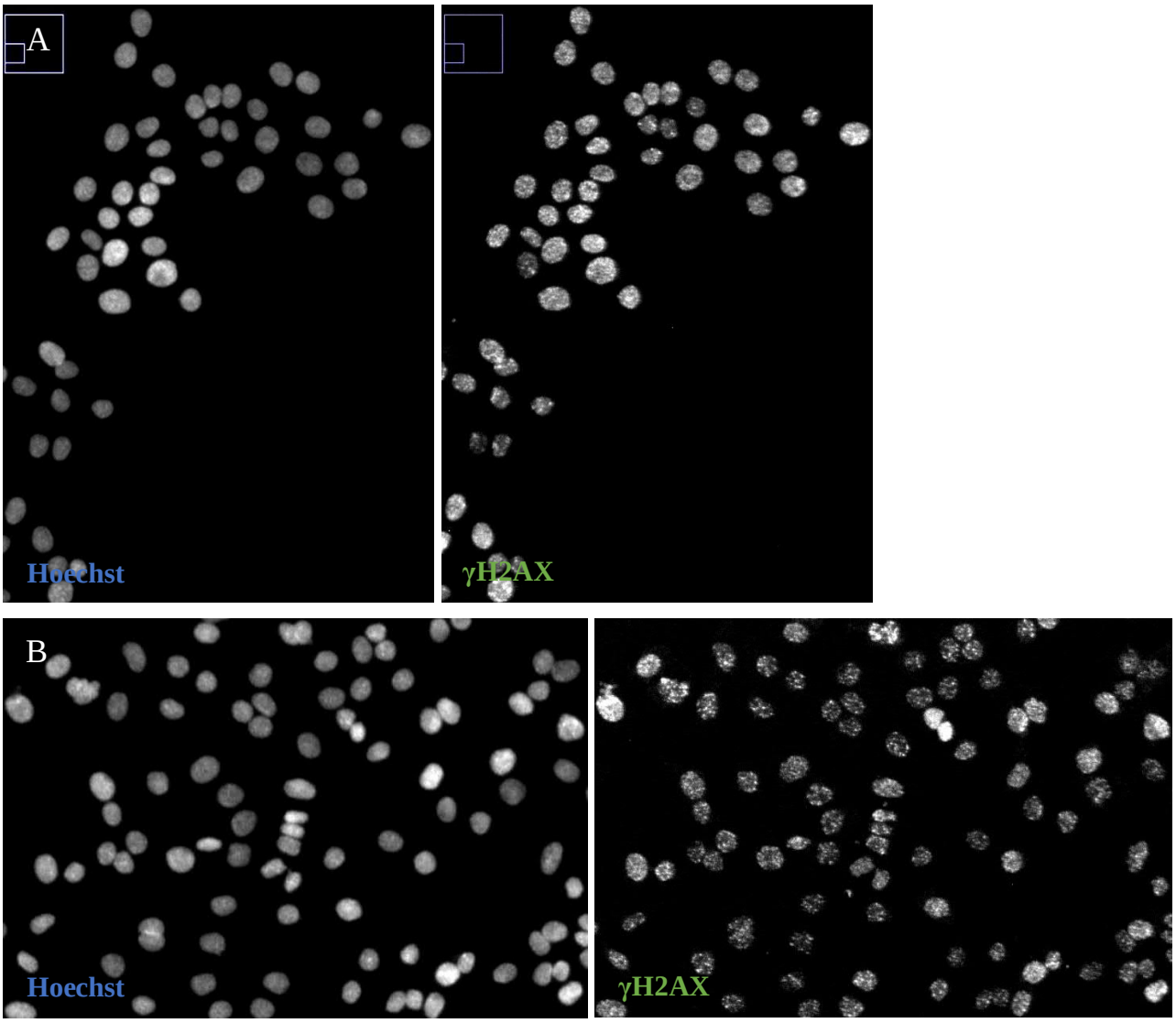

Figure 14. γH2AX results combined from γH2AX+Ki67 and γH2AX+cCasp3 staining combinations used for Kuramochi (A) and OVCAR4 (B) cells in the IR+4h part of the third experiment. Legends indicate metformin treatment durations. Horizontal gray brackets mark statistically significant changes in DNA damage ($p < 0,05$).

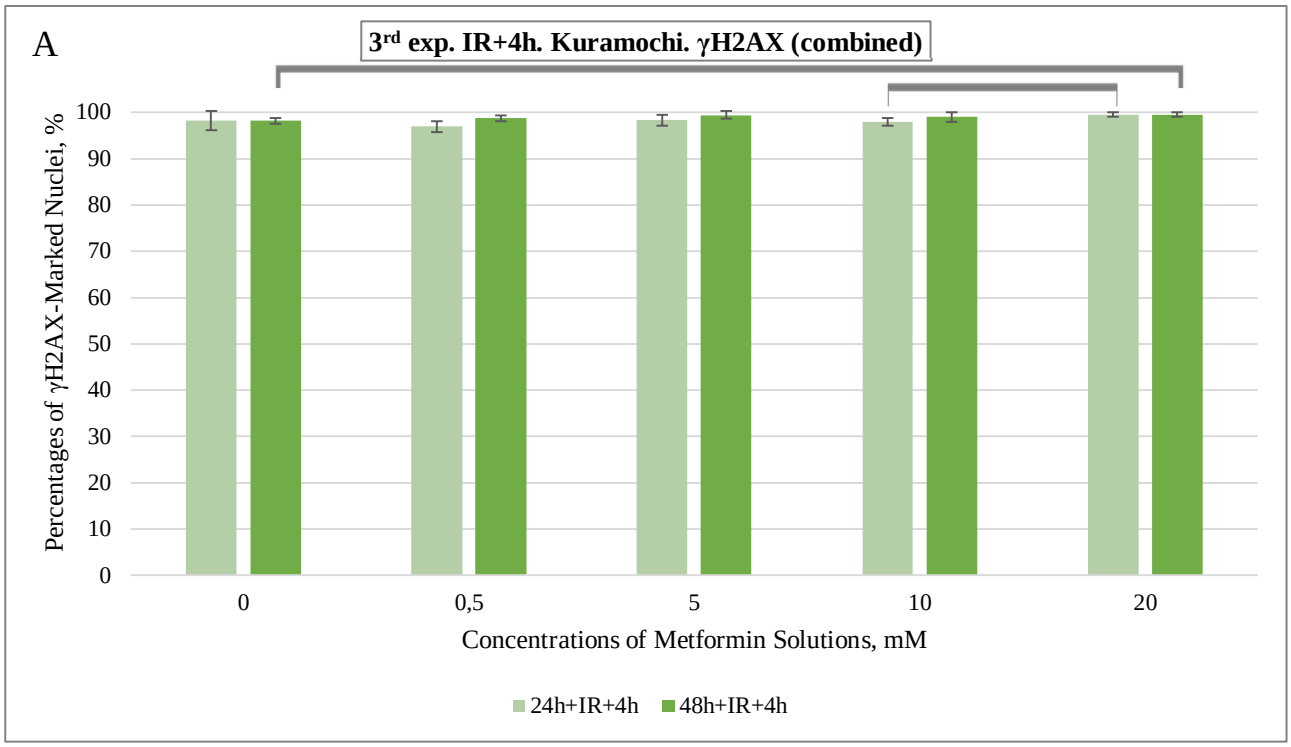

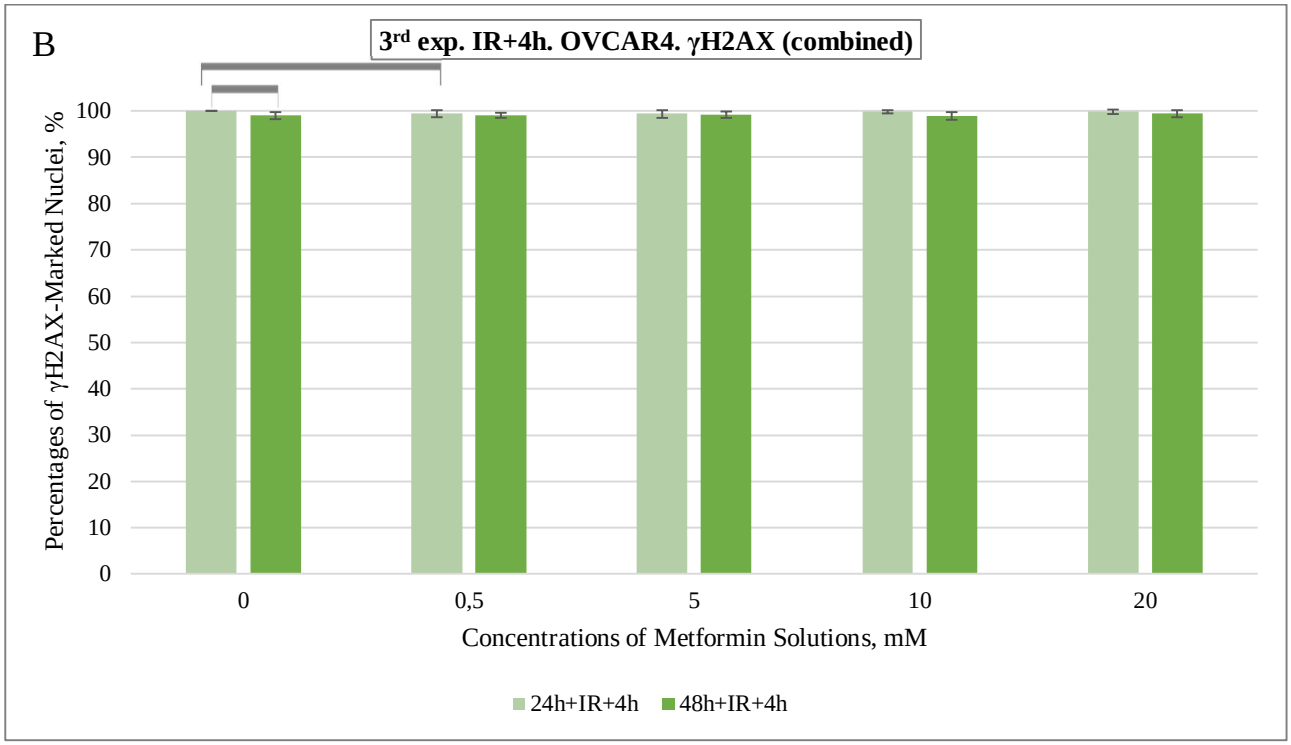

When 24 hours had passed after irradiation (figure 17), Kuramochi cells still had high amounts of DNA damage: around 90% of nuclei were marked with γH2AX, and slightly more nuclei were affected in higher metformin concentrations, particularly 20 mM (the highest concentration used) ($p < 0{,}0001$,

Figure 15. Immunofluorescence images of Kuramochi cells in the IR+24h part of the third experiment: left side – all nuclei in a part of a field as identified with Hoechst; right side – γH2AX-positive nuclei in the same part of the field. A: 48h+IR+24h plate, 0 mM metformin. B: 48h+IR+24h plate, 20 mM metformin. Gray arrows mark γH2AX-negative nuclei.

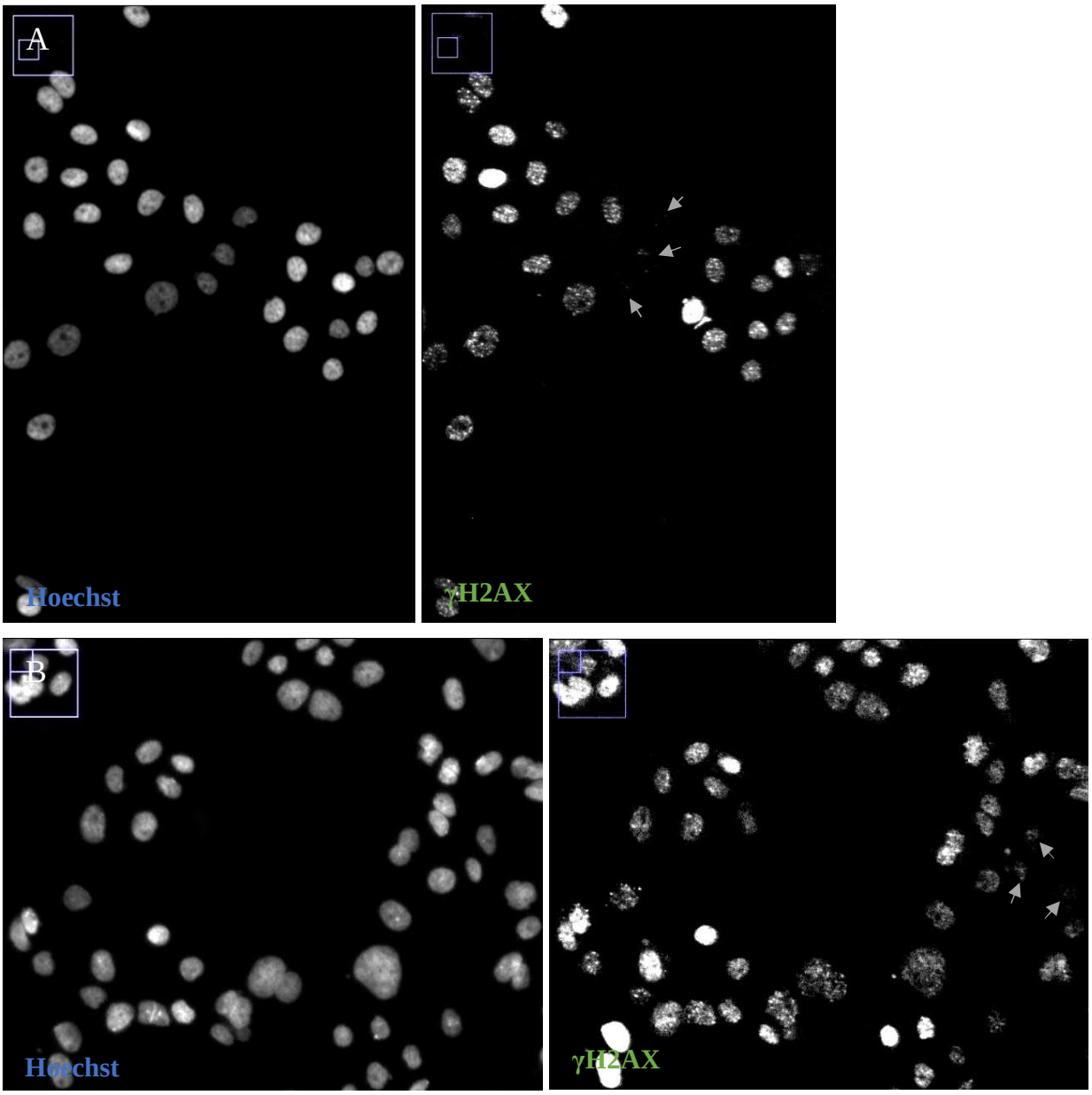

compared to controls, both 24h and 48h treatments) (figure 15). However, OVCAR4 cells in control wells and wells containing lower metformin concentrations exhibited considerably less DNA damage: around 60-70% of nuclei were marked with γH2AX in the 0-10 mM metformin concentration range. Nevertheless, the highest metformin concentration (20 mM) resulted in an elevated percentage of nuclei with persistent damage, 81 ± 4 % in the 24h treatment, and even 94 ± 5 % in the longer, 48h treatment (figure 16). These increases when compared to controls (i.e., 67 ± 4 % in the 24h treatment, and 75 ± 4 % in the 48h treatment) were statistically significant ($p < 0{,}0001$).

Figure 16. Immunofluorescence images of OVCAR4 cells in the IR+24h part of the third experiment: left side – all nuclei in a part of a field as identified with Hoechst; right side – γH2AX-positive nuclei in the same part of the field. A: 48h+IR+24h plate, 0 mM metformin. B: 48h+IR+24h plate, 20 mM metformin. Gray arrows mark γH2AX-negative nuclei; the absence of arrows indicates that all nuclei are γH2AX-positive.

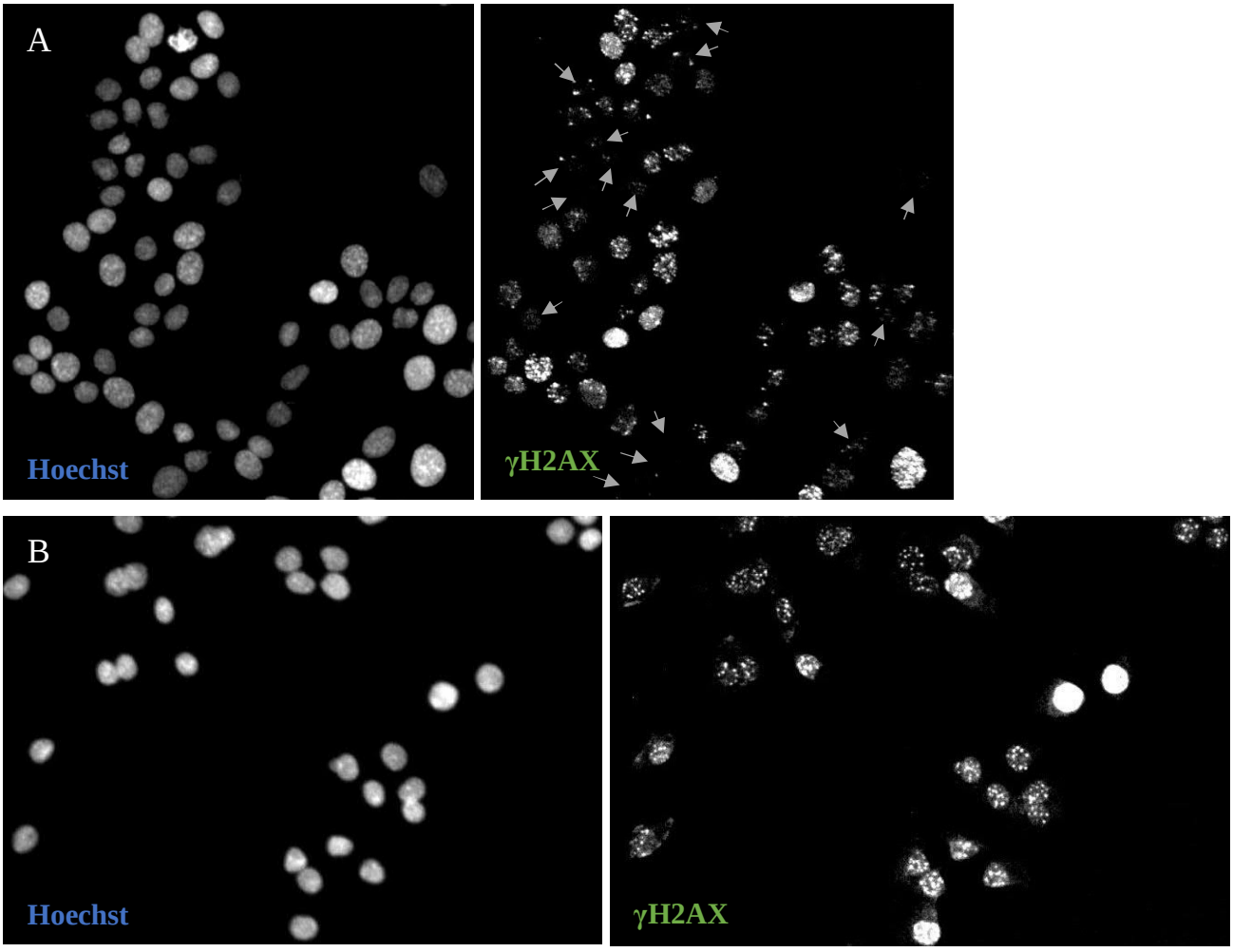

Figure 17. γH2AX results combined from γH2AX+Ki67 and γH2AX+cCasp3 staining combinations used for Kuramochi (A) and OVCAR4 (B) cells in the IR+24h part of the third experiment. Legends indicate metformin treatment durations. Gray text fields indicate statistically significant changes in DNA damage ($p < 0,05$).

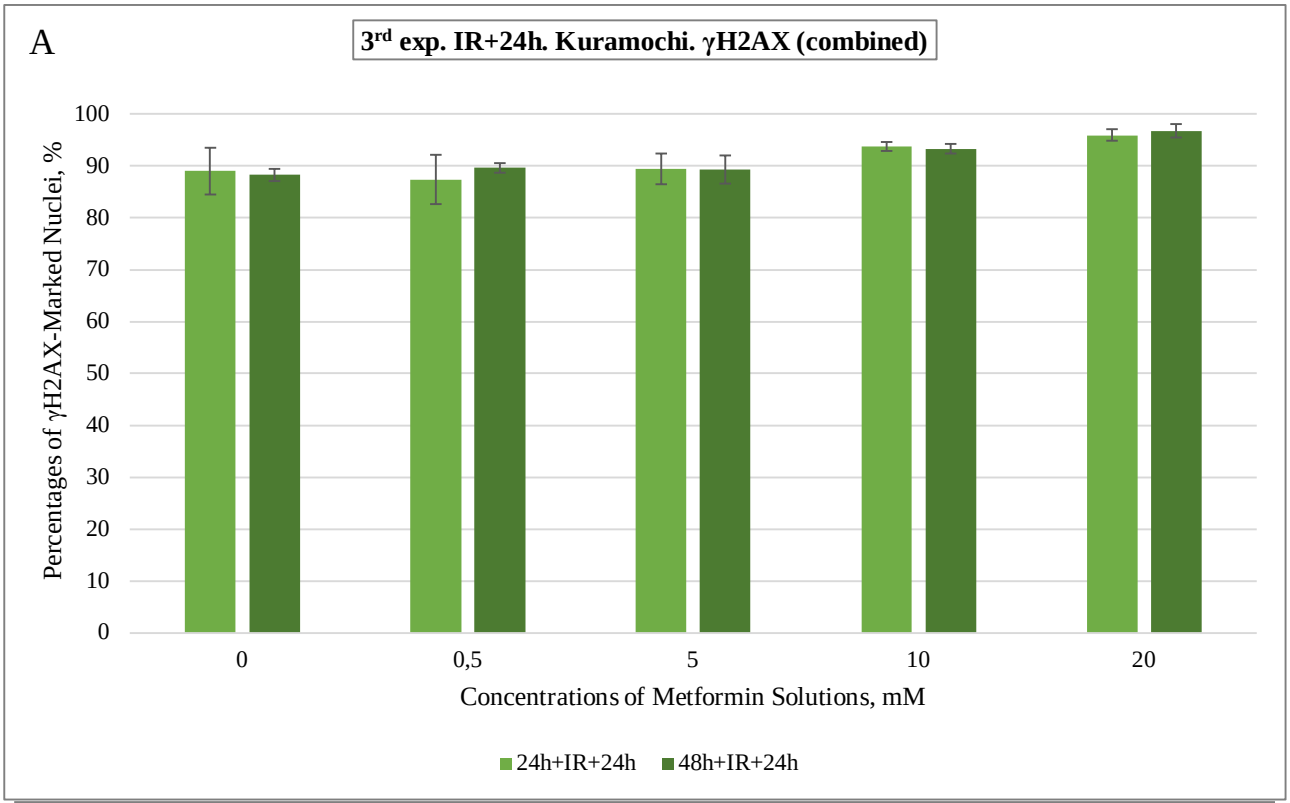

Note: Statistically significant changes ($p < 0,05$): 0 mM vs. 10 mM (both treatments), 0 mM vs. 20 mM (both treatments), 0,5 mM vs. 10 mM (only 24h+IR+24h treatment), 0,5 mM vs. 20 mM (both treatments), 5 mM vs. 10 mM (only 24h+IR+24h treatment), 5 mM vs. 20 mM (both treatments), 10 mM vs. 20 mM (only 48h+IR+24h treatment).

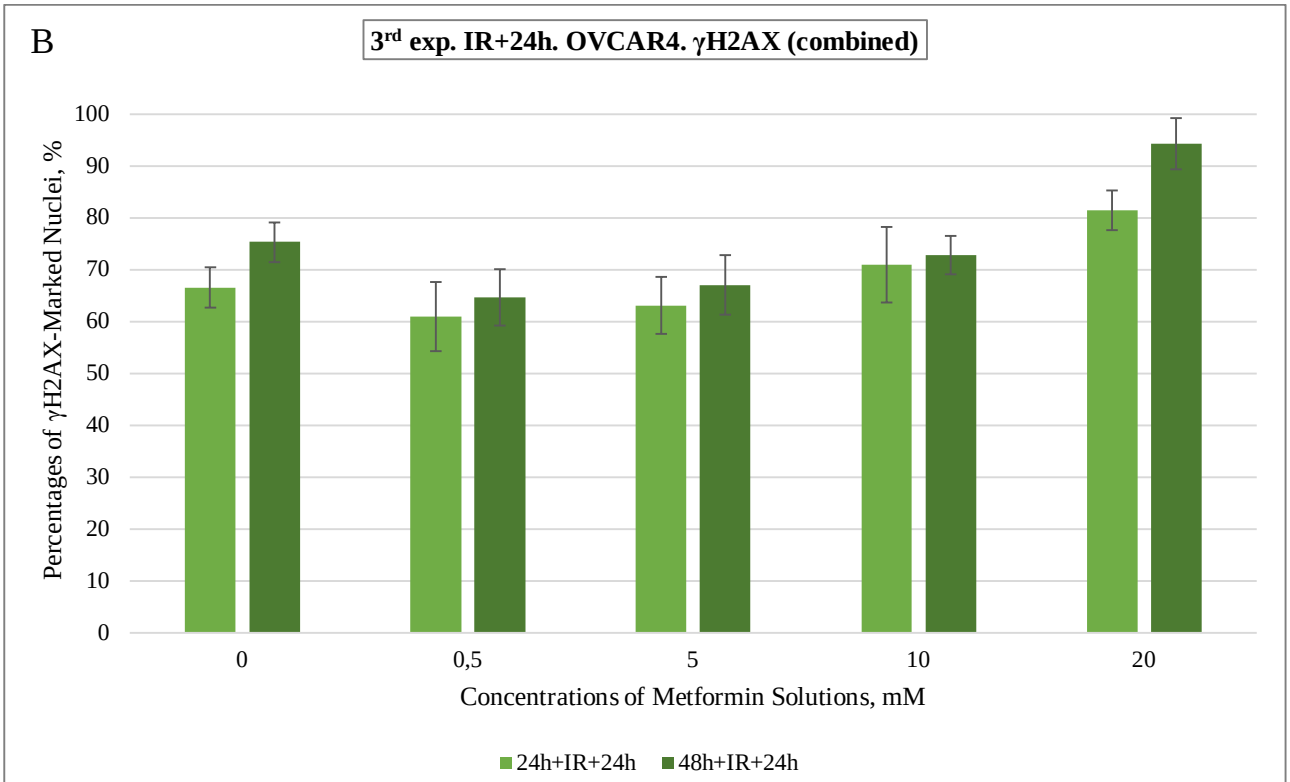

Note: Statistically significant changes ($p < 0,05$): 0 mM vs. 0,5 mM (only 48h+IR+24h treatment), 0 mM vs. 5 mM (only 48h+IR+24h treatment), 0 mM vs. 20 mM (both treatments), 0,5 mM vs. 10 mM (both treatments), 0,5 mM vs. 20 mM (both treatments), 5 mM vs. 10 mM (only 24h+IR+24h treatment), 5 mM vs. 20 mM (both treatments), 10 mM vs. 20 mM (both treatments), 24h+IR+24h vs. 48h+IR+24h at 0 mM and 20 mM.

4.2. Ki67 results

A primary antibody against Ki67 is an extensively used marker for assessing cell proliferation (Li et al., 2015). Ki67 is a nuclear protein whose elevated expression has been associated with malignant cell proliferation, making it also useful for cancer diagnosis and prognosis (Li et al., 2015).

In the first experiment (figure 19), only the highest metformin concentration, i.e., 25 mM visibly reduced proliferation of Kuramochi cells in all three treatment durations. This is in accordance with DNA damage data from this experiment, where only this highest metformin concentration was effective as well. In the 24h treatment, 45 ± 23 % of nuclei were Ki67-positive in the 25 mM metformin concentration compared to 67 ± 3 % of nuclei in controls ($p < 0,0001$), 36 ± 15 % compared to 68 ± 9 % in the 48h

treatment ($p < 0,0001$) (figure 18), and 48 ± 24 % compared to 56 ± 11 % in the 72h treatment ($p = 0,0448$).

Figure 18. Immunofluorescence images of Kuramochi cells in the first experiment: left – all nuclei in a part of a field as identified with Hoechst; right – Ki67-positive nuclei in the same part of the field. A: 48h plate, 0 mM metformin. B: 48h plate, 25 mM metformin. Red arrows mark Ki67-positive nuclei.

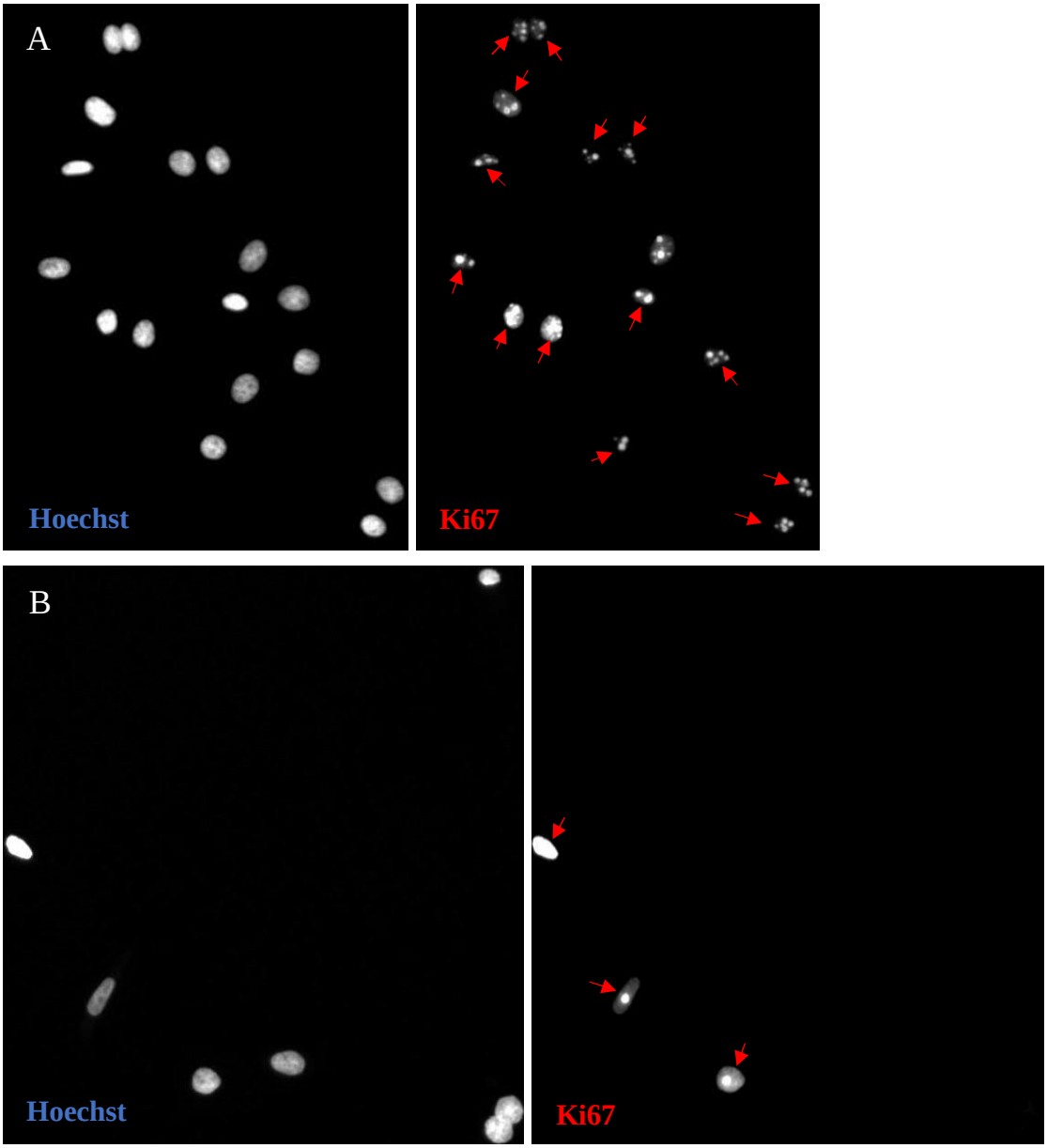

Figure 19. Ki67 results from Kuramochi cells used in the first experiment. 24 h refers to 24h metformin treatment, 48 h refers to 48h metformin treatment, 72 h refers to 72h metformin treatment. Horizontal gray brackets mark statistically significant changes in proliferation ($p < 0,05$).

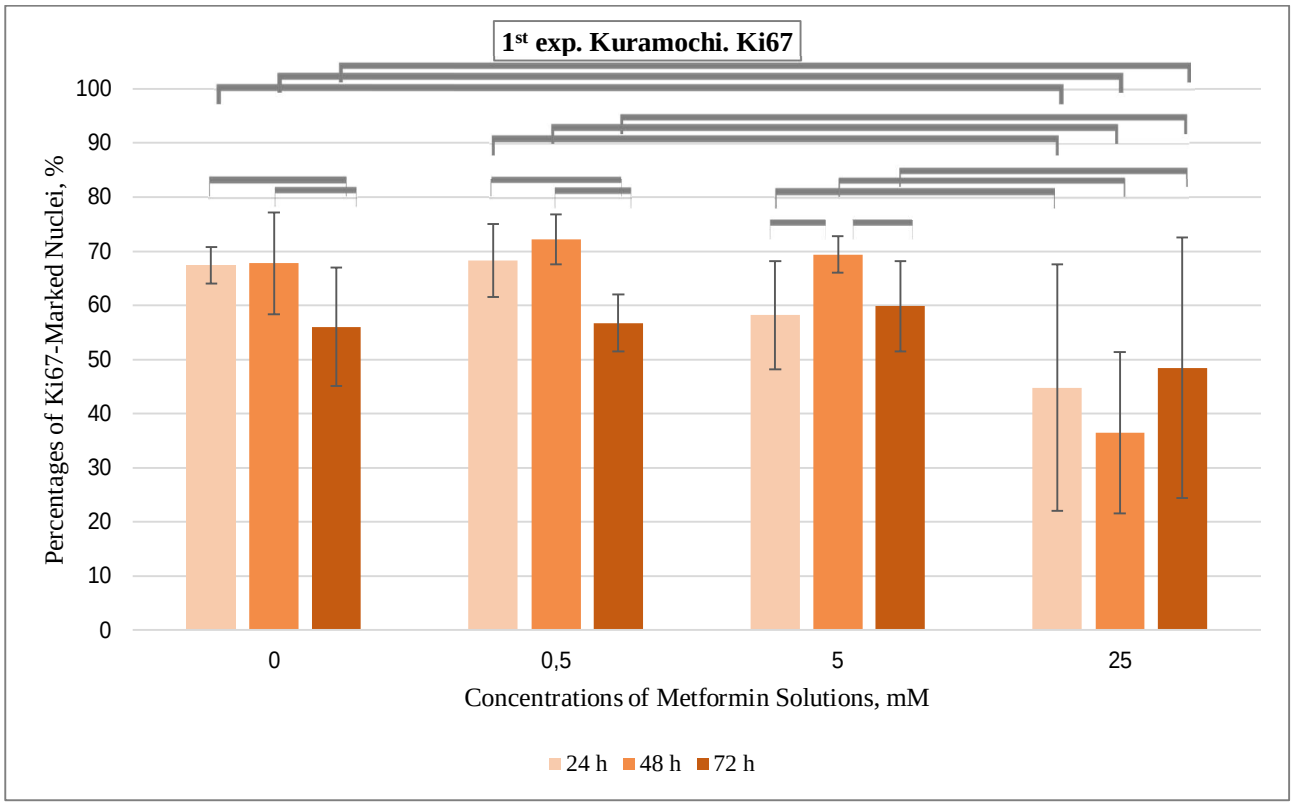

In the second experiment (figure 22), proliferation did not change much with the varying metformin concentrations and treatment durations, but OVCAR4 cells proliferated significantly less than Kuramochi cells. Nevertheless, there was a slight reduction in Kuramochi proliferation in the presence of metformin, compared to controls with no metformin in both treatment durations. In the 24h treatment, all used metformin concentrations produced similar results which were only marginally, but statistically significantly ($p \leq 0,0004$) different from controls. The highest metformin concentration (i.e., 20 mM) resulted in 78 ± 4 % of nuclei being marked for proliferation as compared to 84 % (no CI obtained due to one of the duplicate wells being unsuitable for analysis) of nuclei that were not treated with metformin ($p < 0,0001$). The 48h treatment displayed more a trend of gradually reduced Kuramochi proliferation with increasing metformin concentration, starting with 10 mM ($p < 0,0001$ for 0 mM vs. 5 mM / 10 mM, 10 mM vs. 15 mM, and 15 mM vs. 20 mM). The highest, i.e., 20 mM concentration considerably reduced Kuramochi proliferation from 85 ± 1 % (in controls) to 69 ± 4 % ($p < 0,0001$) (figure 20). OVCAR4

cells, again, were more resistant to metformin, and only the highest metformin concentration (i.e., 20 mM) and the longest treatment duration (i.e., 48h) slightly decreased proliferation from 50 % (no CI obtained due to one of the duplicate wells being unsuitable for analysis) (in controls) to 43 ± 1 % ($p < 0,0001$) (figure 21).

Figure 20. Immunofluorescence images of Kuramochi cells in the second experiment: left side – all nuclei in a part of a field as identified with Hoechst; right side – Ki67-positive nuclei in the same part of the field. A: 48h plate, 0 mM metformin. B: 48h plate, 20 mM metformin. Red arrows mark Ki67-positive nuclei.

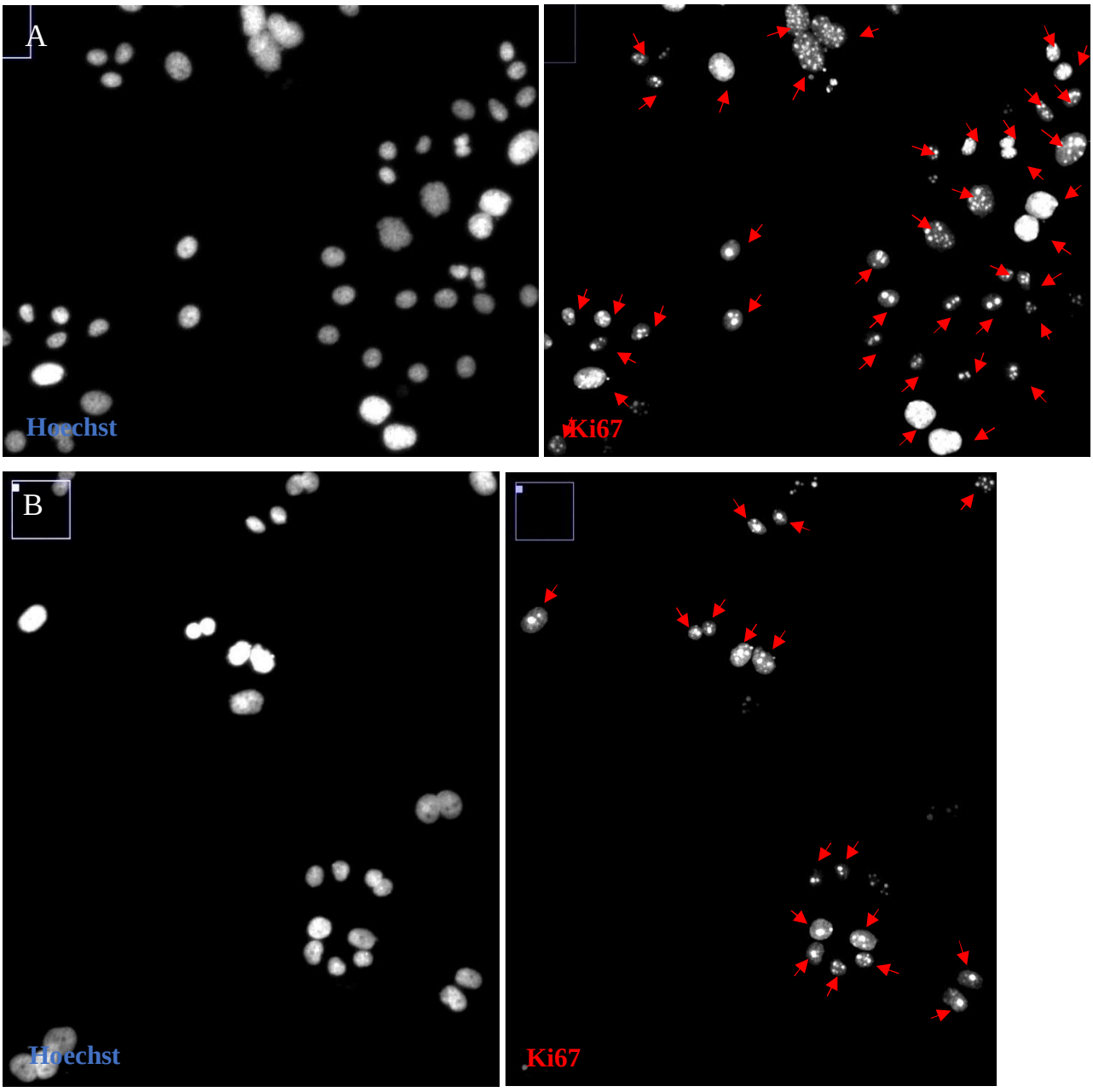

Figure 21. Immunofluorescence images of OVCAR4 cells in the second experiment: left side – all nuclei in a part of a field as identified with Hoechst; right side – Ki67-positive nuclei in the same part of the field. A: 48h plate, 0 mM metformin. B: 48h plate, 20 mM metformin. Red arrows mark Ki67-positive nuclei.

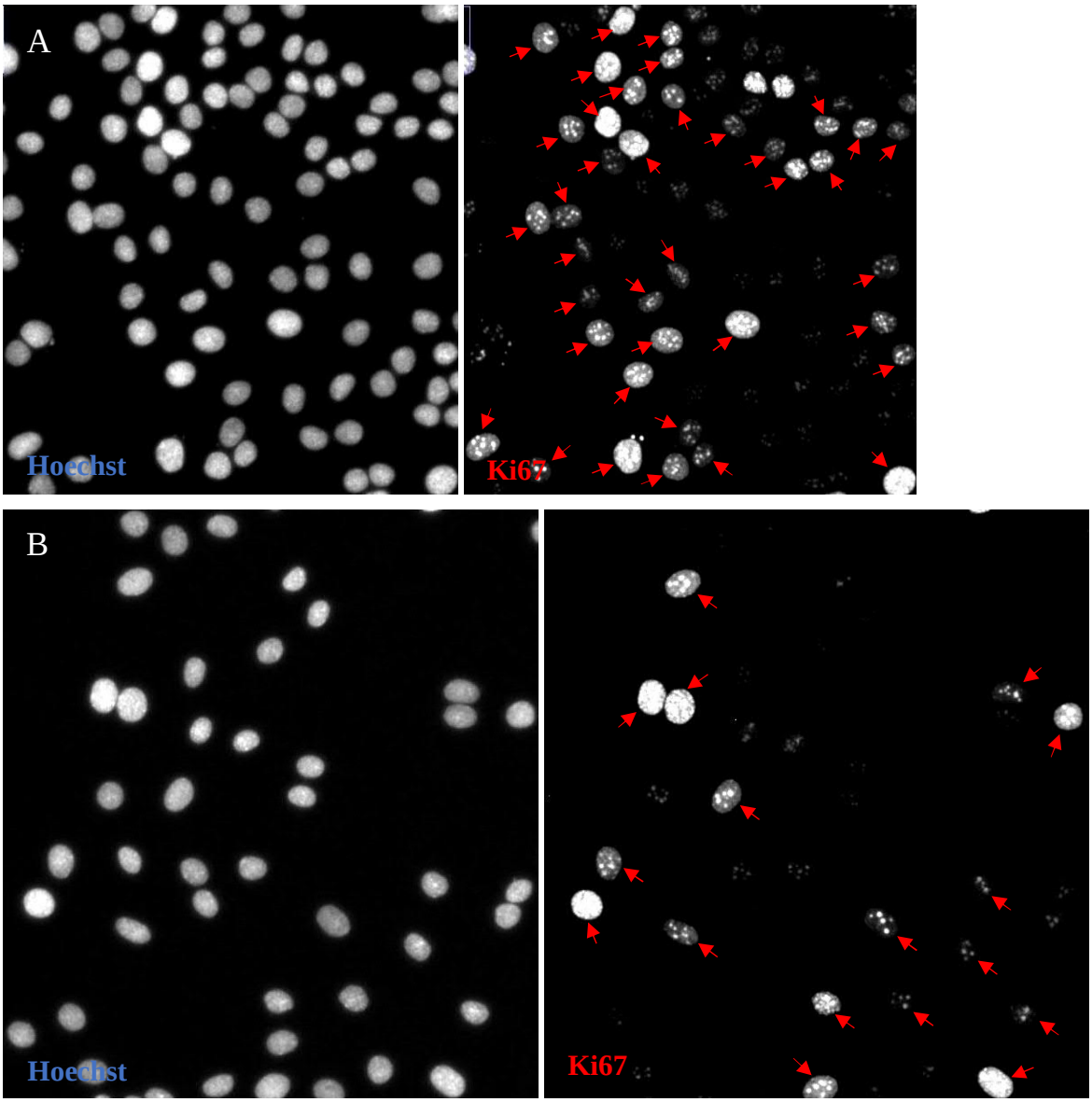

Figure 22. Ki67 results from Kuramochi (A) and OVCAR4 (B) cells used in the second experiment. 24 h refers to 24h metformin treatment, 48 h refers to 48h metformin treatment. Gray text fields indicate statistically significant changes in proliferation ($p < 0,05$).

A

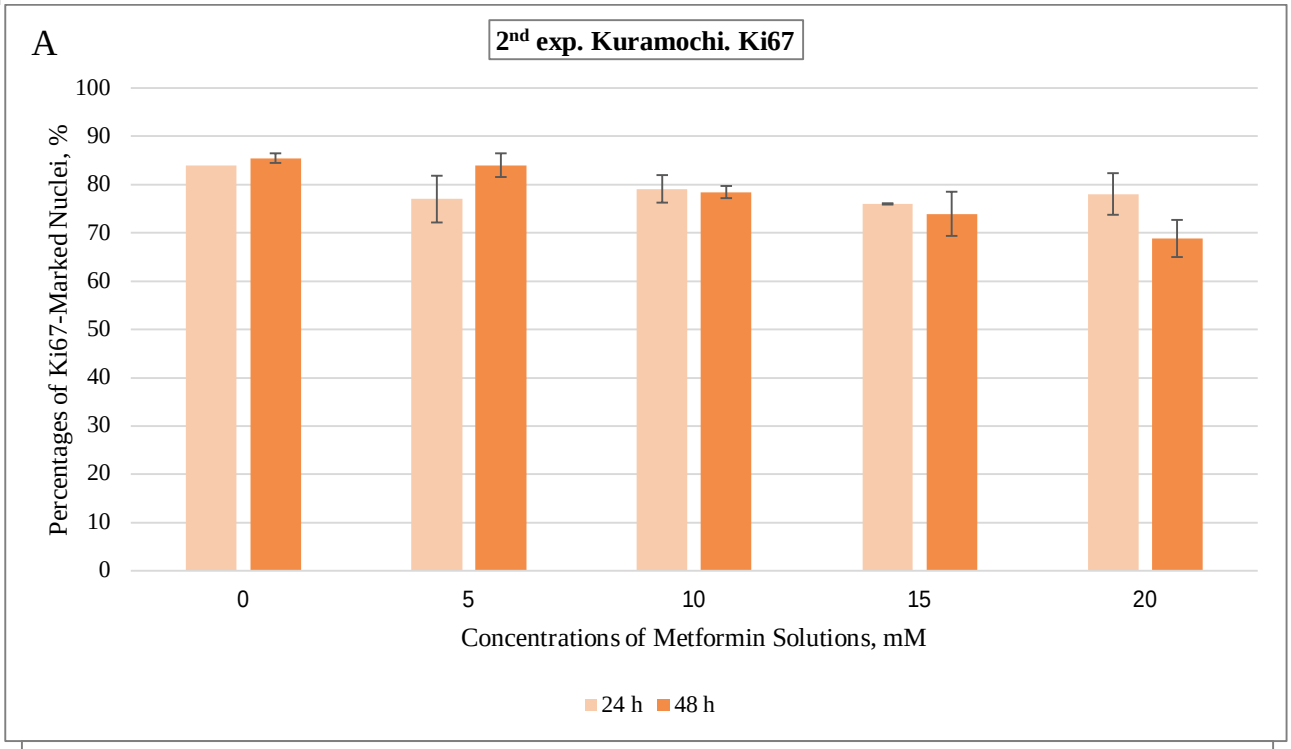

Note: All changes are statistically significant ($p < 0,05$) except for 5 mM vs. 10 mM / 15 mM / 20 mM, 10 mM vs. 15 mM / 20 mM, and 15 mM vs. 20 mM in the 24h treatment, 0 mM vs. 5 mM in the 48h treatment, as well as 24h treatment vs. 48h treatment at 0 mM and 10 mM.

B

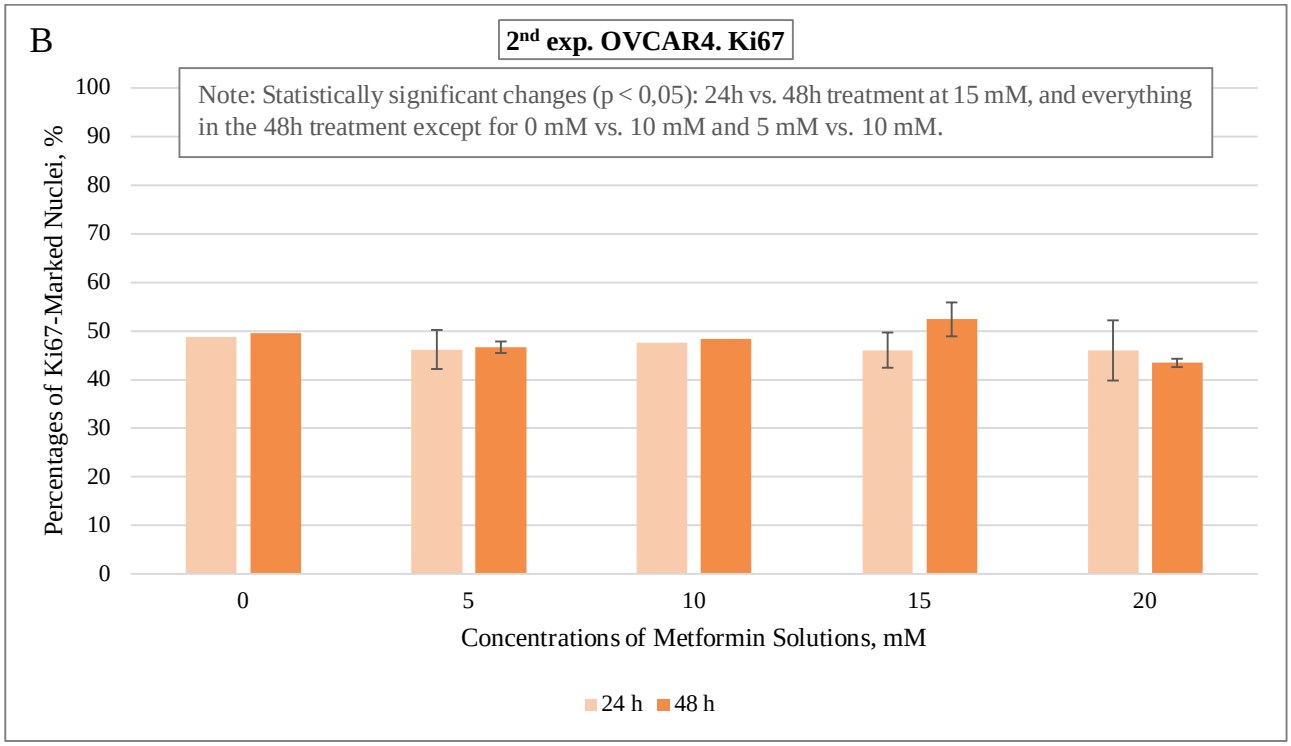

In the third experiment (figure 25), non-irradiated Kuramochi cells did not display substantial changes in the percentage of Ki67-positive nuclei numbers with the different metformin concentrations, as compared to controls except for slightly reduced proliferation using 20 mM metformin (i.e., the highest concentration) in the 48h+no IR+4h treatment (from 75 ± 11 % to 68 ± 4 %), the 24h+no IR+24h treatment (from 83 ± 4 % to 74 ± 7 %), and the 48h+no IR+24h treatment (from 64 ± 2 % to 61 ± 2 %) (figure 23) ($p < 0{,}0001$ for all). Also, Kuramochi cells in the longest treatment, i.e., 48h+no IR+24h, proliferated to a smaller extent compared to the other treatments. Non-irradiated OVCAR cells in general

Figure 23. Immunofluorescence images of Kuramochi cells in the no IR part of the third experiment: left side – all nuclei in a part of a field as identified with Hoechst; right side – Ki67-positive nuclei in the same part of the field. A: 48h+no IR+24h plate, 0 mM metformin. B: 48h+no IR+24h plate, 20 mM. Red arrows mark Ki67-positive nuclei.

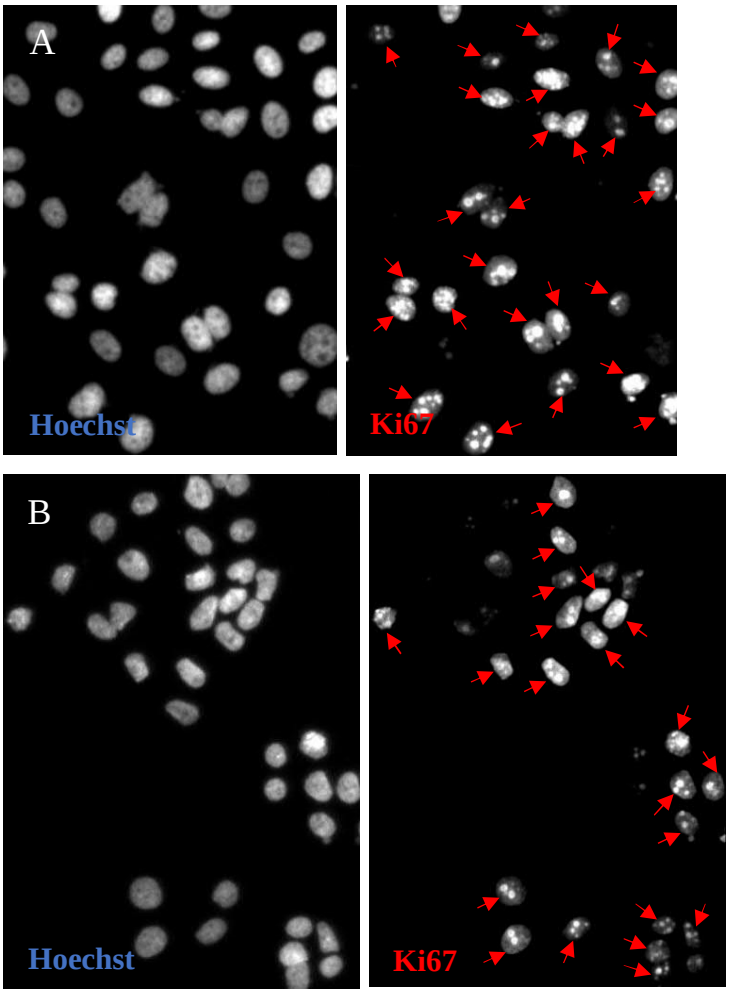

proliferated less than Kuramochi cells, which is in line with the data from the second experiment. Also, notable decreases of OVCAR4 proliferation were observed at the same conditions as in the cases of Kuramochi proliferation in this third experiment: 63 ± 1 % of nuclei were marked for proliferation at 0 mM as opposed to 43 ± 1 % of nuclei at 20 mM in the 48h+no IR+4h treatment, and respectively, 53 ± 1 % compared to 45 ± 4 % in the 24h+no IR+24h treatment, and 58 ± 3 % compared to 44 ± 5 % in the 48h+no IR+24h treatment (figure 24) ($p < 0{,}0001$ for all).

Figure 24. Immunofluorescence images of OVCAR4 cells in the no IR part of the third experiment: left side – all nuclei in a part of a field as identified with Hoechst; right side – Ki67-positive nuclei in the same part of the field. A: 48h+no IR+24h plate, 0 mM metformin. B: 48h+no IR+24h plate, 20 mM. Red arrows mark Ki67-positive nuclei.

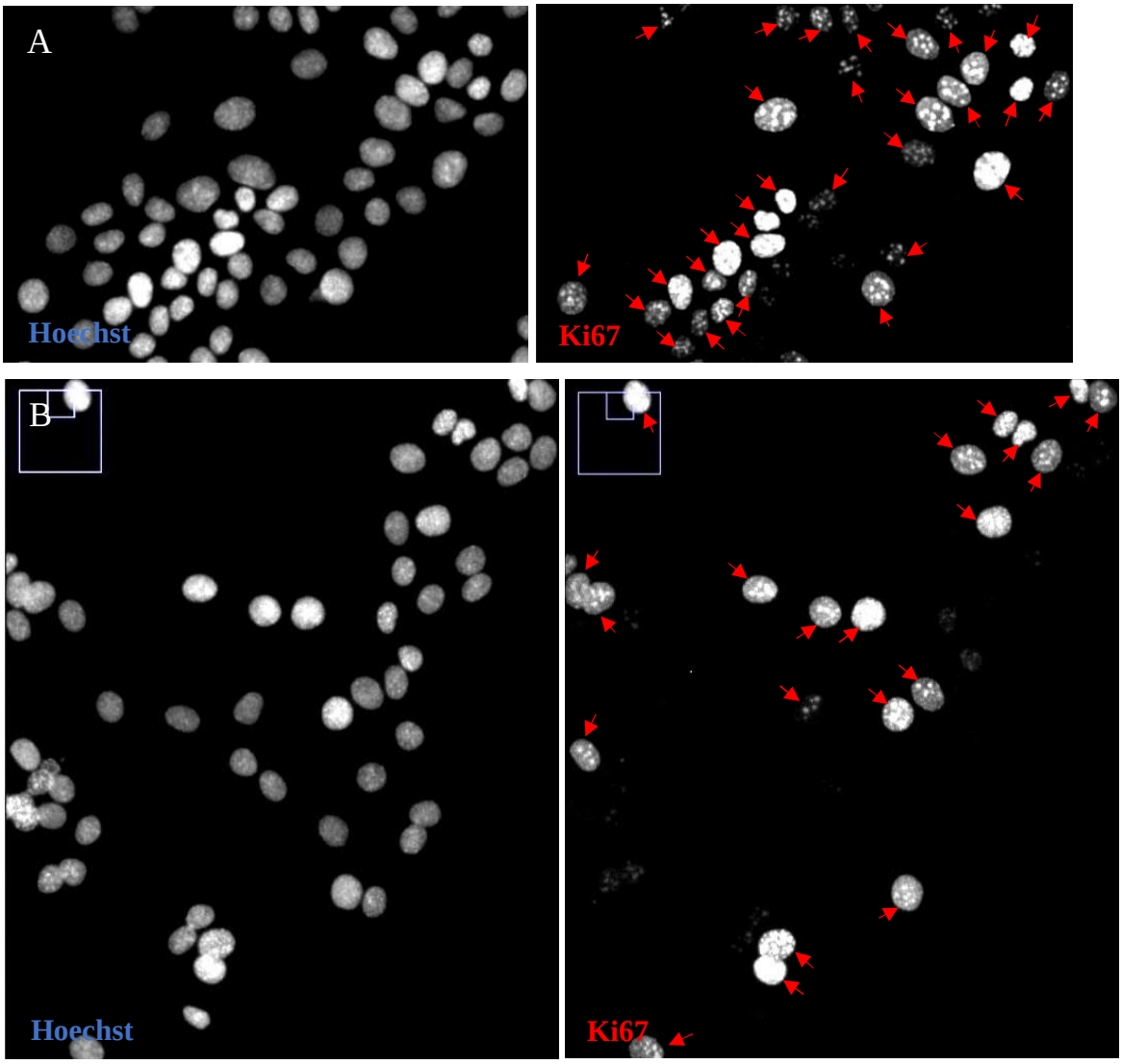

Figure 25. Ki67 results from Kuramochi cells in the no IR+4h (A) and the no IR+24h (C) parts of the third experiment, and from OVCAR4 cells in the no IR+4h (B) and the no IR+24h (D) parts of the third experiment. Legends indicate metformin treatment durations. Gray text fields indicate statistically significant changes in proliferation ($p < 0,05$).

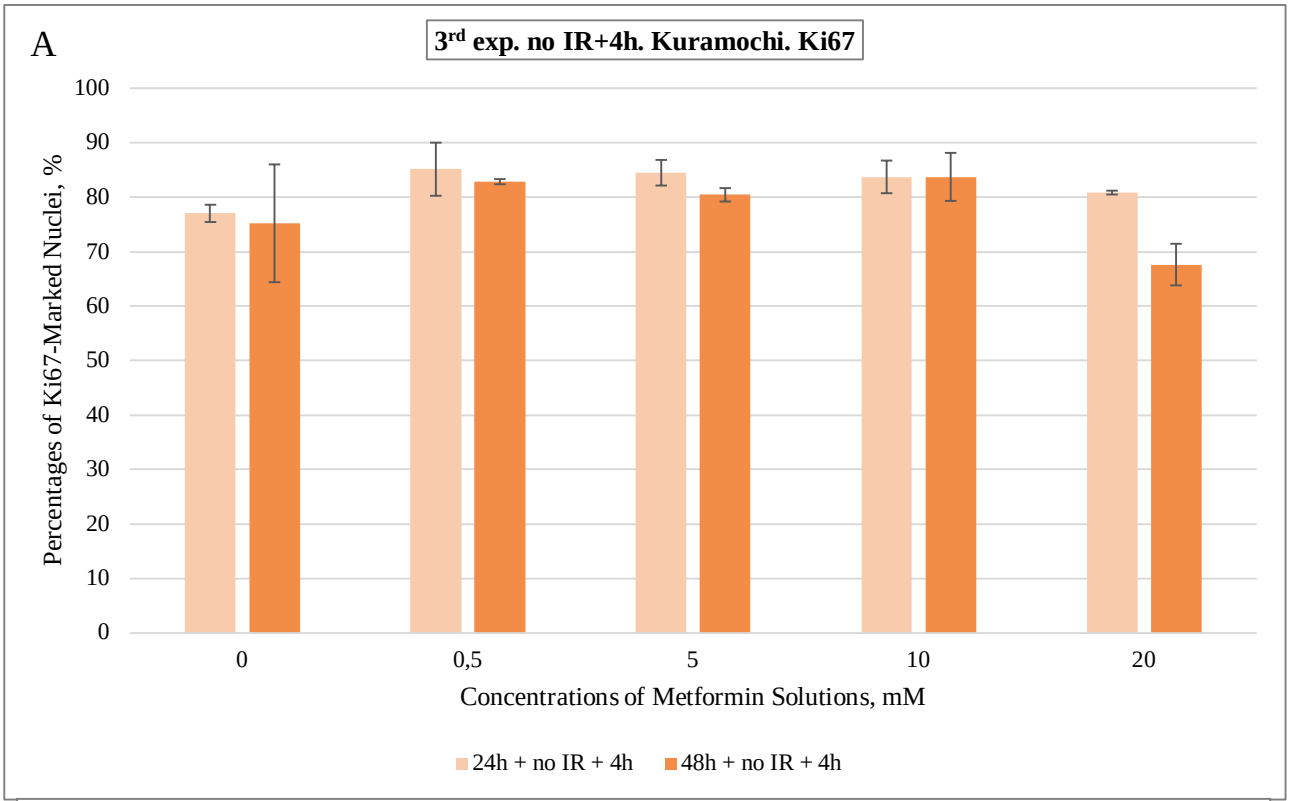

Note: All changes are statistically significant ($p < 0,05$) except for 0,5 mM vs. 5 mM and 5 mM vs. 10 mM in the 24h+no IR+4h treatment, and 24h+no IR+4h treatment vs. 48h+no IR+4h treatment at 10 mM.

B

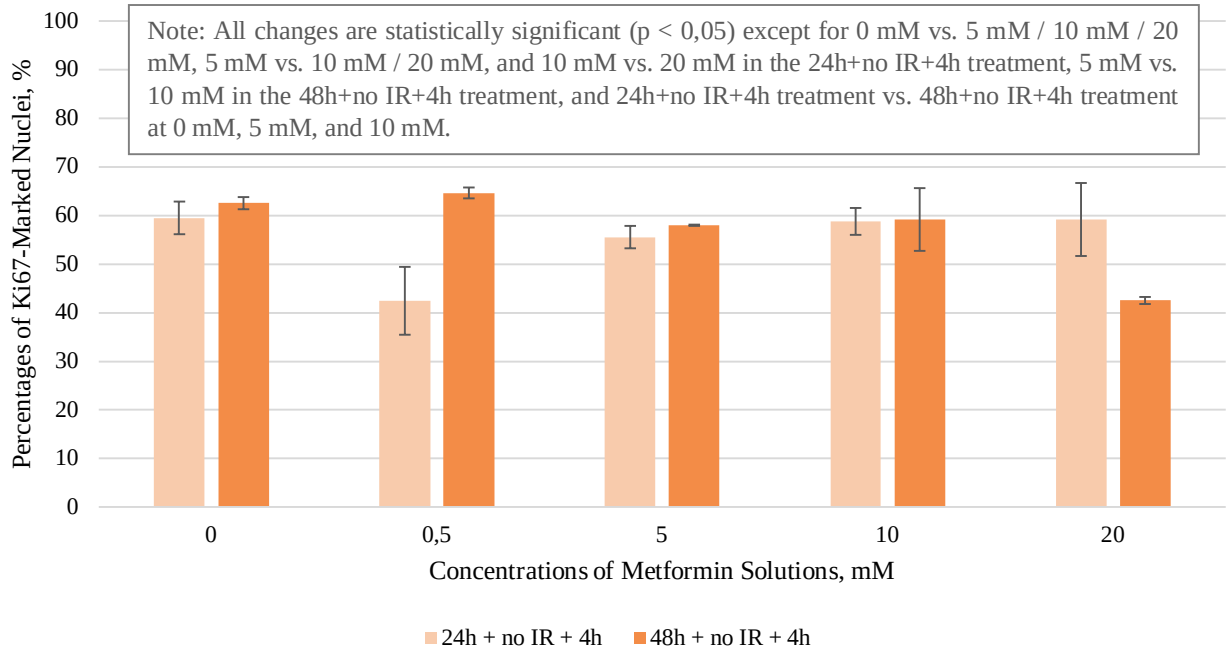

C

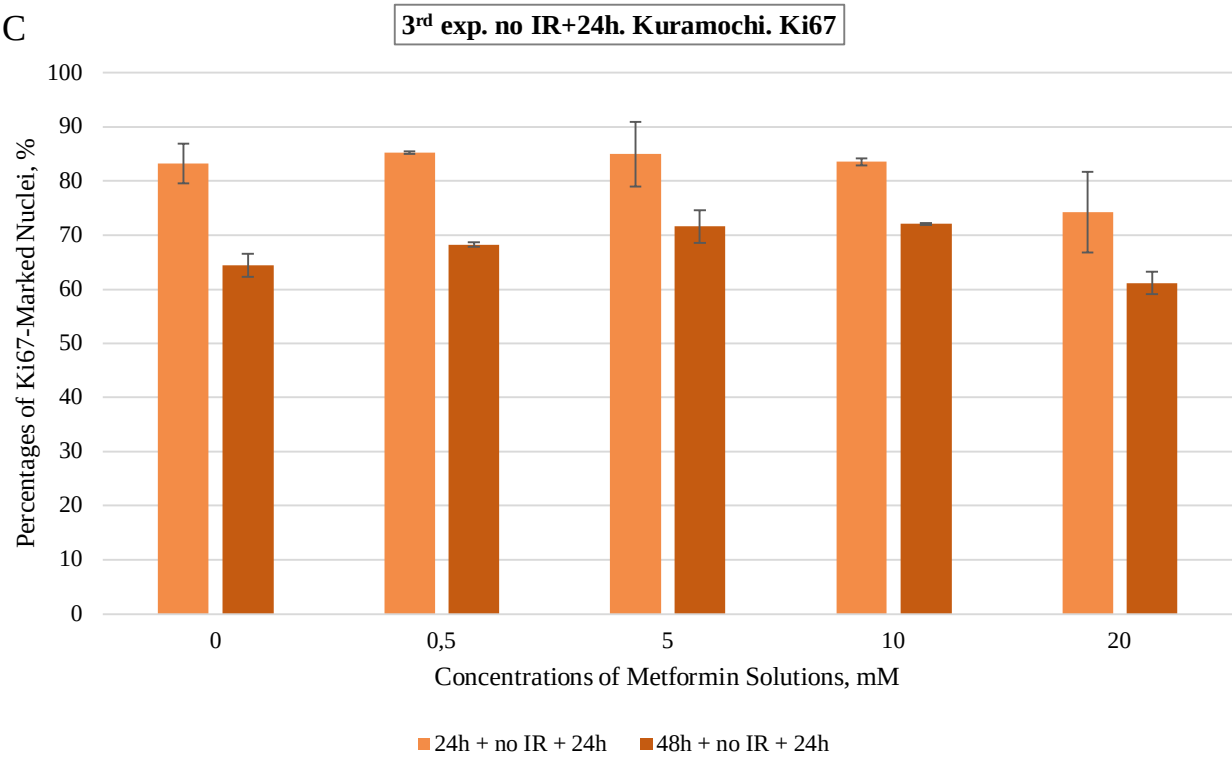

Note: All changes are statistically significant (p < 0,05) except for 0 mM vs. 10 mM and 0,5 mM vs. 5 mM in the 24h+no IR+24h treatment, and 5 mM vs. 10 mM in the 48h+no IR+24h treatment.

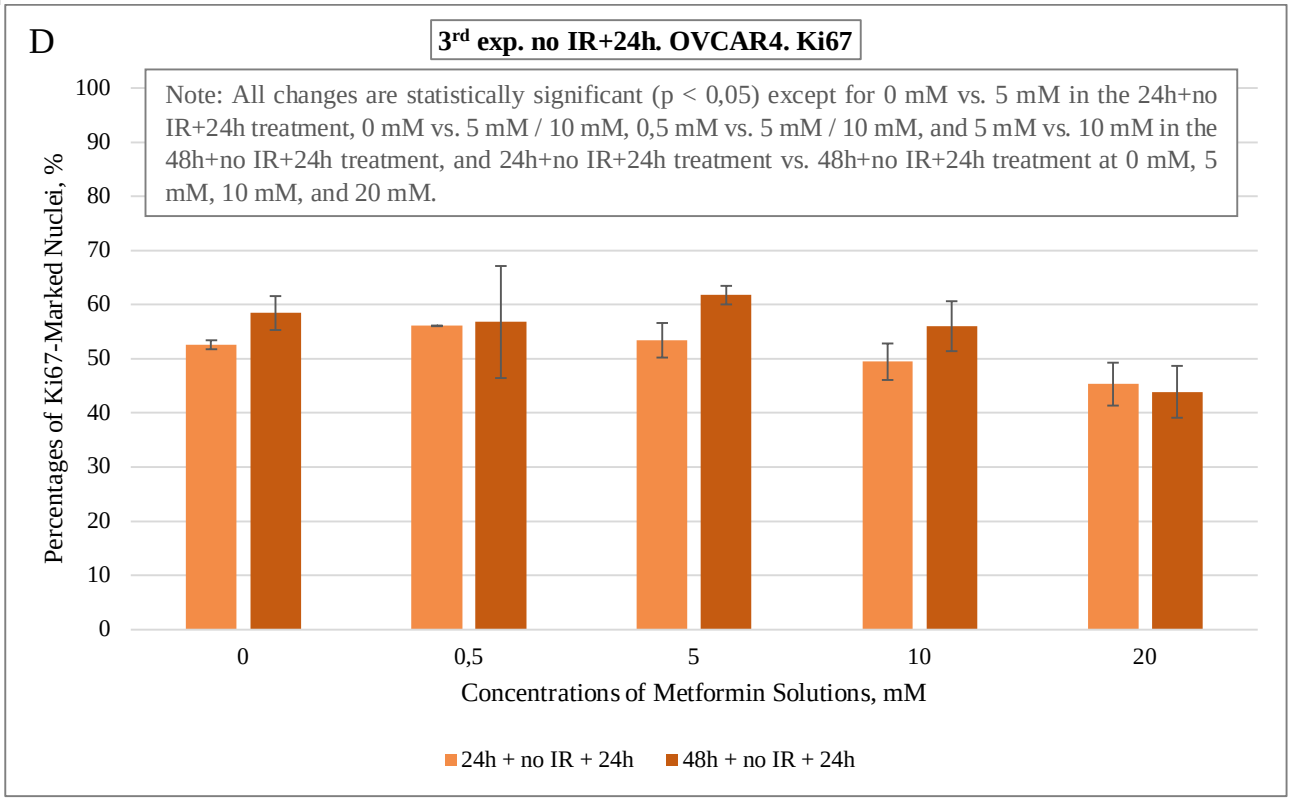

In the pooled data from all non-irradiated cells used in the three experiments (figure 26), the highest (20 mM) metformin concentration was effective in slightly reducing Kuramochi proliferation only in the 48h treatment group from 75 ± 6 % of Ki67-positive nuclei at 0 mM to 70 ± 3 % of nuclei at 20 mM ($p < 0,0001$). Kuramochi proliferation was overall less intense in the longer, 72h treatment group compared to proliferation in the shorter treatment groups, but proliferation results at 20 mM metformin were not very different from controls. Compared to Kuramochi proliferation, OVCAR4 proliferation was slightly lower across all metformin concentrations (including controls) and treatment groups. Substantial reduction in OVCAR4 proliferation was observed using 20 mM metformin in the same 48h treatment group (just like in the case of Kuramochi proliferation), but also an additional 72h treatment duration was just as efficient in reducing OVCAR4 proliferation: from 56 ± 5 % to 44 ± 1 % ($p < 0,0001$), and from 58 ± 3 % to 44 ± 5 % ($p < 0,0001$), respectively. In addition, there was aberrant decrease in OVCAR4 proliferation at 0,5 mM metformin in the 24h treatment group, from 56 ± 7 % of Ki67-positive nuclei at 0 mM to 42 ± 7 % of nuclei at 0,5 mM ($p < 0,0001$). However, this result stems from one experiment only. Therefore, it could have appeared due to chance and its reproducibility should be checked in the future.

Figure 26. Pooled Ki67 results from all non-irradiated Kuramochi (A) and OVCAR4 (B) cells. Legends indicate metformin treatment duration groups. Gray text fields indicate statistically significant changes in proliferation ($p < 0,05$).

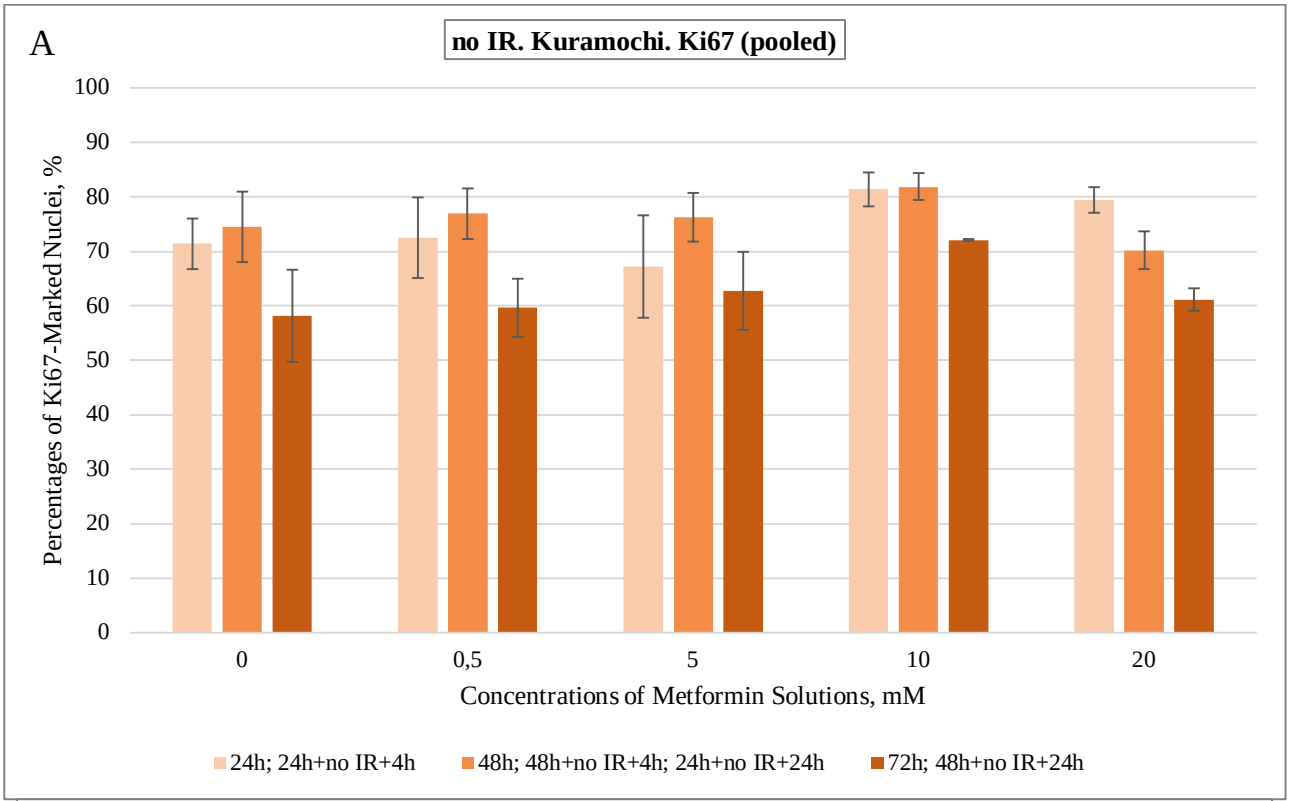

Note: All changes are statistically significant ($p < 0,05$) except for 0 mM vs. 20 mM and 5 mM vs. 20 mM in the 24h treatment group, 5 mM vs. 10 mM in the 48h treatment group, 5 mM vs. 10 mM the 72h treatment group, and 24h treatment group vs. 48h treatment group at 10 mM.

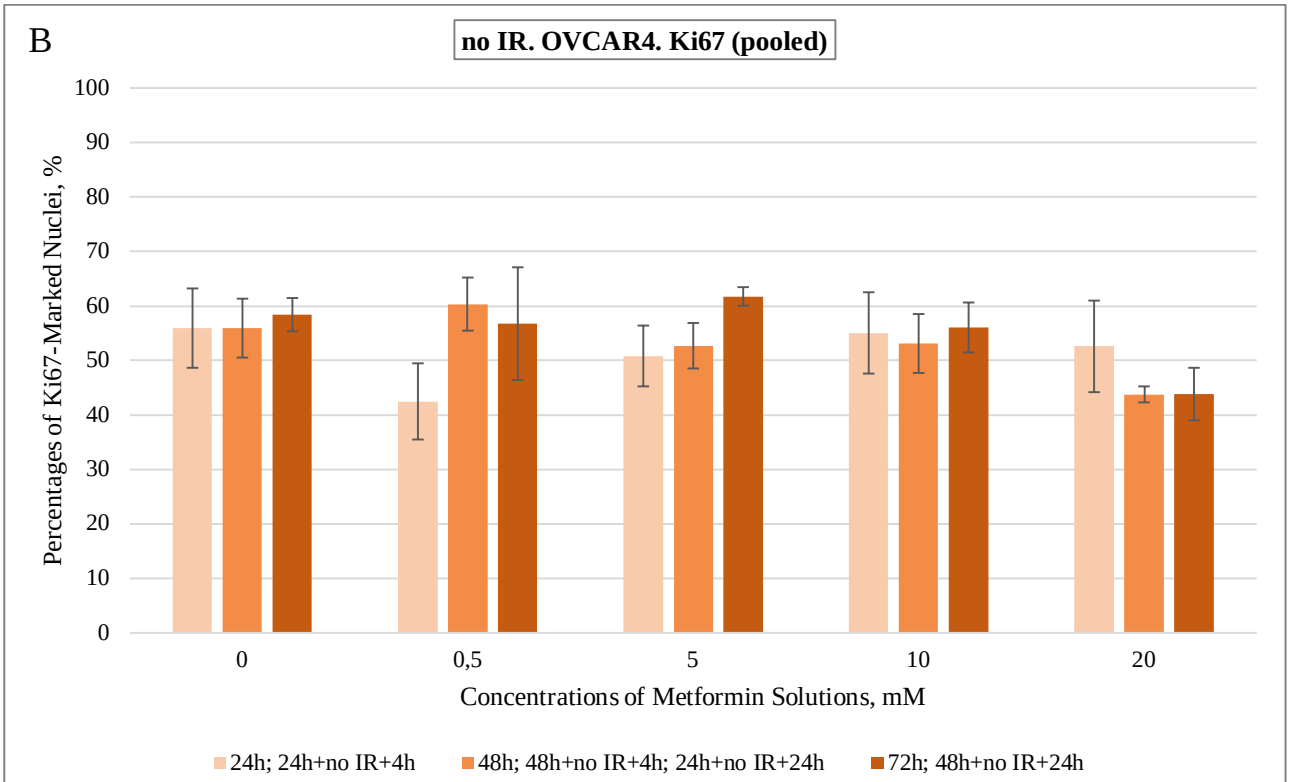

Note: All changes are statistically significant ($p < 0,05$) except for 0 mM vs. 10 mM / 20 mM in the 24h treatment group, 0 mM vs. 5 mM in the 48h treatment group, 0 mM vs. 5 mM / 10 mM in the 72h treatment group, 0,5 mM vs. 5 mM / 10 mM in the 72h treatment group, 5 mM vs. 10 mM in the 72h treatment group, and also, 24h treatment group vs. 48h treatment group at 5 mM, 24h treatment group vs. 72h treatment group at 0 mM and 10 mM, and 48h treatment group vs. 72h treatment group at 0 mM, 5 mM, 10 mM, and 20 mM.

Considering data from the post-metformin irradiation experiments, 4h after irradiation time point (figure 29) generally gave proliferation results similar to those seen in the non-irradiated cells. At first sight, this result is a bit unexpected, since IR-induced unrepaired damage should theoretically halt proliferation. This matter is reviewed in more detail in Discussion. The highest metformin concentration, i.e., 20 mM was the only one able to visibly reduce Kuramochi proliferation in both 24h+IR+4h and 48h+IR+4h treatments, decreasing the proportions of Ki67-positive nuclei from 80 ± 1 % at 0 mM to 67 ± 6 % at 20 mM ($p < 0,0001$) (figure 27), and from 75 ± 8 % at 0 mM to 71 ± 0,4 % at 20 mM ($p < 0,0001$), respectively. In addition, 10 mM metformin concentration reduced Kuramochi proliferation in the 24h+IR+4h treatment with enough statistical significance ($p < 0,0001$), but the decrease was modest: from 80 ± 1 % at 0 mM to 76 ± 7 % at 10 mM. In comparison, OVCAR4 cells experienced a reduction in proliferation only in the longer treatment, the 48h+IR+4h time point, going from 63 ± 1 % of nuclei marked for proliferation at 0 mM to 43 ± 6 % of nuclei at 20 mM ($p < 0,0001$) (figure 28). However, in

addition to 20 mM metformin concentration, 10 mM was also efficient in this treatment duration for OVCAR4 cells, as well as 5 mM although to a much smaller extent, decreasing the proliferating nuclei portion to 48 ± 0,1 % ($p < 0,0001$), and 59 ± 9 % ($p < 0,0028$), respectively. Finally, there was an irregularity in OVCAR4 proliferation results at 0,5 mM in the 24h+IR+4h treatment, where the portion of Ki67-marked nuclei drastically diminished from 46 ± 1 % to 32 ± 1 % ($p < 0,0001$), but increased

Figure 27. Immunofluorescence images of Kuramochi cells in the IR+4h part of the third experiment: left side – all nuclei in a part of a field as identified with Hoechst; right side – Ki67-positive nuclei in the same part of the field. A: 24h+IR+4h plate, 0 mM metformin. B: 24h+IR+4h plate, 20 mM metformin. Red arrows mark Ki67-positive nuclei.

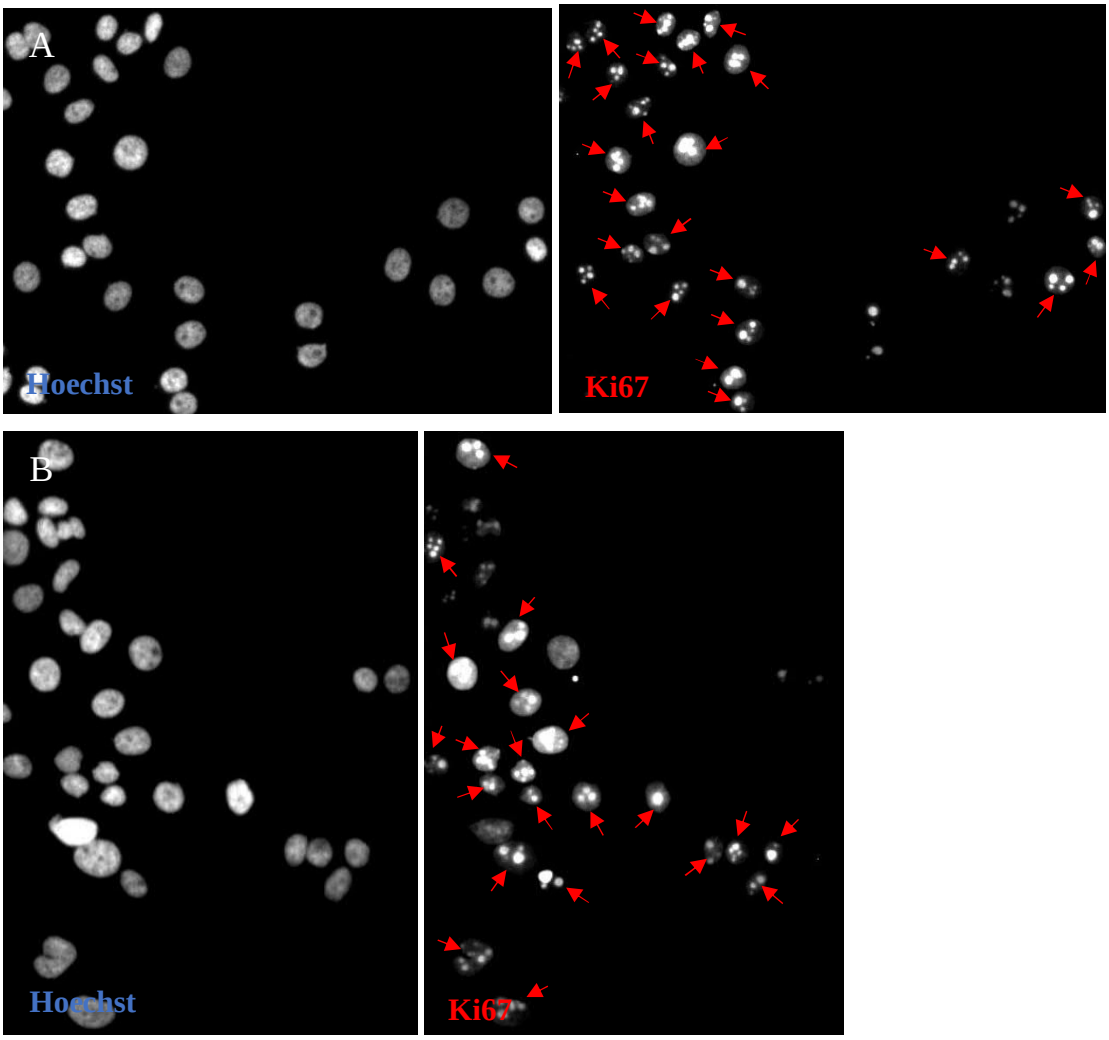

again at higher metformin concentrations. Since this effect was not visible in the 48h+IR+4h treatment, it could be a sporadic event, and performing more experiments like this could be beneficial in order to determine whether such a result is reproducible.

Figure 28. Immunofluorescence images of OVCAR4 cells in the IR+4h part of the third experiment: left side – all nuclei in a part of a field as identified with Hoechst; right side – Ki67-positive nuclei in the same part of the field. A: 48h+IR+4h plate, 0 mM metformin. B: 48h+IR+4h plate, 20 mM metformin. Red arrows mark Ki67-positive nuclei.

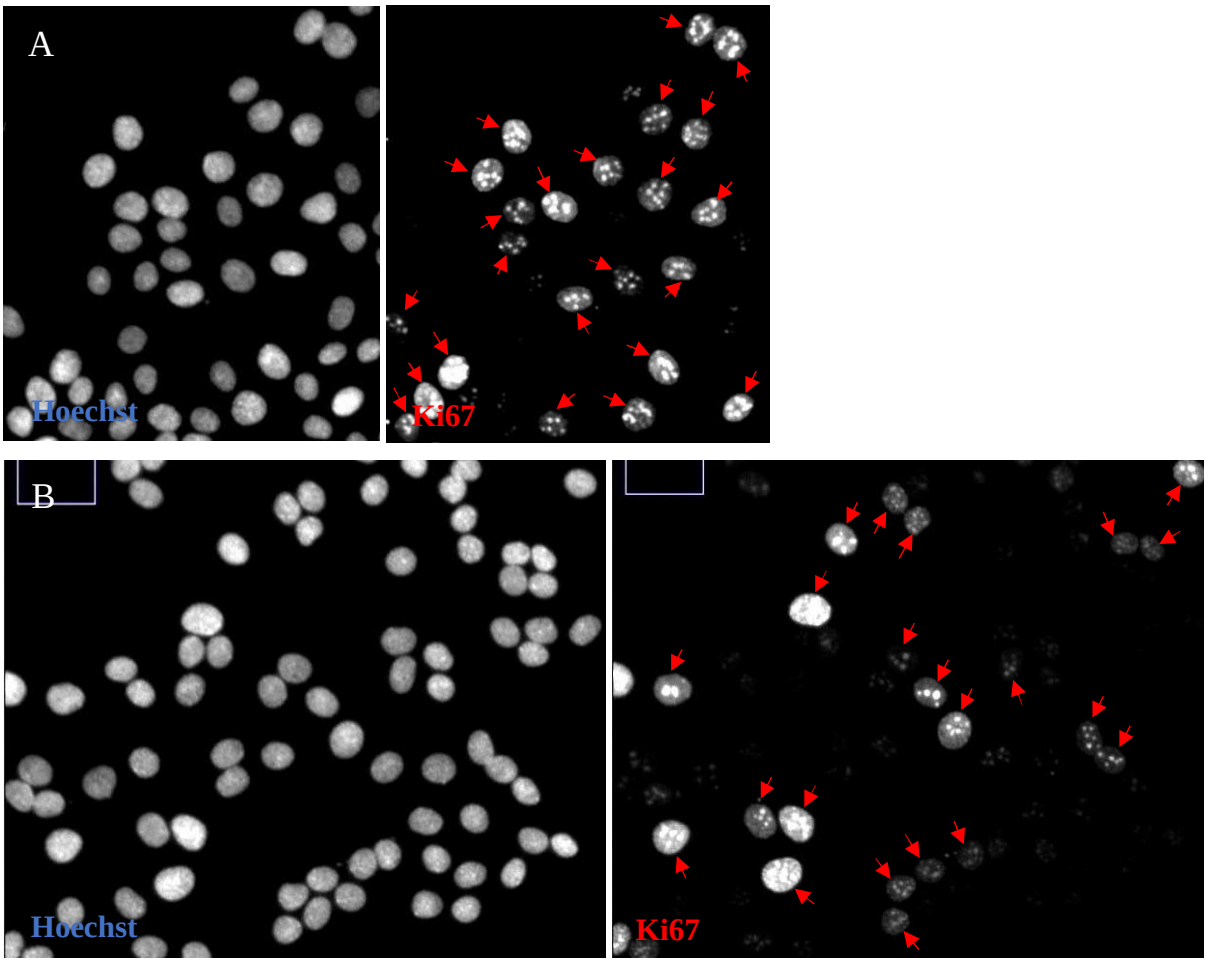

Figure 29. Ki67 results from Kuramochi (A) and OVCAR4 (B) cells in the IR+4h part of the third experiment. Legends indicate metformin treatment durations. Gray text fields indicate statistically significant changes in proliferation ($p < 0,05$).

A

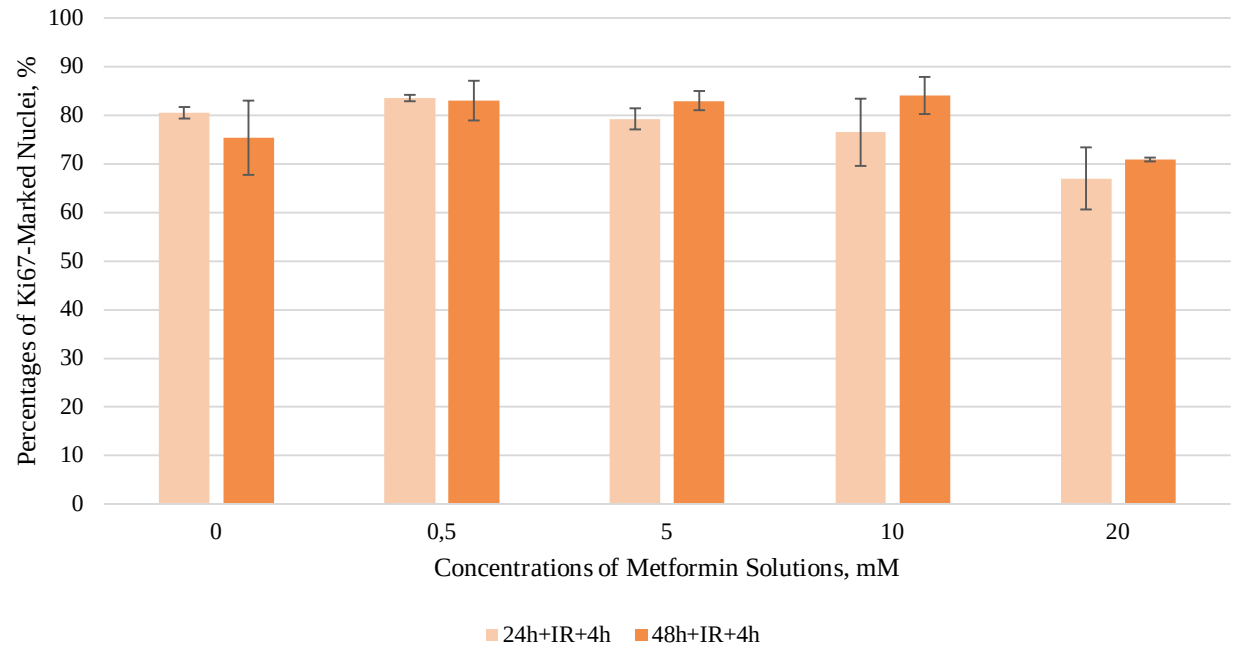

Note: All changes are statistically significant ($p < 0,05$) except for 0 mM vs. 5 mM in the 24h+IR+4h treatment, 0,5 mM vs. 5 mM and 5 mM vs. 10 mM in the 48h+IR+4h treatment, and 24h+IR+4h treatment vs. 48h+IR+4h treatment at 0 mM and 0,5 mM.

B

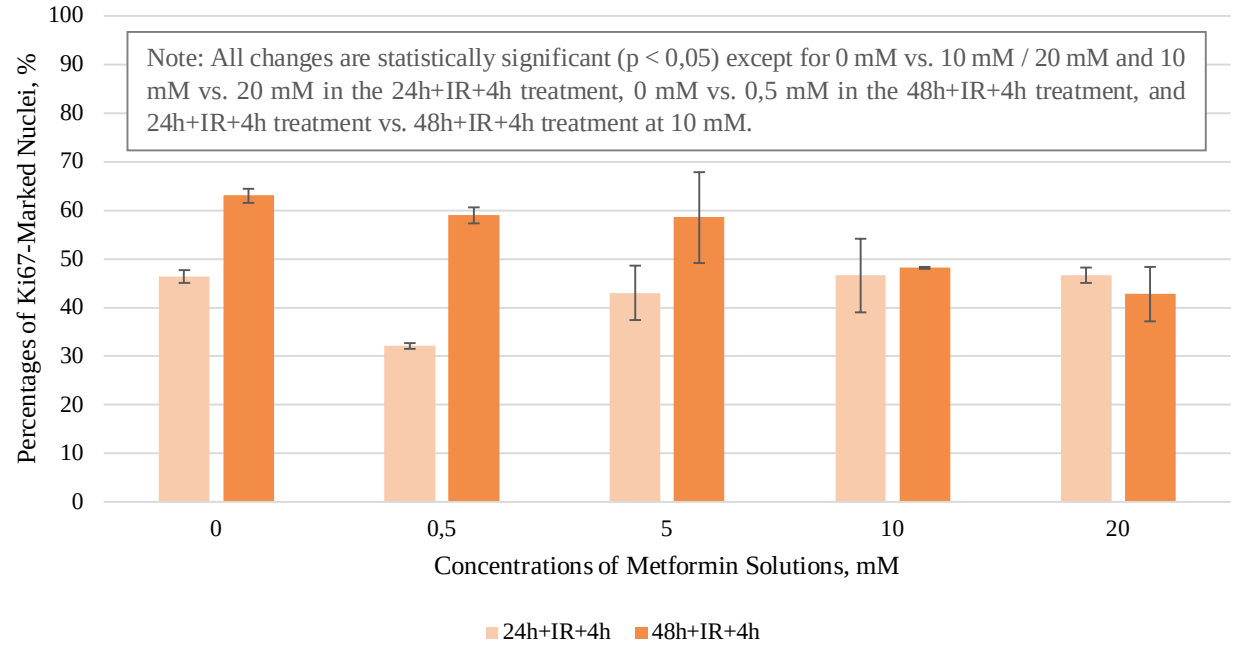

When 24 hours had passed since irradiation (figure 32), Kuramochi proliferation rates were similar to the ones seen at the earlier time point, but only in the shorter, 24h+IR+24h treatment, where only 20 mM metformin concentration was effective again, reducing the proliferating nuclei portion from 83 ± 1 % at 0 mM to 69 ± 5 % at 20 mM ($p < 0{,}0001$) (figure 30). The longer, 48h+IR+24h treatment resulted in overall considerably diminished Kuramochi proliferation, but the part of Ki67-marked nuclei remained virtually the same between controls and the different metformin concentrations, around 60 %. Finally,

Figure 30. Immunofluorescence images of Kuramochi cells in the IR+24h part of the third experiment: left side – all nuclei in a part of a field as identified with Hoechst; right side – Ki67-positive nuclei in the same part of the field. A: 24h+IR+24h plate, 0 mM metformin. B: 24h+IR+24h plate, 20 mM metformin. Red arrows mark Ki67-positive nuclei.

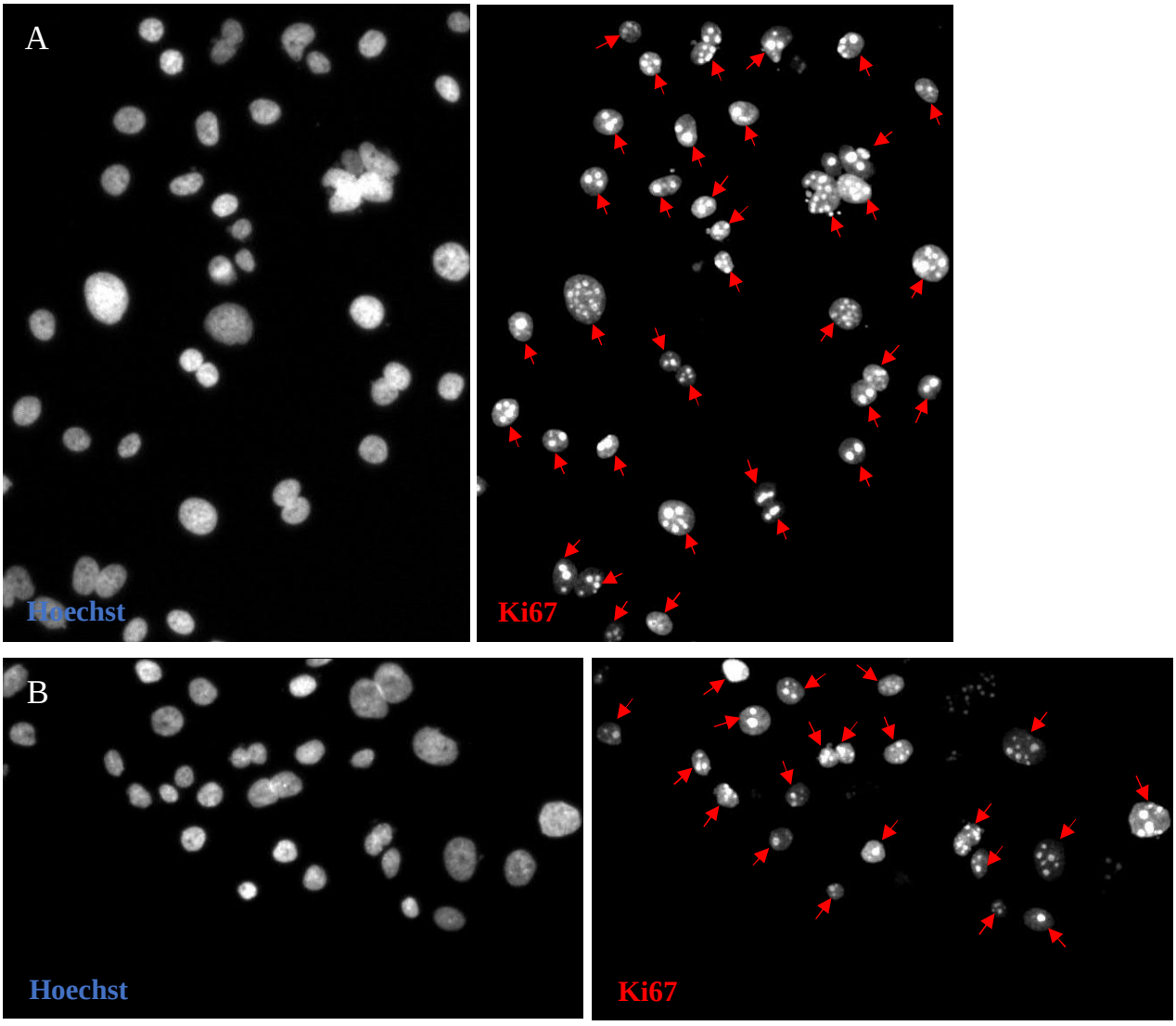

OVCAR4 cells proliferated considerably more at this 24h after irradiation time point compared to the 4h after irradiation time point, and the numbers of proliferating nuclei were similar in controls and at lower metformin concentrations. However, the highest metformin concentration, i.e., 20 mM successfully managed to weaken OVCAR4 proliferation ability, trimming the proliferating nuclei fraction from 64 ± 1 % at 0 mM to 58 ± 2 % at 20 mM in the 24h+IR+24h treatment ($p < 0,0001$), and from 78 ± 5 % at 0 mM to a drastic number of just 39 ± 7 % at 20 mM in the 48h+IR+24h treatment ($p < 0,0001$) (figure 31).

Figure 31. Immunofluorescence images of OVCAR4 cells in the IR+24h part of the third experiment: left side – all nuclei in a part of a field as identified with Hoechst; right side – Ki67-positive nuclei in the same part of the field. A: 48h+IR+24h plate, 0 mM metformin. B: 48h+IR+24h plate, 20 mM. Red arrows mark Ki67-positive nuclei.

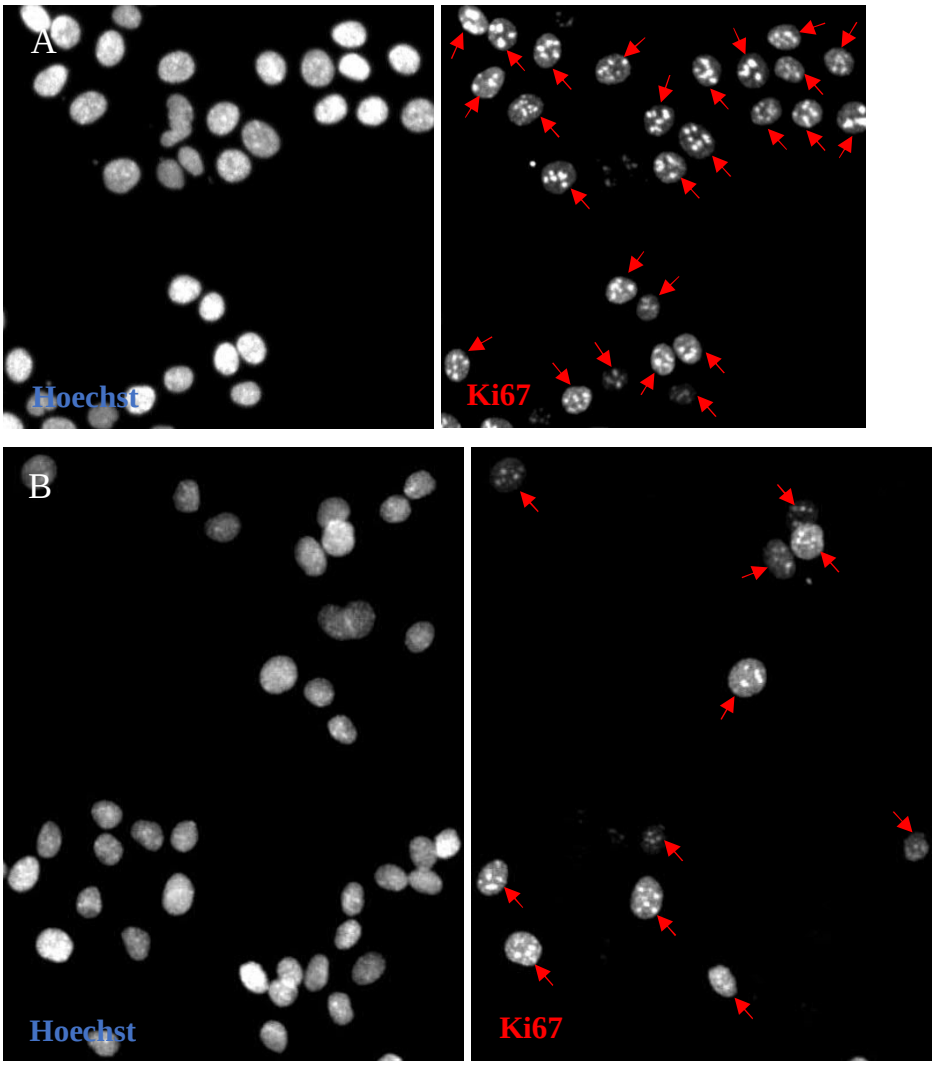

Figure 32. Ki67 results from Kuramochi (A) and OVCAR4 (B) cells in the IR+24h part of the third experiment. Legends indicate metformin treatment durations. Gray text fields indicate statistically significant changes in proliferation ($p < 0,05$).

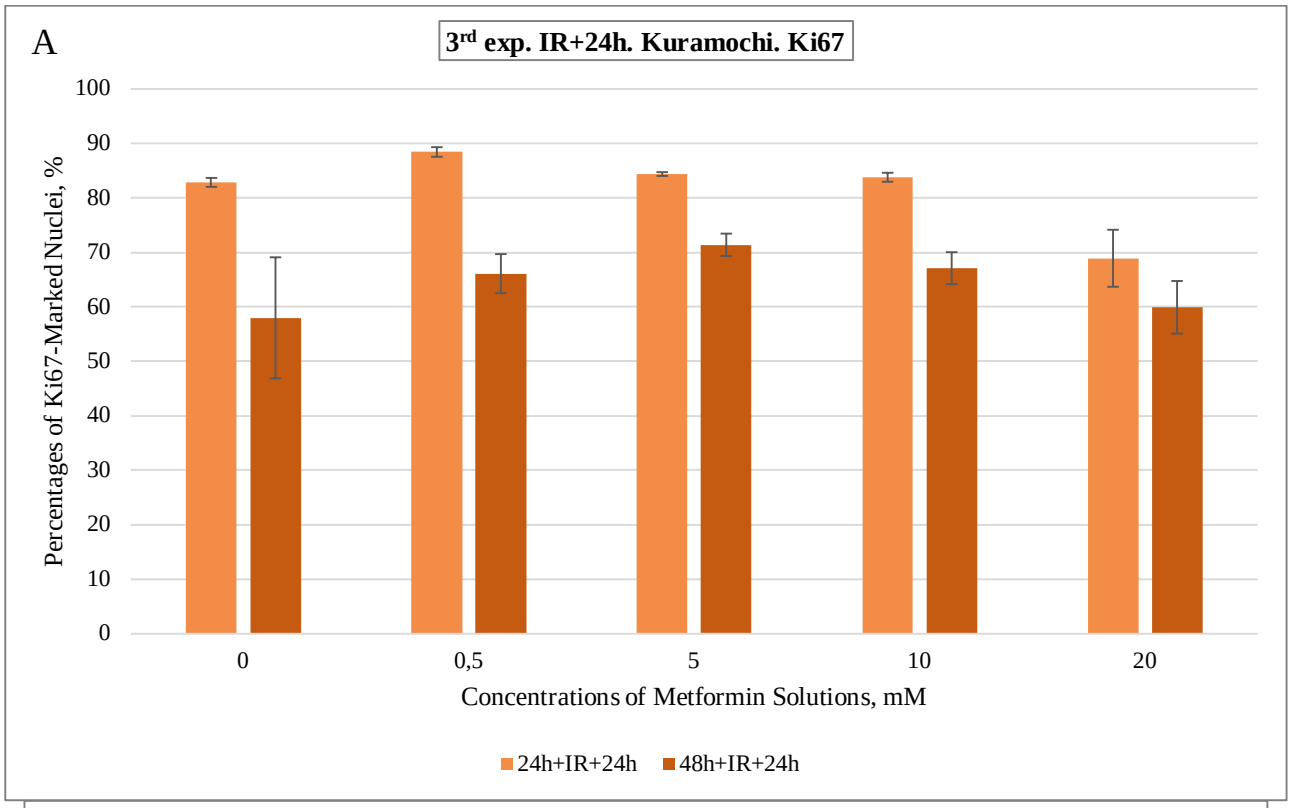

Note: All changes are statistically significant ($p < 0,05$) except for 0 mM vs. 5 mM / 10 mM and 5 mM vs. 10 mM in the 24h+IR+24h treatment, 0 mM vs. 20 mM and 0,5 mM vs. 5 mM in the 48h+IR+24h treatment.

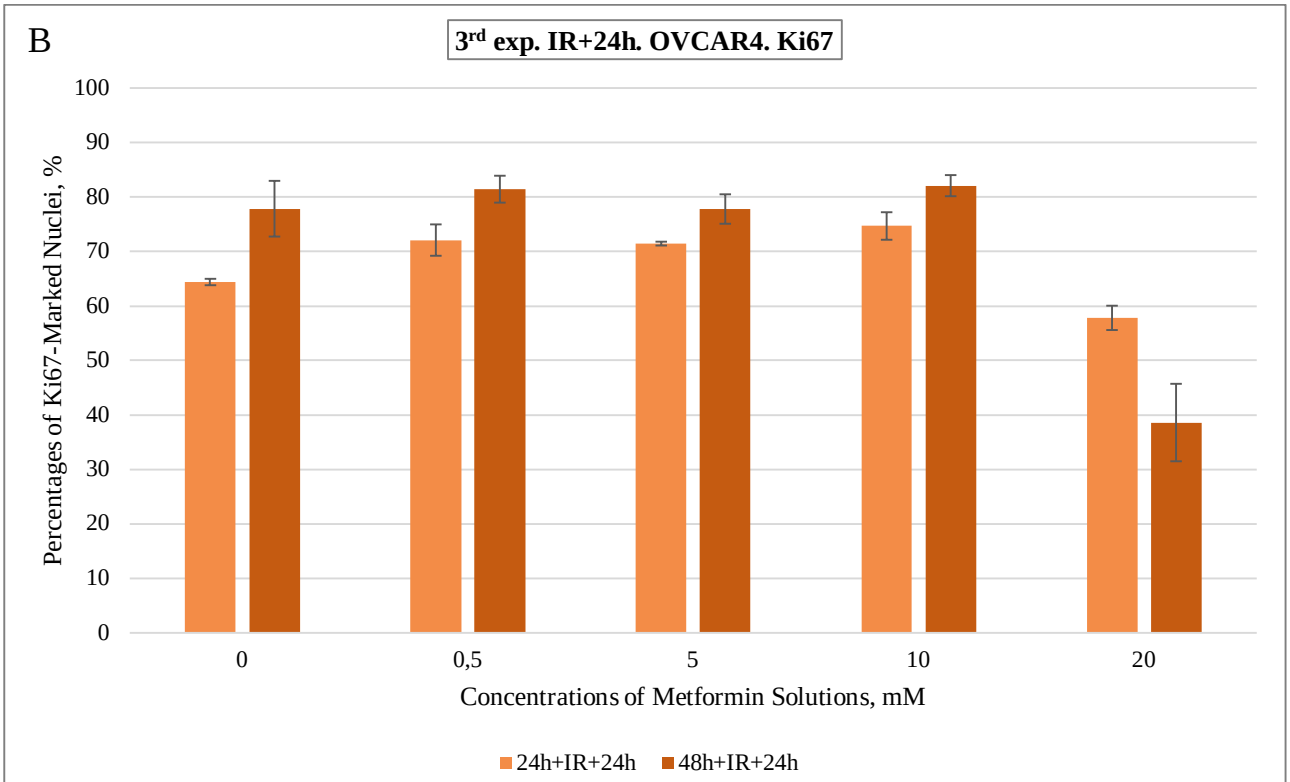

Note: All changes are statistically significant ($p < 0,05$) except for 0,5 mM vs. 5 mM in the 24h+IR+24h treatment, 0 mM vs. 0,5 mM / 5 mM / 10 mM, 0,5 mM vs. 5 mM / 10 mM, and 5 mM vs. 10 mM in the 48h+IR+24h treatment.

4.3. cCasp3 results

Caspase 3 is a pivotal executioner caspase that can be activated by any of the initiator caspases (i.e., caspases 8-10) participating in the different apoptotic pathways (Elmore, 2007). Activation prompts cleavage, and the cleaved caspase 3 (or, cCasp3) cleaves, activates, and inactivates various proteins that partake in apoptotic events resulting in morphological and biochemical alterations characteristic to apoptotic cells (Elmore, 2007; Al-Hassan et al., 2019). Being one of the hallmarks of apoptosis, cCasp3 is utilized in apoptosis detection (Elmore, 2007; Meng et al., 2018). In this study, cCasp3 was assessed by using a primary antibody against it.

Figure 34 contains a bar chart with cCasp3 results. There is only one set of data, from Kuramochi cells that survived the first experiment. In this data set, only the highest metformin concentration, i.e., 25 mM significantly increased apoptosis in all three treatment durations. In the 24h treatment, 63 ± 9 % of nuclei were marked for apoptosis at the 25 mM metformin concentration compared to 52 ± 18 % of nuclei

in controls, and respectively, 97 ± 4 % compared to 35 ± 18 % in the 48h treatment, and 76 ± 14 % compared to 14 ± 12 % in the 72h treatment (figure 33) ($p < 0{,}0001$ for all). However, 5 mM metformin concentration in the 48h treatment, as well as 0,5 mM and 5 mM metformin concentrations in the 72h treatment also increased apoptosis compared to controls, although these increases were modest: from 35 ± 18 % of cCasp3-marked nuclei at 0 mM to 41 ± 21 % at 5 mM in the 48h treatment, from 14 ± 12 %

Figure 33. Immunofluorescence images of Kuramochi cells in the first experiment: left – all nuclei in a part of a field as identified with Hoechst; right – cCasp3-positive nuclei in the same part of the field. A: 72h plate, 0 mM metformin. B: 72h plate, 25 mM metformin. Yellow arrows mark cCasp3-positive nuclei.

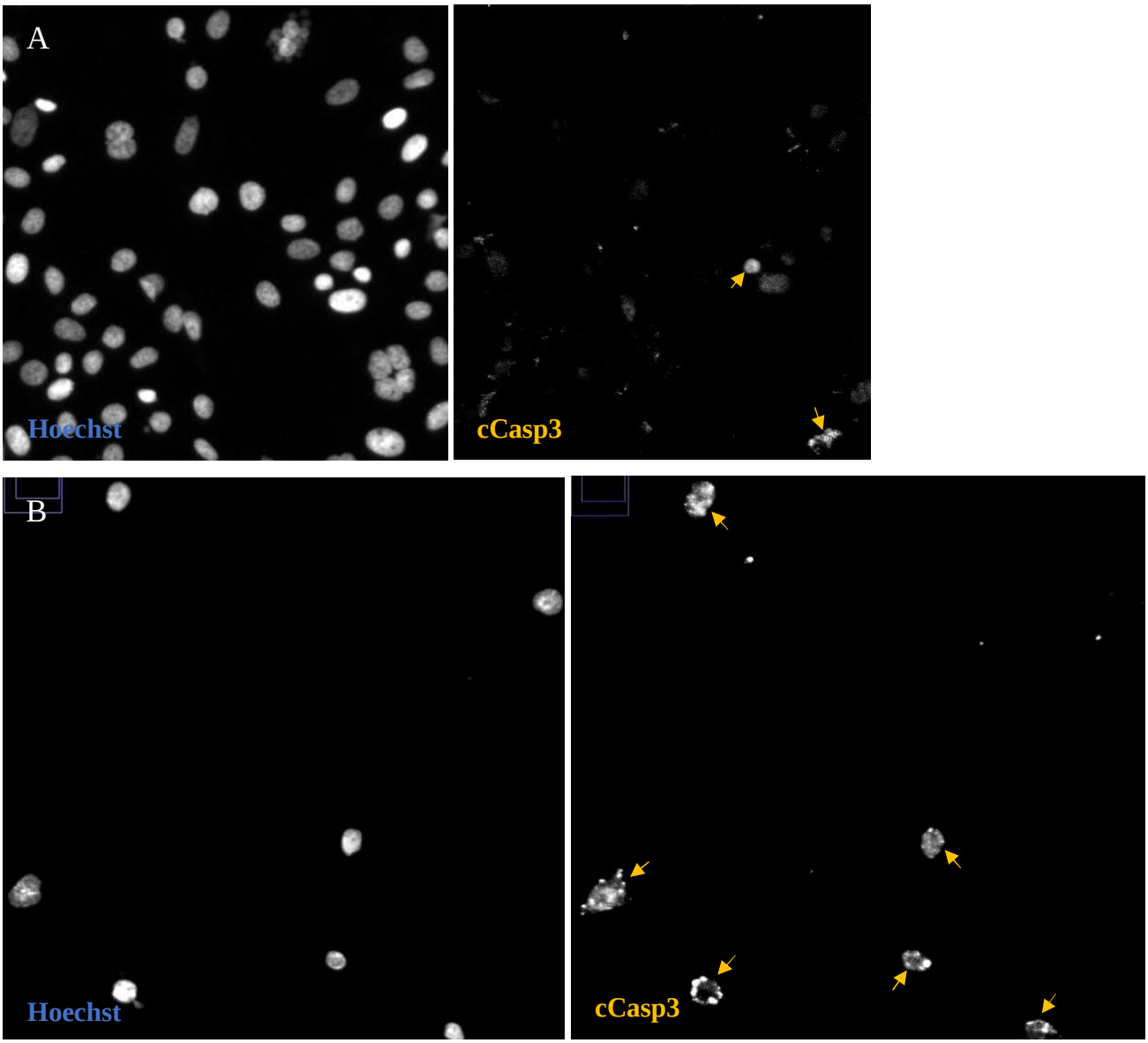

at 0 mM to 27 ± 10 % at 0,5 mM and to 24 ± 12 % at 5 mM in the 72h treatment ($p < 0,0001$ for all). Interestingly, there was a slight variation in apoptotic nuclei numbers between different treatment durations: the 24h metformin treatment produced the most apoptotic nuclei in controls and lower metformin concentrations (i.e., 0 mM, 0,5 mM, and 5 mM), but the least apoptotic nuclei in the highest metformin concentration (i.e., 25 mM), and the 48h metformin treatment was slightly more effective in inducing apoptosis in all metformin concentrations and controls than the 72h treatment. The decreasing trend with time in the 0-5 mM range could be due to the shock caused to the cells by thawing the ampule shortly before plating. The effect could still be visible at the 24h time point, but then later cells appeared to recover from it. The lower metformin concentrations do not seem to have a large effect, so cells may react in a more similar trend as controls do, but when metformin concentration is high enough to be profoundly effective, longer treatments give rise to more apoptosis.

Figure 34. cCasp3 results from Kuramochi cells used in the first experiment. 24 h refers to 24h metformin treatment, 48 h refers to 48h metformin treatment, 72 h refers to 72h metformin treatment. The gray text field indicates statistically significant changes in apoptosis ($p < 0,05$).

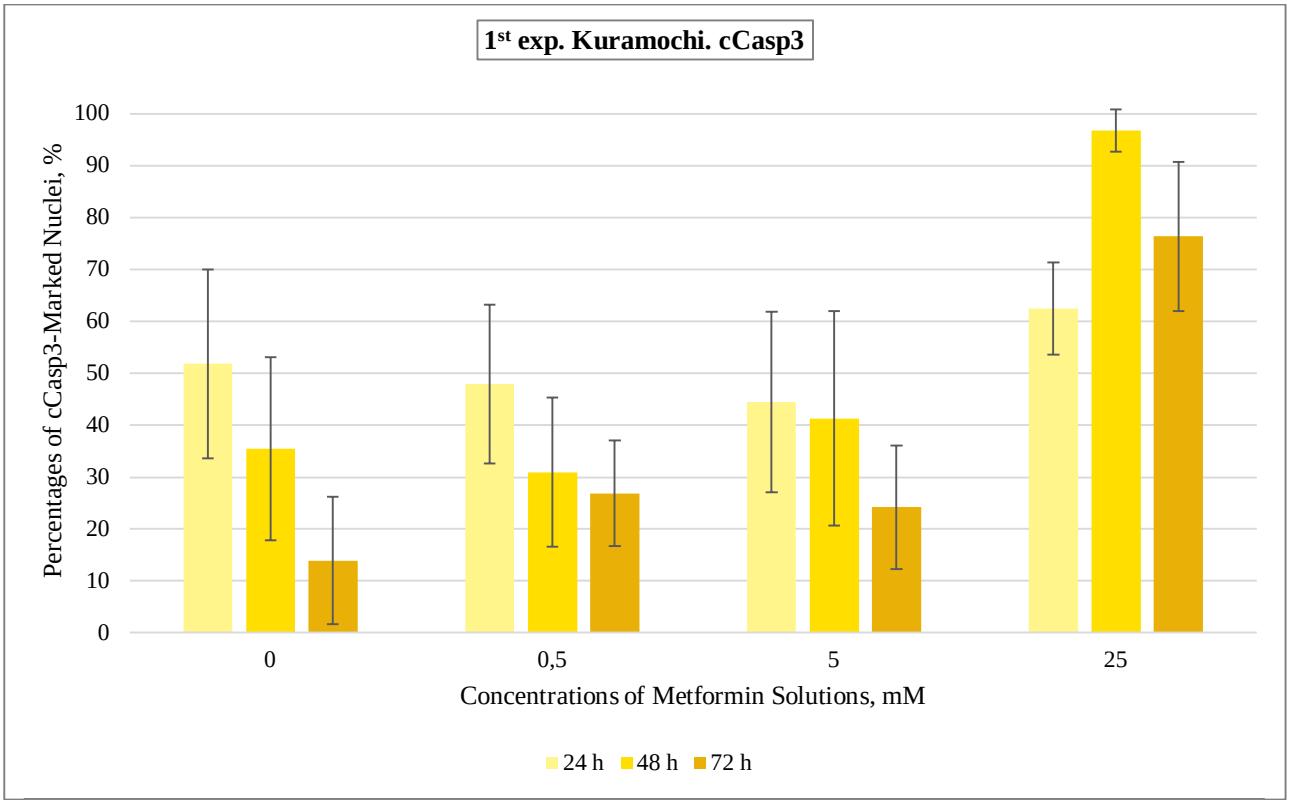

Note: All changes are statistically significant ($p < 0,05$) except for 0 mM vs. 0,5 mM / 5 mM in the 24h treatment, 0,5 mM vs. 5 mM in all three treatments, and 48h treatment vs. 72h treatment at 0,5 mM.

There are no substantial cCasp3 data from the second and third experiments. In roughly 1000 analyzed nuclei per field, only a couple or a few were marked for apoptosis. Figure 35 illustrates this absence of apoptotic nuclei.

Figure 35. Immunofluorescence images from the second and third experiments: left – all nuclei in a part of a field as identified with Hoechst; right – cCasp3-positive nuclei in the same part of the field. A: Kuramochi, 48h plate, 15 mM metformin. B: OVCAR4, 24h+IR+4h plate, 10 mM metformin. The nuclei lack cCasp3 positivity as well as apoptotic properties like blebbing and nuclear fragmentation.

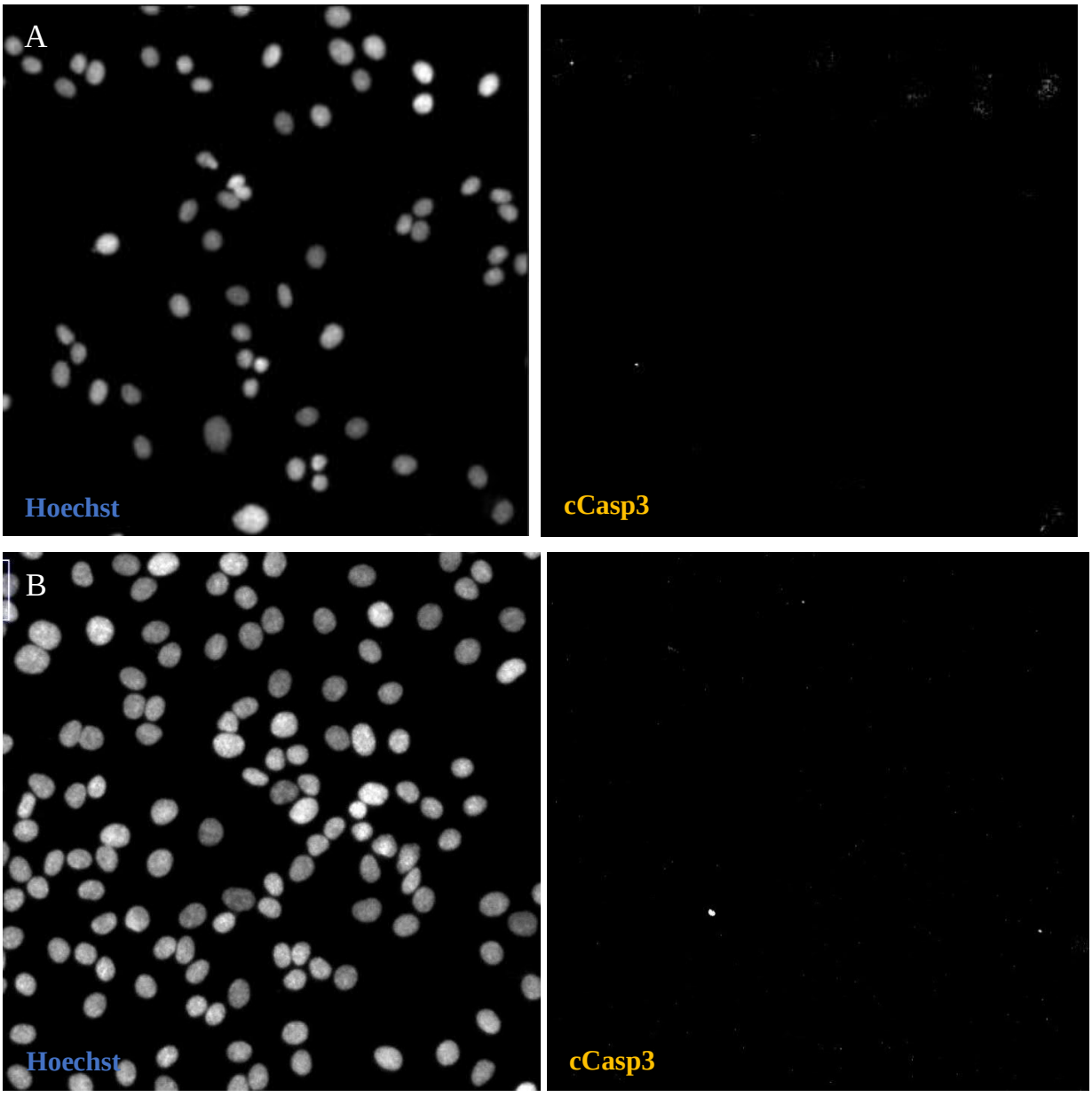

5. DISCUSSION

Several studies have described the association between metformin intake and improved survival rate in diabetic ovarian cancer patients, as well as metformin's anti-proliferative and pro-apoptotic effects on various cancer, including ovarian cancer, cells. However, there was a lack of comprehensive data and understanding about metformin effect on DNA damage in HGSOC cells, particularly with regards to HR. It is important to take into consideration the HR status of analyzed HGSOC cells, because HR proficiency is known to determine chemo-resistance, while HR deficiency correlates with better prognosis and improved survival.

This study aimed to test what kind of an effect different metformin concentrations and treatment lengths have with and without IR on DNA damage, as well as proliferation and apoptosis in two HGSOC cell lines of different HR status: Kuramochi, which is an HR-deficient cell line, and OVCAR4, an HR-proficient cell line. Cells were exposed to metformin (0,5-25 mM) and incubated for 24-72 hours, and a part of cells was additionally irradiated after the metformin pre-treatment, followed by incubation for 4 or 24 more hours (figure 2). After that, cells were fixed, stained, and imaged. Finally, the acquired data were processed (including pooling, when possible) and analyzed. This study has found that the highest used metformin concentrations give the most substantial results with regards to increasing DNA damage, decreasing proliferation, and increasing apoptosis, and that sometimes only longer treatments (48h and 72h treatment) give a desirable effect, especially considering proliferation. OVCAR4 cell line was found to be more resistant to metformin treatment than Kuramochi cell line, but high metformin concentrations (such as 20 mM) and longer treatments coupled with IR very efficiently increased DNA damage and reduced proliferation even for this HR-proficient cell line (no data was obtained on apoptosis though).

Although this study examined just two ovarian cancer cell lines, it still contributes to the cause of obtaining more information about metformin impact on DNA damage in ovarian cancer – a matter on which the previously existing knowledge was very scarce and incomplete. Moreover, to our knowledge, this is the first study that investigated metformin effects on DNA damage, as well as proliferation and apoptosis in HGSOC cell lines while taking into consideration their HR status. In addition, this study chose to use cell lines whose culture media does not require insulin, which by itself would affect results. Metformin increases insulin uptake by sensitizing tissues to insulin, which then lowers glucose levels (Bailey et al., 1996). Hence, both agents, in general, have the glucose-lowering effect, and having insulin in the media would not allow proper examination of specific metformin effects. Not all previously

performed studies took this into account (Gotlieb et al., 2008; Rattan et al., 2011a), and in this aspect, my study provides improved accuracy for metformin-dependent cellular read-outs.

Based on the literature review, I expected the HR-proficient OVCAR4 cells to be affected by metformin with regards to increased DNA damage, reduced proliferation, and increased apoptosis. Several metformin concentrations and treatment durations were selected in order to test this idea, also based on what could be found in previous publications. When the highest chosen metformin concentration in the first experiment, i.e., 25 mM killed many cells, and OVCAR4 cells essentially did not survive that whole experiment (see also Appendix E), it was decided to lower the metformin concentration and use cells that were kept in long-term culture, with the reasoning that recent thawing, in addition to metformin treatment, might cause too big of a shock to cells. The long-term culture aspect proved to be extremely important in this experimental setup, because further experiments yielded substantially higher numbers of cells in both cell lines, no matter how the high metformin concentration was (see Appendix E). The highest metformin concentration in further experiments was selected to be 20 mM, and essentially, it ended up being the only significant concentration considering the study aims.

The 20 mM metformin concentration was the most effective in the HR-deficient Kuramochi cell line in terms of changing both DNA damage and proliferation. Some lower metformin concentrations had a noticeable effect on Kuramochi cells too, but they were overall ineffective on the HR-proficient OVCAR4 cell line. Only 20 mM metformin increased DNA damage in both non-irradiated and irradiated OVCAR4 cells when compared to controls (i.e., 0 mM metformin) (figure 11, B; figure 17, B). The effect of the 20 mM concentration was particularly visible 24 hours after irradiation: at this time point, HR-proficient OVCAR4 cells had sufficient time to repair the induced DNA damage, resulting in a decreased percentage of nuclei with DNA damage, by roughly a third or a quarter in control wells and the wells with lower metformin concentrations. However, the high metformin concentration (20 mM) was able to raise this number again – in the longer treatment (48h) even close to the one seen at the 4h time point after irradiation (over 90%) (figure 16; figure 13). The findings from the DNA damage part of the experiment were in agreement with the findings from the proliferation part. Only 20 mM metformin concentration reduced proliferation in non-irradiated and irradiated OVCAR4 cells (figure 26, B; figure 32, B). The most illustrative and substantial effect was observed at the 24h after irradiation time point with the longest metformin pre-treatment (48h+IR+24h) where OVCAR4 proliferation dropped by approximately half (figure 31).

One more finding from γH2AX and Ki67 analyses is worth additional discussion. Interestingly, at the 4h after irradiation time point, the fractions of Ki67-positive Kuramochi and OVCAR4 nuclei were similar to the ones seen without irradiation at corresponding metformin treatment durations and concentrations (figure 26, figure 29). This is somewhat counter-intuitive, because one might expect the IR-induced unrepaired damage to halt proliferation. I was unable to find suitable previous publications to compare my findings to others, but at least at 8 hours after irradiation, another HR-deficient cell line, OVCAR8, had only a marginal Ki67-positive nuclei percentage difference from the percentage observed in non-irradiated cells, and another HR-proficient cell line, OVCAR3, virtually did not exhibit any differences in proliferation between these two groups (Tumiati et al., 2018 (supplementary data)). In addition, comparing my findings to the ones published by Tumiati et al. (2018), there were a couple of other visible similarities in γH2AX- and Ki67-positivity trends among my tested untreated HR-deficient and HR-proficient cell lines (Kuramochi and OVCAR4, respectively), and their examined HR-deficient and HR-proficient cell lines (OVCAR8 and OVCAR3, respectively). For instance, in the referenced publication, the fraction of proliferating OVCAR8 nuclei was bigger than OVCAR3 by more than a third, which was similar to the proliferation results of my study, where I also observed higher Ki67-positive nuclei percentages in Kuramochi cell line than in OVCAR4 cell line. Another similarity was only a slight reduction of γH2AX positivity at 24 hours after irradiation for OVCAR8 in the referenced study and for Kuramochi in my study, but a significant decrease in γH2AX positivity at the same time point for OVCAR3 and OVCAR4, respectively. Even the percentages themselves in both γH2AX and Ki67 analyses did not extremely differ between these two studies among the examined corresponding HR-deficient and HR-proficient cell lines.

However, γH2AX and Ki67 analyses in one of the experiments had a caveat of partly automated / partly manual scoring of γH2AX- and Ki67-positive nuclei. Each well had a replicate well, but in the unfortunate cases in the third experiment when both wells had large non-cellular objects and could not be used for the automated scoring, manual scoring was used analyzing only the good-quality areas of the wells. Ideally, in such a case, manual scoring should be performed in all of the wells, so that the data would be more comparable, or both wells unsuitable for automated scoring should be excluded from the analysis. However, in this study, I wanted to reduce the amount of missing data as much as possible, and since manual scoring is a long process that had not been intended in the project plan considering the length of the project, it was decided to score Ki67 manually only in the poorer-quality wells and apply the automated scoring to the rest of the wells. In addition, it was problematic to make the software work

equally well for the two γH2AX staining combinations in the third experiment. Therefore, γH2AX was scored manually in this experiment – this time, in all of the wells. Appendix E marks all the cases when manual scoring was applied.

Unfortunately, the experiments described in this thesis generated little data on apoptosis (figures 33-34; Appendix E). Only the first experiment that used recently thawn cells yielded results, but only for Kuramochi cells, the only ones that survived that experiment. The first experiment had a few other problems besides the missing OVCAR4 data, such as large confidence intervals due to a rather small number of scanned fields that were chosen randomly and contained unevenly distributed numbers of nuclei. Also, as already mentioned, high metformin concentration (25 mM) proved to be lethal to many recently thawn cells and it also increased confidence intervals even more. It was then decided not to repeat that particular experiment, with the reasoning that more information would be gained with further experiments that would also include more concentrations, and irradiation, making the data also more informative. Nevertheless, in these further experiments, there were just a few signals of cCasp3 (figure 35) – not enough to form conclusive deductions. One possible explanation for the lack of a cCasp3 signal is short-term culture vs. long-term culture. The first experiment used cells that had been thawed only approximately 72 hours earlier, and thawing could cause stress, making cells more apoptotic. In contrast, the second and third experiments used cells that had been regularly passaged, i.e., kept in long-term culture. Therefore, they were less sensitive. Another explanation for the absence of a cCasp3 signal could be that there was apoptosis, but perhaps it could not be detectable with this particular marker. However, this is unlikely, because apoptotic nuclei typically have certain characteristics, mainly nuclear fragmentation and cytoplasmic blebbing (Patel et al., 2015), which were predominantly absent in the analyzed nuclei, even in the irradiated cells. The most likely explanation is that the selected time points were not suitable to detect apoptosis. Ideally, after irradiation, cCasp3 should be analyzed at the 8h time point, which was missing in these experiments. It was decided to simplify the experimental setup in order to have fewer time points to test with the intention to detect cCasp3 signal at the 24h time point, but it is possible that it was too late (cells either repaired the induced damage or died, but the cCasp3 signal was missed), while the 4h time point was too early. The 24h and 48h time points in the second experiment might have had the same fault of being unsuitable. Future experiments of this kind should certainly include the 8h time point. Nevertheless, the obtained cCasp3 data from Kuramochi cells from the first experiment suggest that, again, only high metformin concentrations, such as 25 mM, have the ability to

increase apoptosis eminently. More apoptosis experiments should be performed in order to verify this, and it is necessary to analyze an HR-proficient cell line as well.

A comparison of my metformin analysis results to the ones obtained in previous publications of similar design brings both concordance and discrepancy. A study by Lengyel et al. (2015) did not find Kuramochi proliferation to decrease with 10 mM metformin (MTT assay was used for assessment), which is in agreement with my finding. In the same study, however, they found other cell lines, namely OVCAR5, Kras/PTEN, SKOV3ip1, and Hey A8 to respond to 10 mM metformin, unlike Kuramochi. A discrepancy example is a study by Gotlieb et al. (2008) that reported proliferation inhibition of OVCAR4 and OVCAR3 cells (which are both HR-proficient) induced by 72h metformin treatment starting already at 1 mM, the inhibitory effect increasing with increasing metformin concentrations (up to 100 mM), though their used analysis method was different – cell viability determination using AlamarBlue colorimetric assay. I could not find more studies that used the same cell lines as I did. There were several studies that analyzed SKOV3 cells, and I referred to these studies when selecting metformin conditions for my experiments, but it is important to note that SKOV3 is not an HGSOC cell line, and metformin effect on these cells can be very different from the ones seen in HGSOC cells. Even among these SKOV3 studies, varying results are reported. For example, a study by Shank et al. (2012) found that SKOV3 proliferation is inhibited by 3-day metformin treatment starting at 1 mM (the method of choice was cell viability evaluation by performing cell count using trypan blue and flow cytometry). However, another study (Patel et al., 2015) determined that SKOV3 cell viability is inhibited by applying 48h treatment using only a range of rather high metformin concentrations, 15-30 mM (the method used was MTT assay), which is more in line with my findings. The same study also found that 48h metformin treatment at 15 mM prompts SKOV3 cell cycle arrest and apoptosis (from 5,1 % detected apoptosis in untreated cells to 14,5 % in treated cells; analysis method – flow cytometry). Finally, one more study (Wu et al., 2012) reported substantially larger inhibition of proliferation in 48h and 72h treatments using the range of 5-50 mM metformin, compared to 24h treatment, but no apoptosis was detected in SKOV3 cells following 24h 0-20 mM metformin treatment (for this purpose, annexin V expression was assessed using flow cytometry).

Despite the discussed shortcomings, this study still gathered novel and scientifically valuable data on metformin effects on two HGSOC cell lines of different HR status. Overall, my findings indicate that HR-proficient cells, such as OVCAR4, are still able to repair induced DNA damage, survive and proliferate when treated with lower metformin concentrations (0,5-10 mM), but become impaired when

exposed to high metformin concentrations, such as 20 mM. This is a promising finding suggesting that it might be possible to affect even chemo-resistant HR-proficient cell lines with appropriate metformin concentrations. A point to consider, though, is the feasibility of delivering metformin concentrations as high as 20 mM to the human body without causing noxious effects, in spite of metformin being a safe and well-tolerated drug (Patel et al., 2015). Even though the selected concentrations are in accordance with the ones used in cell biology experiments of similar design (Gotlieb et al., 2008; Rattan et al., 2011a; Shank et al., 2012; Wu et al., 2012; Lengyel et al., 2015; Patel et al., 2015; Dos Santos Guimarães et al., 2018; Yang et al., 2019), it is important to note that they are supra-physiological. Type 2 diabetic patients treated with metformin have less than 50 μM concentration of this drug in their blood (Martin-Castillo et al., 2010). However, it has been shown that tissues can accumulate metformin and thus higher concentrations can be reached locally (Owen et al., 2000). In fact, one already presented study by Wu et al. (2012), that found SKOV3 proliferation to be effectively inhibited with ~20 mM without apoptosis, postulates that this suggests that such doses are potentially not directly toxic and are at a therapeutic level. Refined translation of this into clinical use would need to be developed, which is a fine opportunity for future research. Regarding other future research possibilities, since the irradiation part of one of the experiments was performed only once, it would be wise to replicate that particular experiment. Future experiments could also include higher metformin concentrations than 20 mM, if desired, but it is essential to apply metformin to cells kept in long-term culture. It could also be beneficial to perform more apoptosis experiments with the adjusted setup, since the current experiment lacked the data on this cellular process. Apoptosis is often investigated in cancer-related experiments, because acquired resistance to chemotherapeutic therapies and the consequent cancer progression can be caused by faults in the apoptotic machinery (Patel et al., 2015). Most importantly, it is necessary to investigate whether high metformin concentrations affect specifically the HR-mediated DNA repair pathway. If the findings are positive, it would also be a good idea to perform the same experiments with more HR-proficient and HR-deficient commercial cell lines (provided they do not need insulin in the medium). In the case of encouraging findings, it would also be worthy to perform the experiments with primary ovarian cancer cells instead of commercial cell lines, because primary cells better resemble the physiological state of cancer cells *in vivo*, and thus, more meaningful data can be obtained using them (Patel et al., 2015).

In conclusion, this thesis work provides preliminary evidence that metformin concentrations of at least 20 mM in combination with IR are effective in increasing DNA damage and reducing proliferation even in an HR-proficient HGSOC cell line, and thereby lays the groundwork for more detailed investigations

of metformin's suppressive effects on HR-proficient high-grade serous ovarian tumors. In the long term, such studies can provide novel, well-tolerated chemo-sensitization options for patients with hard-to-treat HGSOC.

ACKNOWLEDGEMENTS

Firstly, I would like to thank my primary supervisor Liisa Kauppi for giving me the opportunity to do this thesis in her lab, for kindly providing abundant guidance and help whenever I needed it, and for being incredibly supportive, patient, and understanding. I also want to thank my secondary supervisors Manuela Tumiati and Taina Turunen for sharing their knowledge and wisdom and for consistent help and support in the experimental part of the project. In addition, I would like to express my gratitude to the Biomedicum Imaging Unit for giving me microscopy training and subsequent support with the equipment. Lastly, I thank the Sigrid Jusélius foundation for financial aid.

REFERENCES

1. Aletti, G.D., Gallenberg, M.M., Cliby, W.A., Jatoi, A., and Hartmann, L.C. (2007). Current management strategies for ovarian cancer. Mayo Clin Proc. *82*, 751-770.
2. Algire, C., Moiseeva, O., Deschênes-Simard, X., Amrein, L., Petruccelli, L., Birman, E., Viollet, B., Ferbeyre, G., and Pollak, M.N. (2012). Metformin reduces endogenous reactive oxygen species and associated DNA damage. Cancer Prev Res (Phila). *5*, 536-543.
3. Al-Hassan, J.M., Fang Liu Y., Khan, M.A., Yang, P., Guan, R., Wen, X., Afzal, M., Oommen, S., Paul, B.M., Nair, D., Palaniyar, N., and Pace-Asciak, C. (2019). Furanoic Lipid F-6, A Novel Anti-Cancer Compound that Kills Cancer Cells by Suppressing Proliferation and Inducing Apoptosis. Cancers (Basel). *11*, 960.
4. Amador, R.R., Longo, J.P., Lacava, Z.G., Dórea, J.G., and Almeida Santos M. de F. (2012). Metformin (dimethyl-biguanide) induced DNA damage in mammalian cells. Genet Mol Biol. *35*, 153-158.
5. Ashinuma, H., Takiguchi, Y., Kitazono, S., Kitazono-Saitoh, M., Kitamura, A., Chiba, T., Tada, Y., Kurosu, K., Sakaida, E., Sekine, I., Tanabe, N., Iwama, A., Yokosuka, O., and Tatsumi, K. (2012). Antiproliferative action of metformin in human lung cancer cell lines. Oncol Rep. *28*, 8-14.
6. Bailey, C.J., and Turner, R.C. (1996). Metformin. N Engl J Med. *334*, 574-579.
7. Bell, D.A. (2005). Origins and molecular pathology of ovarian cancer. Mod Pathol. *18*, S19-32.
8. Ben Sahra, I., Laurent, K., Loubat, A., Giorgetti-Peraldi, S., Colosetti, P., Auberger, P., Tanti, J.F., Le Marchand-Brustel, Y., and Bost, F. (2008). The antidiabetic drug metformin exerts an antitumoral effect in vitro and in vivo through a decrease of cyclin D1 level. Oncogene. *27*, 3576-3586.
9. Berns, E.M., and Bowtell, D.D. (2012). The changing view of high-grade serous ovarian cancer. Cancer Res. *72*, 2701-2704.
10. Bodmer, M., Becker, C., Meier, C., Jick, S.S., and Meier, C.R. (2011). Use of metformin and the risk of ovarian cancer: a case-control analysis. Gynecol Oncol. *123*, 200-204.
11. Bolton, K.L., Chenevix-Trench, G., Goh, C., Sadetzki, S., Ramus, S.J., Karlan, B.Y., Lambrechts, D., Despierre, E., Barrowdale, D., McGuffog, L., Healey, S., Easton, D.F., Sinilnikova, O., Benítez, J., García, M.J., Neuhausen, S., Gail, M.H., Hartge, P., Peock, S., Frost, D., Evans, D.G.,

Eeles, R., Godwin, A.K., Daly, M.B., Kwong, A., Ma, E.S., Lázaro, C., Blanco, I., Montagna, M., D'Andrea, E., Nicoletto, M.O., Johnatty, S.E., Kjær, S.K., Jensen, A., Høgdall, E., Goode, E.L., Fridley, B.L., Loud, J.T., Greene, M.H., Mai, P.L., Chetrit, A., Lubin, F., Hirsh-Yechezkel, G., Glendon, G., Andrulis, I.L., Toland, A.E., Senter, L., Gore, M.E., Gourley, C., Michie, C.O., Song, H., Tyrer, J., Whittemore, A.S., McGuire, V., Sieh, W., Kristoffersson, U., Olsson, H., Borg, Å., Levine, D.A., Steele, L., Beattie, M.S., Chan, S., Nussbaum, R.L., Moysich, K.B., Gross, J., Cass, I., Walsh, C., Li, A.J., Leuchter, R., Gordon, O., Garcia-Closas, M., Gayther, S.A., Chanock, S.J., Antoniou, A.C., Pharoah, P.D., EMBRACE, kConFab Investigators, and Cancer Genome Atlas Research Network. (2012). Association between BRCA1 and BRCA2 mutations and survival in women with invasive epithelial ovarian cancer. JAMA. *307*, 382-390.

12. Bowker, S.L., Majumdar, S.R., Veugelers, P., and Johnson, J.A. (2006). Increased cancer-related mortality for patients with type 2 diabetes who use sulfonylureas or insulin. Diabetes Care. *29*, 254-258.
13. Bowtell, D.D., Böhm, S., Ahmed, A.A., Aspuria, P.J., Bast, R.C. Jr., Beral, V., Berek, J.S., Birrer, M.J., Blagden, S., Bookman, M.A., Brenton, J.D., Chiappinelli, K.B., Martins, F.C., Coukos, G., Drapkin, R., Edmondson, R., Fotopoulou, C., Gabra, H., Galon, J., Gourley, C., Heong, V., Huntsman, D.G., Iwanicki, M., Karlan, B.Y., Kaye, A., Lengyel, E., Levine, D.A., Lu, K.H., McNeish, I.A., Menon, U., Narod, S.A., Nelson, B.H., Nephew, K.P., Pharoah, P., Powell, D.J. Jr., Ramos, P., Romero, I.L., Scott, C.L., Sood, A.K., Stronach, E.A., and Balkwill, F.R. (2015). Rethinking ovarian cancer II: reducing mortality from high-grade serous ovarian cancer. Nat Rev Cancer. *15*, 668-679.
14. Boyd J. (2003). Specific keynote: hereditary ovarian cancer: what we know. Gynecol Oncol. *88*, S8-10.
15. Cancer Genome Atlas Research Network. (2011). Integrated genomic analyses of ovarian carcinoma. Nature. *474*, 609-615.
16. Chien, J.R., Aletti, G., Bell, D.A., Keeney, G.L., Shridhar, V., and Hartmann, L.C. (2007). Molecular pathogenesis and therapeutic targets in epithelial ovarian cancer. J Cell Biochem. *102*, 1117-1129.
17. Damia, G., and D'Incalci, M. (2007). Targeting DNA repair as a promising approach in cancer therapy. Eur J Cancer. *43*, 1791-1801.

18. Delaney, J.R., Patel, C.B., Willis, K.M., Haghighiabyaneh, M., Axelrod, J., Tancioni, I., Lu, D., Bapat, J., Young, S., Cadassou, O., Bartakova, A., Sheth, P., Haft, C., Hui, S., Saenz, C., Schlaepfer, D.D., Harismendy, O., and Stupack, D.G. (2017). Haploinsufficiency networks identify targetable patterns of allelic deficiency in low mutation ovarian cancer. Nat Commun. *28*, 14423.
19. Desai, A., Xu, J., Aysola, K., Qin, Y., Okoli, C., Hariprasad, R., Chinemerem, U., Gates, C., Reddy, A., Danner, O., Franklin, G., Ngozi, A., Cantuaria, G., Singh, K., Grizzle, W., Landen, C., Partridge, E.E., Rice, V.M., Reddy, E.S., and Rao, V.N. (2014). Epithelial ovarian cancer: An overview. World J Transl Med. *3*, 1-8.
20. Domcke, S., Sinha, R., Levine, D.A., Sander, C., and Schultz, N. (2013). Evaluating cell lines as tumour models by comparison of genomic profiles. Nat Commun. *4*, 2126.
21. Dos Santos Guimarães, I., Ladislau-Magescky, T., Tessarollo, N.G., Dos Santos, D.Z., Gimba, E.R.P., Sternberg, C., Silva, I.V., and Rangel, L.B.A. (2018). Chemosensitizing effects of metformin on cisplatin- and paclitaxel-resistant ovarian cancer cell lines. Pharmacol Rep. *70*, 409-417.
22. Elmore, S. (2007). Apoptosis: a review of programmed cell death. Toxicol Pathol. *35*, 495-516.
23. Erices, R., Cubillos, S., Aravena, R., Santoro, F., Marquez, M., Orellana, R., Ramírez, C., González, P., Fuenzalida, P., Bravo, M.L., Oliva, B., Kato, S., Ibañez, C., Brañes, J., Bravo, E., Alonso, C., García, K., Arab, C., Torres, V.A., Godoy, A.S., Pereira, J., Bustos, G., Cardenas, J.C., Cuello, M.A., and Owen, G.I. (2017). Diabetic concentrations of metformin inhibit platelet-mediated ovarian cancer cell progression. Oncotarget. *8*, 20865-20880.
24. Evans, J.M., Donnelly, L.A., Emslie-Smith, A.M., Alessi, D.R., and Morris, A.D. (2005). Metformin and reduced risk of cancer in diabetic patients. BMJ. *330*, 1304-1305.
25. Fasih, A., Elbaz, H.A., Hüttemann, M., Konski, A.A., and Zielske, S.P. (2014). Radiosensitization of pancreatic cancer cells by metformin through the AMPK pathway. Radiat Res. *182*, 50-59.
26. Ferlay, J., Soerjomataram, I., Dikshit, R., Eser, S., Mathers, C., Rebelo, M., Parkin, D.M., Forman, D., and Bray, F. (2015). Cancer incidence and mortality worldwide: sources, methods and major patterns in GLOBOCAN 2012. Int J Cancer. *136*, E359-E386.
27. Fong, P.C., Boss, D.S., Yap, T.A., Tutt, A., Wu, P., Mergui-Roelvink, M., Mortimer, P., Swaisland, H., Lau, A., O'Connor, M.J., Ashworth, A., Carmichael, J., Kaye, S.B., Schellens,

J.H., and de Bono, J.S. (2009). Inhibition of poly(ADP-ribose) polymerase in tumors from BRCA mutation carriers. N Engl J Med. *361*, 123-134.

28. Gotlieb, W.H., Saumet, J., Beauchamp, M.C., Gu, J., Lau, S., Pollak, M.N., and Bruchim, I. (2008). In vitro metformin anti-neoplastic activity in epithelial ovarian cancer. Gynecol Oncol. *110*, 246-250.
29. Haince, J.F., Rouleau, M., Hendzel, M.J., Masson, J.Y., and Poirier, G.G. (2005). Targeting poly(ADP-ribosyl)ation: a promising approach in cancer therapy. Trends Mol Med. *11*, 456-463.
30. Halicka, H.D., Zhao, H., Li, J., Traganos, F., Zhang, S., Lee, M., and Darzynkiewicz, Z. (2011). Genome protective effect of metformin as revealed by reduced level of constitutive DNA damage signaling. Aging (Albany NY). *3*, 1028-1038.
31. Hennessy, B.T.J., Timms, K.M., Carey, M.S., Gutin, A., Meyer, L.A., Flake, D.D. 2nd, Abkevich, V., Potter, J., Pruss, D., Glenn, P., Li, Y., Li, J., Gonzalez-Angulo, A.M., McCune, K.S., Markman, M., Broaddus, R.R., Lanchbury, J.S., Lu, K.H., and Mills, G.B. (2010). Somatic mutations in BRCA1 and BRCA2 could expand the number of patients that benefit from poly (ADP ribose) polymerase inhibitors in ovarian cancer. J Clin Oncol. *28*, 3570-3576.
32. Hijaz, M., Chhina, J., Mert, I., Taylor, M., Dar, S., Al-Wahab, Z., Ali-Fehmi, R., Buekers, T., Munkarah, A.R., and Rattan, R. (2016). Preclinical evaluation of olaparib and metformin combination in BRCA1 wildtype ovarian cancer. Gynecol Oncol. *142*, 323-331.
33. Hoeijmakers, J.H. (2001). Genome maintenance mechanisms for preventing cancer. Nature. *411*, 366-374.
34. Jeong, Y.K., Kim, M.S., Lee, J.Y., Kim, E.H., and Ha, H. (2015). Metformin radiosensitizes p53-deficient colorectal cancer cells through induction of G2/M arrest and inhibition of DNA repair proteins. PLoS One. *10*, e0143596.
35. Kelland, L. (2007). The resurgence of platinum-based cancer chemotherapy. Nat Rev Cancer. *7*, 573-584.
36. Kennedy, R.D., and D'Andrea, A.D. (2006). DNA repair pathways in clinical practice: lessons from pediatric cancer susceptibility syndromes. J Clin Oncol. *24*, 3799-3808.
37. Khanna, K.K., and Jackson, S.P. (2001). DNA double-strand breaks: signaling, repair and the cancer connection. Nat Genet. *27*, 247-254.

38. Kisfalvi, K., Eibl, G., Sinnett-Smith, J., and Rozengurt, E. (2009). Metformin disrupts crosstalk between G protein-coupled receptor and insulin receptor signaling systems and inhibits pancreatic cancer growth. Cancer Res. *69*, 6539-6545.
39. Konecny, G.E., Wang, C., Hamidi, H., Winterhoff, B., Kalli, K.R., Dering, J., Ginther, C., Chen, H.W., Dowdy, S., Cliby, W., Gostout, B., Podratz, K.C., Keeney, G., Wang, H.J., Hartmann, L.C., Slamon, D.J., and Goode, E.L. (2014). Prognostic and therapeutic relevance of molecular subtypes in high-grade serous ovarian cancer. J Natl Cancer Inst. *106*, dju249.
40. Konstantinopoulos, P.A., Ceccaldi, R., Shapiro, G.I., and D'Andrea, A.D. (2015). Homologous recombination deficiency: Exploiting the fundamental vulnerability of ovarian cancer. Cancer Discov. *5*, 1137-1154.
41. Kumar, S., Meuter, A., Thapa, P., Langstraat, C., Giri, S., Chien, J., Rattan, R., Cliby, W., and Shridhar, V. (2013). Metformin intake is associated with better survival in ovarian cancer: a case-control study. Cancer. *119*, 555-562.
42. Kuo, J.L., and Yang, L. (2008). Gamma-H2AX - a novel biomarker for DNA double-strand breaks. In vivo (Athens, Greece). *22*, 305-309.
43. Kurman, R.J., and Shih, Ie-M. (2016). The dualistic model of ovarian carcinogenesis: Revisited, revised, and expanded. Am J Pathol. *186*, 733-747.
44. Lee, J., An, S., Jung, J.H., Kim, K., Kim, J.Y., An, I.S., and Bae, S. (2019). MUL1 E3 ligase regulates the antitumor effects of metformin in chemoresistant ovarian cancer cells via AKT degradation. Int J Oncol. *54*, 1833-1842.
45. Lee, Y.S., Doonan, B.B., Wu, J.M., and Hsieh, T.C. (2016). Combined metformin and resveratrol confers protection against UVC-induced DNA damage in A549 lung cancer cells via modulation of cell cycle checkpoints and DNA repair. Oncol Rep. *35*, 3735-3741.
46. Lengyel, E., Litchfield, L.M., Mitra, A.K., Nieman, K.M., Mukherjee, A., Zhang, Y., Johnson, A., Bradaric, M., Lee, W., and Romero, I.L. (2015). Metformin inhibits ovarian cancer growth and increases sensitivity to paclitaxel in mouse models. Am J Obstet Gynecol. *212:479*, e1-e10.
47. Li, L.T., Jiang, G., Chen, Q, and Zheng, J.N. (2015). Ki67 is a promising molecular target in the diagnosis of cancer (Review). Mol Med Rep. *11*, 1566-1572.
48. Lisio, M.A., Fu, L., Goyeneche, A., Gao, Z.H., and Telleria, C. (2019). High-grade serous ovarian cancer: Basic sciences, clinical and therapeutic standpoints. Int J Mol Sci. *20*, E952.

49. Liu, J., Hou, M., Yuan, T., Yi, G., Zhang, S., Shao, X., Chen, J., Jia, X., and He, Z. (2012). Enhanced cytotoxic effect of low doses of metformin combined with ionizing radiation on hepatoma cells via ATP deprivation and inhibition of DNA repair. Oncol Rep. *28*, 1406-1412.
50. Liu, J., Li, M., Song, B., Jia, C., Zhang, L., Bai, X., and Hu, W. (2013). Metformin inhibits renal cell carcinoma in vitro and in vivo xenograft. Urol Oncol. *31*, 264-270.
51. Martin-Castillo, B., Vazquez-Martin, A., Oliveras-Ferraros, C., and Menendez, J.A. (2010). Metformin and Cancer: Doses, Mechanisms and the Dandelion and Hormetic Phenomena. Cell Cycle. *9*, 1057-64.
52. Meng, L., Jan, S.Z., Hamer, G., van Pelt, A.M., van der Stelt, I., Keijer, J., and Teerds, K.J. (2018). Preantral follicular atresia occurs mainly through autophagy, while antral follicles degenerate mostly through apoptosis. Biol Reprod. *99*, 853-863.
53. Moore, K., Colombo, N., Scambia, G., Kim, B.G., Oaknin, A., Friedlander, M., Lisyanskaya, A., Floquet, A., Leary, A., Sonke, G.S., Gourley, C., Banerjee, S., Oza, A., González-Martín, A., Aghajanian, C., Bradley, W., Mathews, C., Liu, J., Lowe, E.S., Bloomfield, R., and DiSilvestro, P. (2018). Maintenance Olaparib in Patients with Newly Diagnosed Advanced Ovarian Cancer. N Engl J Med. *379*, 2495-2505.
54. Najafi, M., Cheki, M., Rezapoor, S., Geraily, G., Motevaseli, E., Carnovale, C., Clementi, E., and Shirazi, A. (2018). Metformin: Prevention of genomic instability and cancer: A review. Mutat Res Genet Toxicol Environ Mutagen. *827*, 1-8.
55. Ohnishi, S., Mizutani, H., and Kawanishi, S. (2016). The enhancement of oxidative DNA damage by anti-diabetic metformin, buformin, and phenformin, via nitrogen-centered radicals. Free Radic Res. *50*, 929-937.
56. Onaran, I., Guven, G.S., Ozdaş, S.B., Kanigur, G., and Vehid, S. (2006). Metformin does not prevent DNA damage in lymphocytes despite its antioxidant properties against cumene hydroperoxide-induced oxidative stress. Mutat Res. *611*, 1-8.
57. Owen, M.R., Doran, E., and Halestrap, A.P. (2000). Evidence that metformin exerts its anti-diabetic effects through inhibition of complex 1 of the mitochondrial respiratory chain. Biochem J. *348*, 607-614.
58. Ozols, R.F., Bookman, M.A., Connolly, D.C., Daly, M.B., Godwin, A.K., Schilder, R.J., Xu, X., and Hamilton, T.C. (2004). Focus on epithelial ovarian cancer. Cancer Cell. *5*, 19-24.

59. Park, J.H., Kim, Y.H., Park, E.H., Lee, S.J., Kim, H., Kim, A., Lee, S.B., Shim, S., Jang, H., Myung, J.K., Park, S., Lee, S.J., and Kim, M.J. (2019). Effects of metformin and phenformin on apoptosis and epithelial-mesenchymal transition in chemoresistant rectal cancer. Cancer Sci. *110*, 2834-2845.

60. Patel, S., Kumar, L., and Singh, N. (2015). Metformin and epithelial ovarian cancer therapeutics. Cell Oncol (Dordr). *38*, 365-375.

61. Phelan, C.M., Kuchenbaecker, K.B., Tyrer, J.P., Kar, S.P., Lawrenson, K., Winham, S.J., Dennis, J., Pirie, A., Riggan, M.J., Chornokur, G., Earp, M.A., Lyra, P.C. Jr., Lee, J.M., Coetzee, S., Beesley, J., McGuffog, L., Soucy, P., Dicks, E., Lee, A., Barrowdale, D., Lecarpentier, J., Leslie, G., Aalfs, C.M., Aben, K.K.H., Adams, M., Adlard, J., Andrulis, I.L., Anton-Culver, H., Antonenkova, N., AOCS study group, Aravantinos, G., Arnold, N., Arun, B.K., Arver, B., Azzollini, J., Balmaña, J., Banerjee, S.N., Barjhoux, L., Barkardottir, R.B., Bean, Y., Beckmann, M.W., Beeghly-Fadiel, A., Benitez, J., Bermisheva, M., Bernardini, M.Q., Birrer, M.J., Bjorge, L., Black, A., Blankstein, K., Blok, M.J., Bodelon, C., Bogdanova, N., Bojesen, A., Bonanni, B., Borg, Å., Bradbury, A.R., Brenton, J.D., Brewer, C., Brinton, L., Broberg, P., Brooks-Wilson, A., Bruinsma, F., Brunet, J., Buecher, B., Butzow, R., Buys, S.S., Caldes, T., Caligo, M.A., Campbell, I., Cannioto, R., Carney, M.E., Cescon, T., Chan, S.B., Chang-Claude, J., Chanock, S., Chen, X.Q., Chiew, Y.E., Chiquette, J., Chung, W.K., Claes, K.B.M., Conner, T., Cook, L.S., Cook, J., Cramer, D.W., Cunningham, J.M., D'Aloisio, A.A., Daly, M.B., Damiola, F., Damirovna, S.D., Dansonka-Mieszkowska, A., Dao, F., Davidson, R., DeFazio, A., Delnatte, C., Doheny, K.F., Diez, O., Ding, Y.C., Doherty, J.A., Domchek, S.M., Dorfling, C.M., Dörk, T., Dossu,s L., Duran, M., Dürst, M., Dworniczak, B., Eccles, D., Edwards, T., Eeles, R., Eilber, U., Ejlertsen, B., Ekici, A.B., Ellis, S., Elvira, M., EMBRACE Study, Eng, K.H., Engel, C., Evans, D.G., Fasching, P.A., Ferguson, S., Ferrer, S.F., Flanagan, J.M., Fogarty, Z.C., Fortner, R.T., Fostira, F., Foulkes, W.D., Fountzilas, G., Fridley, B.L., Friebel, T.M., Friedman, E., Frost, D., Ganz, P.A., Garber, J., García, M.J., Garcia-Barberan, V., Gehrig, A., GEMO Study Collaborators, Gentry-Maharaj, A., Gerdes, A.M., Giles, G.G., Glasspool, R., Glendon, G., Godwin, A.K., Goldgar, D.E., Goranova, T., Gore, M., Greene, M.H., Gronwald, J., Gruber, S., Hahnen, E., Haiman, C.A., Håkansson, N., Hamann, U., Hansen, T.V.O., Harrington, P.A., Harris, H.R., Hauke, J., HEBON Study, Hein, A., Henderson, A., Hildebrandt, M.A.T., Hillemanns, P., Hodgson, S., Høgdall, C.K., Høgdall, E., Hogervorst, F.B.L., Holland, H.,

Hooning, M.J., Hosking, K., Huang, R.Y., Hulick, P.J., Hung, J., Hunter, D.J., Huntsman, D.G., Huzarski, T., Imyanitov, E.N., Isaacs, C., Iversen, E.S., Izatt, L., Izquierdo, A., Jakubowska, A., James, P., Janavicius, R., Jernetz, M., Jensen, A., Jensen, U.B., John, E.M., Johnatty, S., Jones, M.E., Kannisto, P., Karlan, B.Y., Karnezis, A., Kast, K., KConFab Investigators, Kennedy, C.J., Khusnutdinova, E., Kiemeney, L.A., Kiiski, J.I., Kim, S.W., Kjaer, S.K., Köbel, M., Kopperud, R.K., Kruse, T.A., Kupryjanczyk, J., Kwong, A., Laitman, Y., Lambrechts, D., Larrañaga, N., Larson, M.C., Lazaro, C., Le, N.D., Le Marchand, L., Lee, J.W., Lele, S.B., Leminen, A., Leroux, D., Lester, J., Lesueur, F., Levine, D.A., Liang, D., Liebrich, C., Lilyquist, J., Lipworth, L., Lissowska, J., Lu, K.H., Lubiński, J., Luccarini, C., Lundvall, L., Mai, P.L., Mendoza-Fandiño, G., Manoukian, S., Massuger, L.F.A.G., May, T., Mazoyer, S., McAlpine, J.N., McGuire, V., McLaughlin, J.R., McNeish, I., Meijers-Heijboer, H., Meindl, A., Menon, U., Mensenkamp, A.R., Merritt, M.A., Milne, R.L., Mitchell, G., Modugno, F., Moes-Sosnowska, J., Moffitt, M., Montagna, M., Moysich, K.B., Mulligan, A.M., Musinsky, J., Nathanson, K.L., Nedergaard, L., Ness, R.B., Neuhausen, S.L., Nevanlinna, H., Niederacher, D., Nussbaum, R.L., Odunsi, K., Olah, E., Olopade, O.I., Olsson, H., Olswold, C., O'Malley, D.M., Ong, K.R., Onland-Moret, N.C., OPAL study group, Orr, N., Orsulic, S., Osorio, A., Palli, D., Papi, L., Park-Simon, T.W., Paul, J., Pearce, C.L., Pedersen, I.S., Peeters, P.H.M., Peissel, B., Peixoto, A., Pejovic, T., Pelttari, L.M., Permuth, J.B., Peterlongo, P., Pezzani, L., Pfeiler, G., Phillips, K.A., Piedmonte, M., Pike, M.C., Piskorz, A.M., Poblete, S.R., Pocza, T., Poole, E.M., Poppe, B., Porteous, M.E, Prieur, F., Prokofyeva, D., Pugh, E., Pujana, M.A., Pujol, P., Radice, P., Rantala, J., Rappaport-Fuerhauser, C., Rennert, G., Rhiem, K., Rice, P., Richardson, A., Robson, M., Rodriguez, G.C., Rodríguez-Antona, C., Romm, J., Rookus, M.A., Rossing, M.A., Rothstein, J.H., Rudolph, A., Runnebaum, I.B., Salvesen, H.B., Sandler, D.P., Schoemaker, M.J., Senter, L., Setiawan, V.W., Severi, G., Sharma, P., Shelford, T., Siddiqui, N., Side, L.E., Sieh, W., Singer, C.F., Sobol, H., Song, H., Southey, M.C., Spurdle, A.B., Stadler, Z., Steinemann, D., Stoppa-Lyonnet, D., Sucheston-Campbell, L.E., Sukiennicki, G., Sutphen, R., Sutter, C., Swerdlow, A.J., Szabo, C.I., Szafron, L., Tan, Y.Y., Taylor, J.A., Tea, M.K., Teixeira, M.R., Teo, S.H., Terry, K.L., Thompson, P.J., Thomsen, L.C.V., Thull, D.L., Tihomirova, L., Tinker, A.V., Tischkowitz, M., Tognazzo, S., Toland, A.E., Tone, A., Trabert, B., Travis, R.C., Trichopoulou, A., Tung, N., Tworoger, S.S., van Altena, A.M., Van Den Berg, D., van der Hout, A.H., van der Luijt, R.B., Van Heetvelde, M., Van Nieuwenhuysen, E., van Rensburg, E.J., Vanderstichele, A., Varon-Mateeva, R., Vega,

A., Edwards, D.V., Vergote, I., Vierkant, R.A., Vijai, J., Vratimos, A., Walker, L., Walsh, C., Wand, D., Wang-Gohrke, S., Wappenschmidt, B., Webb, P.M., Weinberg, C.R., Weitzel, J.N., Wentzensen, N., Whittemore, A.S., Wijnen, J.T., Wilkens, L.R., Wolk, A., Woo, M., Wu, X., Wu, A.H., Yang, H., Yannoukakos, D., Ziogas, A., Zorn, K.K., Narod, S.A., Easton, D.F., Amos, C.I., Schildkraut, J.M., Ramus, S.J., Ottini, L., Goodman, M.T., Park, S.K., Kelemen, L.E., Risch, H.A., Thomassen, M., Offit, K., Simard, J., Schmutzler, R.K., Hazelett, D., Monteiro, A.N., Couch, F.J., Berchuck, A., Chenevix-Trench, G., Goode, E.L., Sellers, T.A., Gayther, S.A., Antoniou, A.C., and Pharoah, P.D.P. (2017). Identification of 12 new susceptibility loci for different histotypes of epithelial ovarian cancer. Nat Genet. *49*, 680-691.

62. Rattan, R., Giri, S., Hartmann, L.C., and Shridhar, V. (2011a). Metformin attenuates ovarian cancer cell growth in an AMP-kinase dispensable manner. J Cell Mol Med. *15*, 166-178.
63. Rattan, R., Graham, R.P., Maguire, J.L., Giri, S., and Shridhar, V. (2011b). Metformin suppresses ovarian cancer growth and metastasis with enhancement of cisplatin cytotoxicity in vivo. Neoplasia. *13*, 483-491.
64. Sanchez-Rangel, E., and Inzucchi, S.E. (2017). Metformin: clinical use in type 2 diabetes. Diabetologia. *60*, 1586-1593.
65. Shank, J.J., Yang, K., Ghannam, J., Cabrera, L., Johnston, C.J., Reynolds, R.K., and Buckanovich, R.J. (2012). Metformin targets ovarian cancer stem cells in vitro and in vivo. Gynecol Oncol. *127*, 390-397.
66. Siegel, R.L., Miller, K.D., and Jemal, A. (2020). Cancer statistics, 2020. CA Cancer J Clin. *70*, 7-30.
67. Stewart, L.M., Spilsbury, K., Jordan, S., Stewart, C., Holman, C.D.J., Powell, A., Reekie, J., and Cohen, P. (2018). Risk of high-grade serous ovarian cancer associated with pelvic inflammatory disease, parity and breast cancer. Cancer Epidemiol. *55*, 110-116.
68. Testa, U., Petrucci, E., Pasquini, L., Castelli, G., and Pelosi, E. (2018). Ovarian cancers: Genetic abnormalities, tumor heterogeneity and progression, clonal evolution and cancer stem cells. Medicines (Basel). *5*, E16.
69. Tebbe, C., Chhina, J., Dar, S.A., Sarigiannis, K., Giri, S., Munkarah, A.R., and Rattan, R. (2014). Metformin limits the adipocyte tumor-promoting effect on ovarian cancer. Oncotarget. *5*, 4746-4764.

70. Tobinick, E.L. (2009). The value of drug repositioning in the current pharmaceutical market. Drug News Perspect. *22*, 119-125.
71. Tseng, S.C., Huang, Y.C., Chen, H.J., Chiu, H.C., Huang, Y.J., Wo, T.Y., Weng, S.H., and Lin, Y.W. (2013). Metformin-mediated downregulation of p38 mitogen-activated protein kinase-dependent excision repair cross-complementing 1 decreases DNA repair capacity and sensitizes human lung cancer cells to paclitaxel. Biochem Pharmacol. *85*, 583-594.
72. Tumiati, M., Hietanen, S., Hynninen, J., Pietilä, E., Färkkilä, A., Kaipio, K., Roering, P., Huhtinen, K., Alkodsi, A., Li, Y., Lehtonen, R., Erkan, E.P., Tuominen, M.M., Lehti, K., Hautaniemi, S.K., Vähärautio, A., Grénman, S., Carpén, O., and Kauppi, L. (2018). A functional homologous recombination assay predicts primary chemotherapy response and long-term survival in ovarian cancer patients. Clin Cancer Res. *24*, 4482-4493.
73. Tumiati, M. (Genome Stability Group, University of Helsinki, Helsinki, Finland). In preparation.
74. Webb, P.M., and Jordan, S.J. (2017). Epidemiology of epithelial ovarian cancer. Best Pract Res Clin Obstet Gynaecol. *41*, 3-14.
75. Wu, B., Li, S., Sheng, L., Zhu, J., Gu, L., Shen, H., La, D., Hambly, B.D., Bao, S., and Di, W. (2012). Metformin inhibits the development and metastasis of ovarian cancer. Oncol Rep. *28*, 903-908.
76. Xu, S., Yang, Z., Jin, P., Yang, X., Li, X., Wei, X., Wang, Y., Long, S., Zhang, T., Chen, G., Sun, C., Ma, D., and Gao, Q. (2018). Metformin suppresses tumor progression by inactivating stromal fibroblasts in ovarian cancer. Mol Cancer Ther. *17*, 1291-1302.
77. Yang, C., Zhao, N., Li, D., Zou, G., and Chen, Y. (2019). Metformin improves the sensitivity of ovarian cancer cells to chemotherapeutic agents. Oncol Lett. *18*, 2404-2411.
78. Zakikhani, M., Dowling, R., Fantus, I.G., Sonenberg, N., and Pollak, M. (2006). Metformin is an AMP kinase-dependent growth inhibitor for breast cancer cells. Cancer Res. *66*, 10269-10273.
79. Zakikhani, Z., Dowling, R.J., Sonenberg, N., and Pollak, M.N. (2008). The effects of adiponectin and metformin on prostate and colon neoplasia involve activation of AMP-activated protein kinase. Cancer Prev Res (Phila). *1*, 369-375.
80. Zhang, N., Liu, X., Li, L., and Legerski, R. (2007). Double-strand breaks induce homologous recombinational repair of interstrand cross-links via cooperation of MSH2, ERCC1-XPF, REV3, and the Fanconi anemia pathway. DNA Repair (Amst). *6*, 1670-1678.

APPENDICES

Appendix A: Table of Resources

	Name, Manufacturer/Source, Additional Information
Cells	• Kuramochi Commercial Cell Line. Initial Passage 20. Source: Genome Stability Group (Kauppi Lab), Biomedicum 1, University of Helsinki. • OVCAR4 Commercial Cell Line. Initial Passage x+3 (explanation: "x" means unknown – laboratory received the cells not knowing the exact passage, and then the cells were additionally passaged 3 times afterward). Source: Genome Stability Group (Kauppi Lab), Biomedicum 1, University of Helsinki.
Chemicals, Nutrients etc.	• Calcium Chloride, fused, granular, general purpose grade. Fisher Scientific, C/1400/53. • Magnesium Chloride hexa-hydrate, BioXtra, ≥ 99,0 %. Sigma-Aldrich, M2670-100G. • Phosphate-Buffered Saline (PBS) Tablets. Medicago, 09-9400-100. • Bovine Serum Albumin (BSA), fatty acids free lyophilized; stored in 4 ºC. biowest, P6156- 100GR. • Glycine, ≥ 99 %. Sigma-Aldrich, G8898-500G. • Triton® X-100. Fisher Scientific, BP151-100. • RPMI 1640 Growth Medium. Corning®, 15-040-CVR. • Fetal Bovine Serum (FBS). gibco, Thermo Fisher Scientific, 10270-106. It is heated to 56 ºC to inactivate the complement, then aliquots are made and stored in -20 ºC. • Glutamine. GlutaMAX™-I(100X), gibco® by Life Technologies, 35050-038. • Penicillin-streptomycin (P/S) ([+] 10,000 units/ml penicillin and [+] 10,000 µg/ml streptomycin). gibco® by Life Technologies, 15140-122. • 0,25 % Trypsin/EDTA (1X). Life Technologies Limited, 25200-056.

	• Dimethyl Sulfoxide (DMSO). MP Biomedicals, 196055. • Trypan Blue Stain, 0,4 %. Logos Biosystems, T13001. • Metformin Hydrochloride. MP Biomedicals, 151691. Molecular Weight: 165,63 g/mol. • Paraformaldehyde (PFA), 96 %, extra pure. Acros Organics, 416780010. • Hoechst 33342, trihydrochloride, trihydrate, 10 mg/ml; stored in 4 ºC. invitrogen, Molecular Probes by Life Technologies, H3570.
Antibodies	• Mouse anti-γH2AX (Ser139+140), Primary Antibody; stored in -20 ºC. abcam, 22551. • Rabbit anti-Ki67, Primary Antibody; stored in -20 ºC. abcam, 15580. • Rabbit anti-cCasp3, Primary Antibody; stored in -20 ºC. Cell Signaling Technology, 9664. • Goat anti-Mouse IgG Alexa Fluor 488, Secondary Antibody; stored in 4 ºC. Molecular Probes, A 11029. • Goat anti-Mouse IgG Alexa Fluor 647, Secondary Antibody; stored in 4 ºC. Molecular Probes, A 21245.
Microscopy Equipment	• Invitrogen™ EVOS™ XL Core Cell Imaging System. Thermo Fisher Scientific. • Thermo Cellinsight High Content Imager. Thermo Fisher Scientific. • ImageXpress® Pico Automated Cell Imaging System. Molecular Devices.
Other Devices and Equipment	• HERAfreeze™ HLE Series Freezer (-80 ºC). Thermo Scientific. Model Number: HLE50086V; Item Number: 155VE5CO2M; Serial Number: 1119782801190221. • Ultra Low Freezer (-150 ºC). Sanyo, MDF-C2156VAN. • CoolCell® LX Cell Freezing Containers. BioCision. • BIOWIZARD Platinum 130 SF Class II Laminar Flow Cabinet. Kojair. • Heraeus BB 15 Function Line Incubator. Thermo Fisher Scientific. • Isotemp® GPD 10 Water Bath. Fisher Scientific. • Eppendorf® Centrifuge 5804R.

	• Luna-fl™ Dual Fluorescence Cell Counter. Logos Biosystems. • Luna™ Cell Counting Slides. Logos Biosystems, L12001. • Mini See-Saw Rocker SSM4. Stuart. • BIOHIT Sartorius mLINE® mechanical pipette, 8-channel (30-300 µl). • BIOHIT Proline Plus single channel pipette (0,5-10 µl). • BIOHIT m (10-100 µl) pipette. • BIOHIT Proline Plus single channel (100-1000 µl) pipette. • BIOHIT MidiPlus pipette. • BioLite Tissue Culture Dish, 100 mm. Thermo Fisher Scientific, 130182. • Nunclon™ Delta Surface 96-Well Cell Culture Plates. Thermo Fisher Scientific, 167008. • Nalgene® Cryoware Cryogenic Vials. Thermo Fisher Scientific, 5000-0020. • Corning® 50 ml Centrifuge Tube, CentriStar™ Cap. 430829. • Corning® 15 ml Centrifuge Tube, CentriStar™ Cap. 430791. • Eppendorf Tubes®, 5,0 ml. 0030119487. • Emerald™ Syringe, 10 ml. Becton Dickinson, 307736. • Inject® Luer Solo Syringe, 20 ml. B. Braun, 4606205V. • Microlance™ 3, 20G 1 ½“ - Nr. 1, 0,9 x 40 mm. Becton Dickinson, 301300. • Millex®GP Filter Unit 0,22 µm, Millipore Express® PES Membrane. Merck Millipore, SLGP033RS. • Parafilm® M Laboratory Film. Bemis, PM-999.
Software	• Cellomics Navigator – software for working with Thermo Cellinsight. • MD.CellReporterXpress® by Molecular Devices® – software for working with ImageXpress® Pico. • ImageJ – public domain Java image processing program. Fiji – image processing package with a variety of plugins for scientific image analysis.

	URL: https://imagej.net/Fiji • Online file conversion tool (CSV to XLSX). URL: https://convertio.co/csv-xlsx/ • Online calculator for statistical significance. URL: https://www.medcalc.org/calc/fisher.php • MS Paint – basic graphics and painting program for creating custom images • Adobe Photoshop CS6 – graphics editing software for creating custom images
Solutions Made in the Laboratory	• Growth Medium: RPMI 1640 growth medium is supplemented with 10 % FBS, 2 mM glutamine, and 1 % P/S. • PBS: 1 PBS tablet is dissolved in 1 l of MilliQ. • PBS++: 1 l of PBS is supplemented with 1 mM $CaCl_2$ and 0,5 mM $MgCl_2$. • 2 % PFA/PBS++: PFA is diluted in PBS++ to make a 2 % solution, which is then stored in -20 ºC. • Permeabilization buffer: 100 ml of PBS++ is supplemented with 0,2 % Triton X-100. • Staining buffer: 250 ml of PBS is supplemented with 0,5 % BSA, 0,15 % glycine, and 0,1 % Triton X-100; stored in 4 ºC.

Appendix B: Macros Used in the First Experiment

Macro for Channel 1 – Hoechst:

```
run("Auto Threshold", "method=Li white");
run("Watershed");
run("Watershed");
run("Analyze Particles...", "size=200-Infinity pixel show=[Masks] exclude summarize");
run("Create Selection");
run("Make Inverse");
```

```
run("Copy");
```

Macro for Channel 2 – γH2AX:

```
run("Paste");
setBackgroundColor(0, 0, 0);
run("Clear", "slice");
run("Select None");
run("Duplicate...", "title=gH2Ax.TIF");
run("Auto Threshold", "method=Default ignore_black ignore_white white");
run("Despeckle");
run("Analyze Particles...", "size=150-Infinity pixel show=Masks exclude summarize");
```

Macro for Channel 3 – Ki67:

```
run("Paste");
run("Undo");
run("Clear", "slice");
run("Select None");
run("Duplicate...", "title=Ki67.TIF");
run("Auto Threshold", "method=Default ignore_black ignore_white white");
run("Despeckle");
run("Options...", "iterations=3 count=2 black pad do=Dilate");
run("Analyze Particles...", "size=150-Infinity pixel show=Masks exclude summarize");
```

Macro for Channel 3 – cCasp3:

```
run("Subtract Background...", "rolling=200");
run("Paste");
run("Undo");
run("Clear Outside");
run("Select None");
run("Duplicate...", "title=cCasp3.TIF");
run("Out [-]");
run("Enhance Contrast...", "saturated=0.3");
run("Auto Threshold", "method=RenyiEntropy white");
run("Options...", "iterations=21 count=3 black do=Dilate");
```

```
run("Analyze Particles...", "size=400-Infinity pixel show=[Bare Outlines] exclude summarize");
run("Out [-]");
```

Appendix C: γH2AX Results from Different Staining Combinations

Figure 1. γH2AX results from the γH2AX+Ki67 staining combination used for Kuramochi cells in the first experiment.

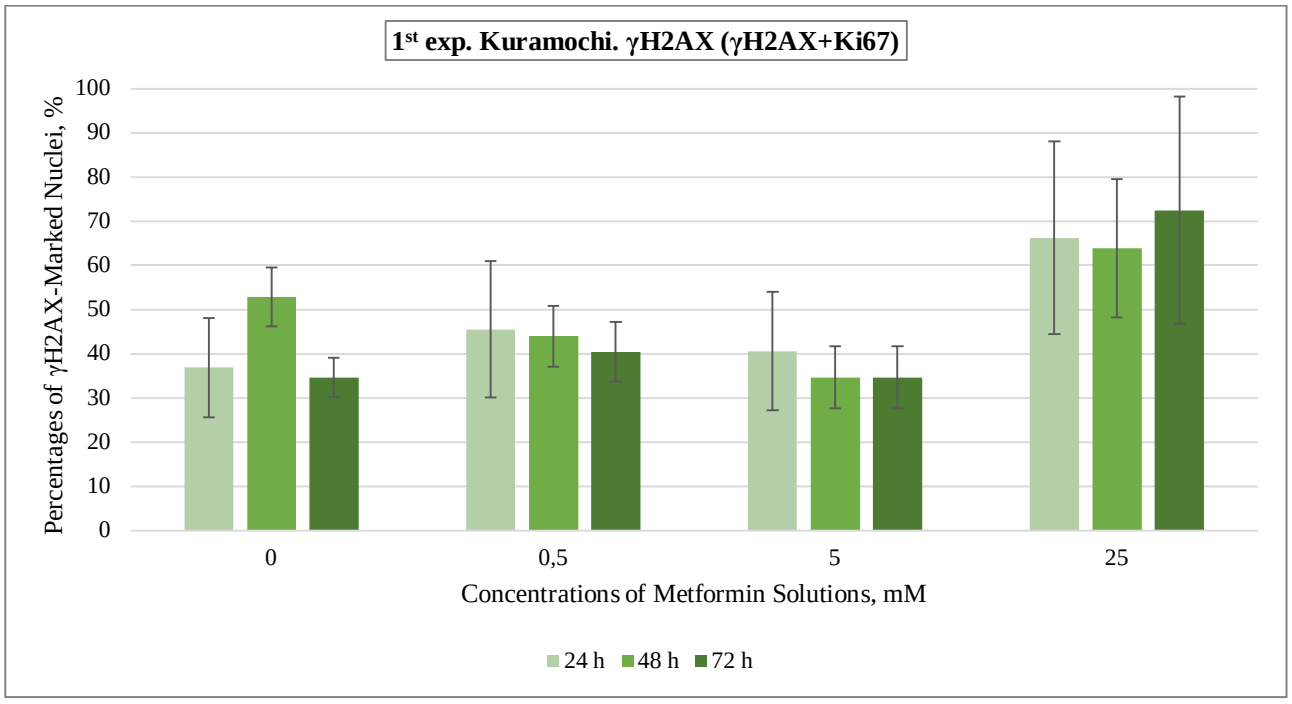

Figure 2. γH2AX results from the γH2AX+cCasp3 staining combination used for Kuramochi cells in the first experiment.

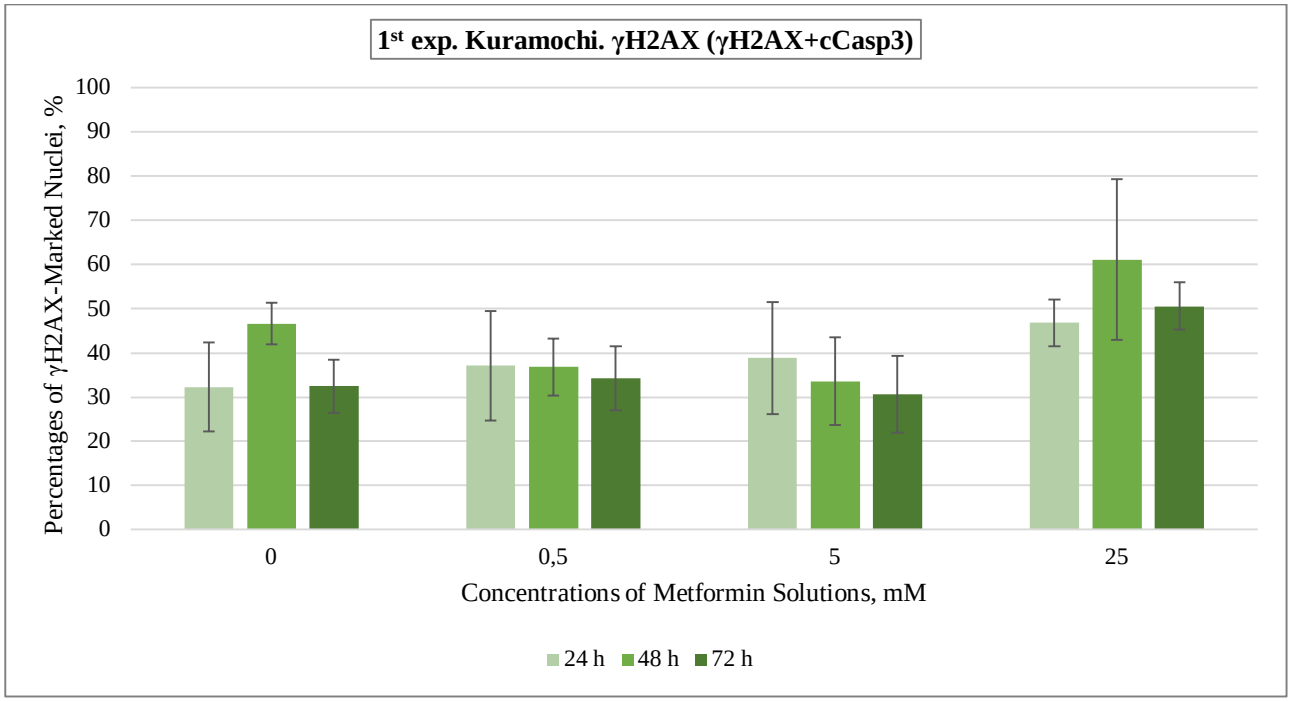

Figure 3. γH2AX results from the γH2AX+Ki67 staining combination used for Kuramochi cells in the second experiment.

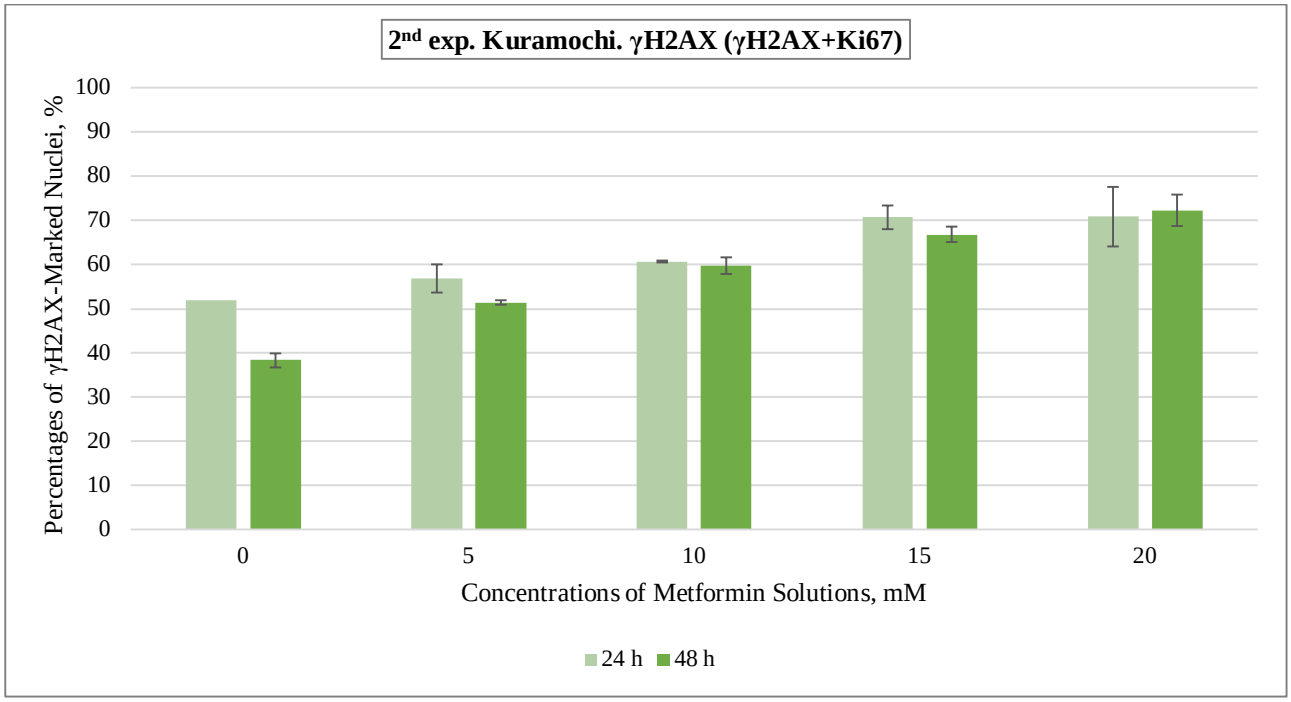

Figure 4. γH2AX results from the γH2AX+cCasp3 staining combination used for Kuramochi cells in the second experiment.

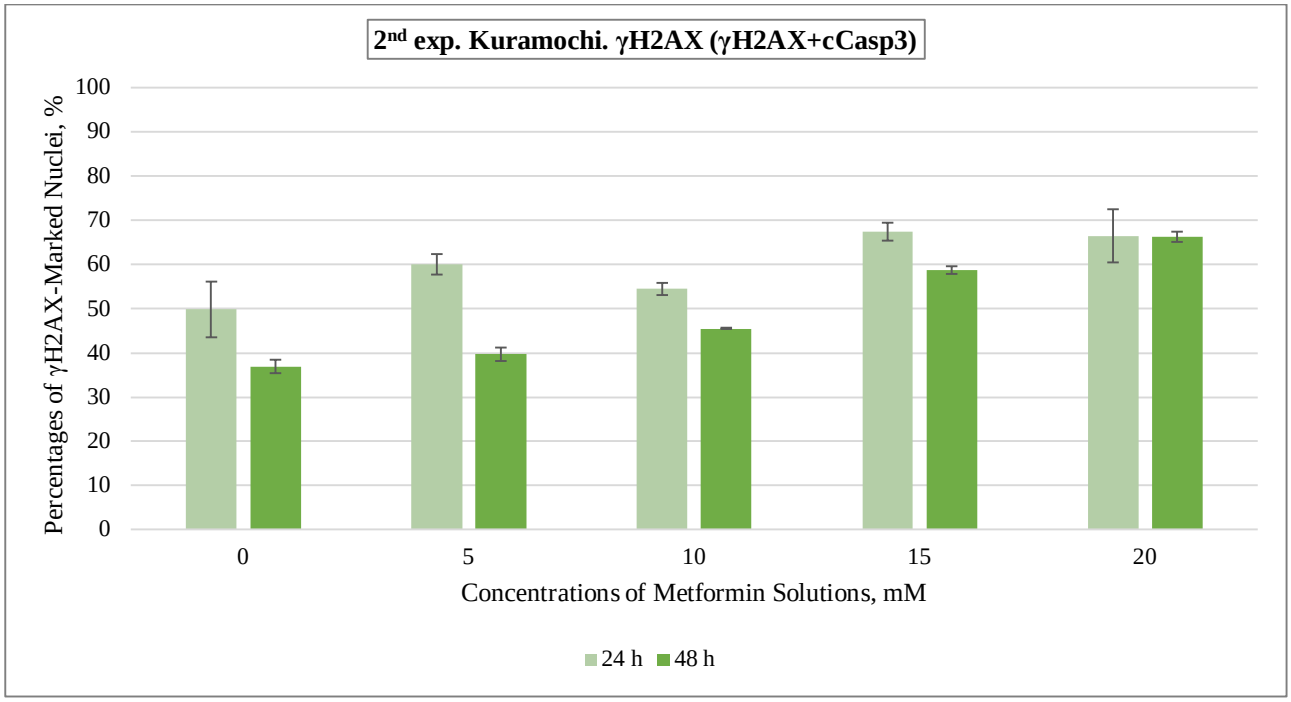

Figure 5. γH2AX results from the γH2AX+Ki67 staining combination used for OVCAR4 cells in the second experiment.

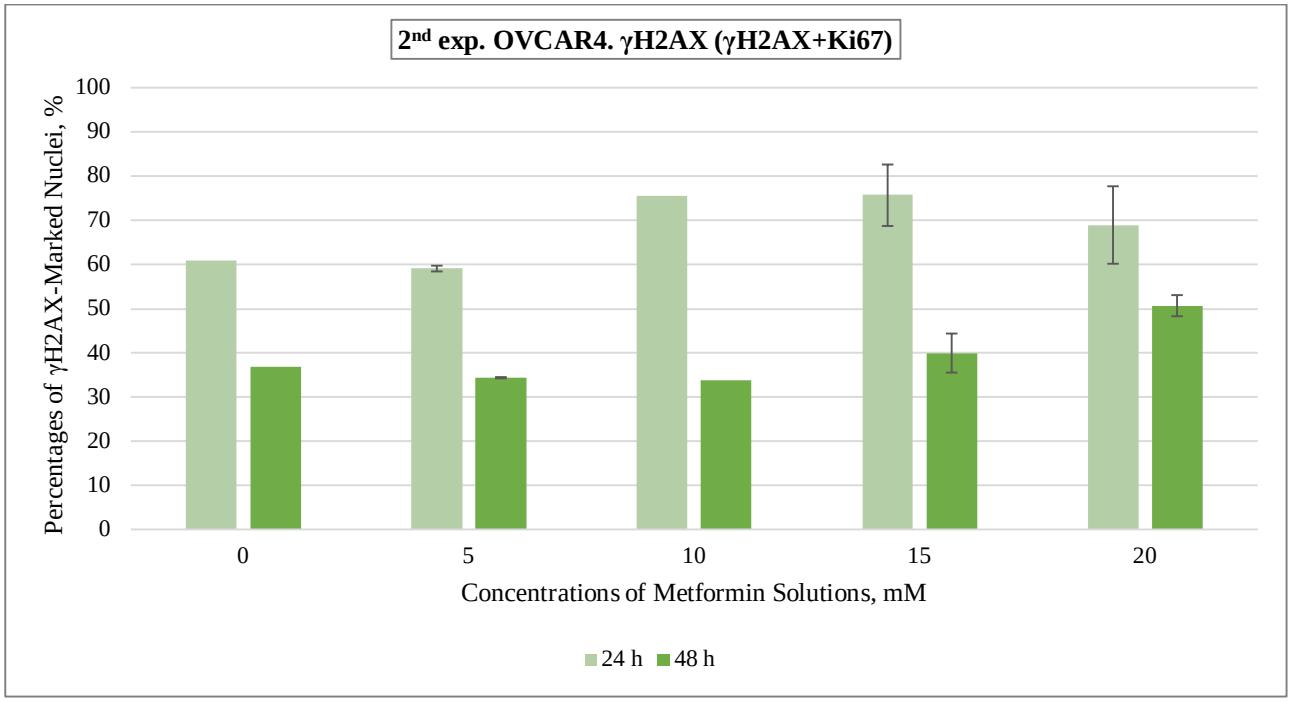

Figure 6. γH2AX results from the γH2AX+cCasp3 staining combination used for OVCAR4 cells in the second experiment.

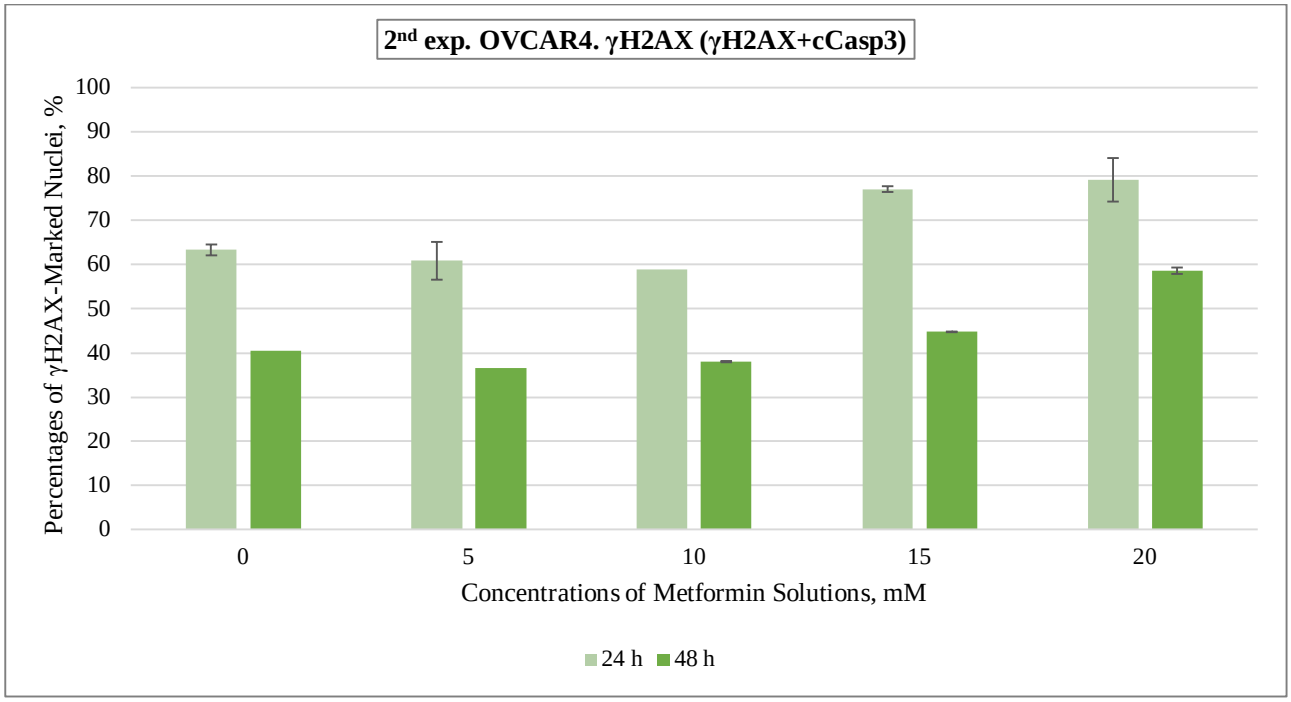

Figure 7. γH2AX results from the γH2AX+Ki67 staining combination used for Kuramochi cells in the no IR+4h part of the third experiment.

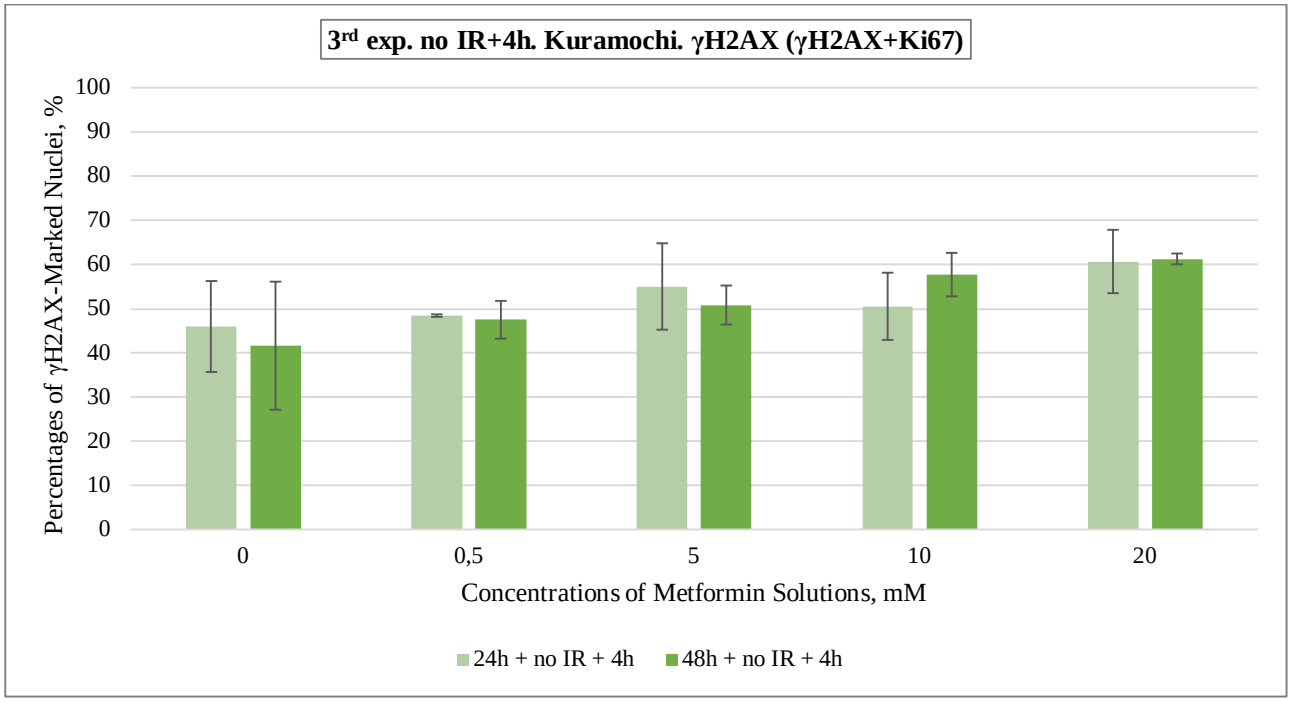

Figure 8. γH2AX results from the γH2AX+cCasp3 staining combination used for Kuramochi cells in the no IR+4h part of the third experiment.

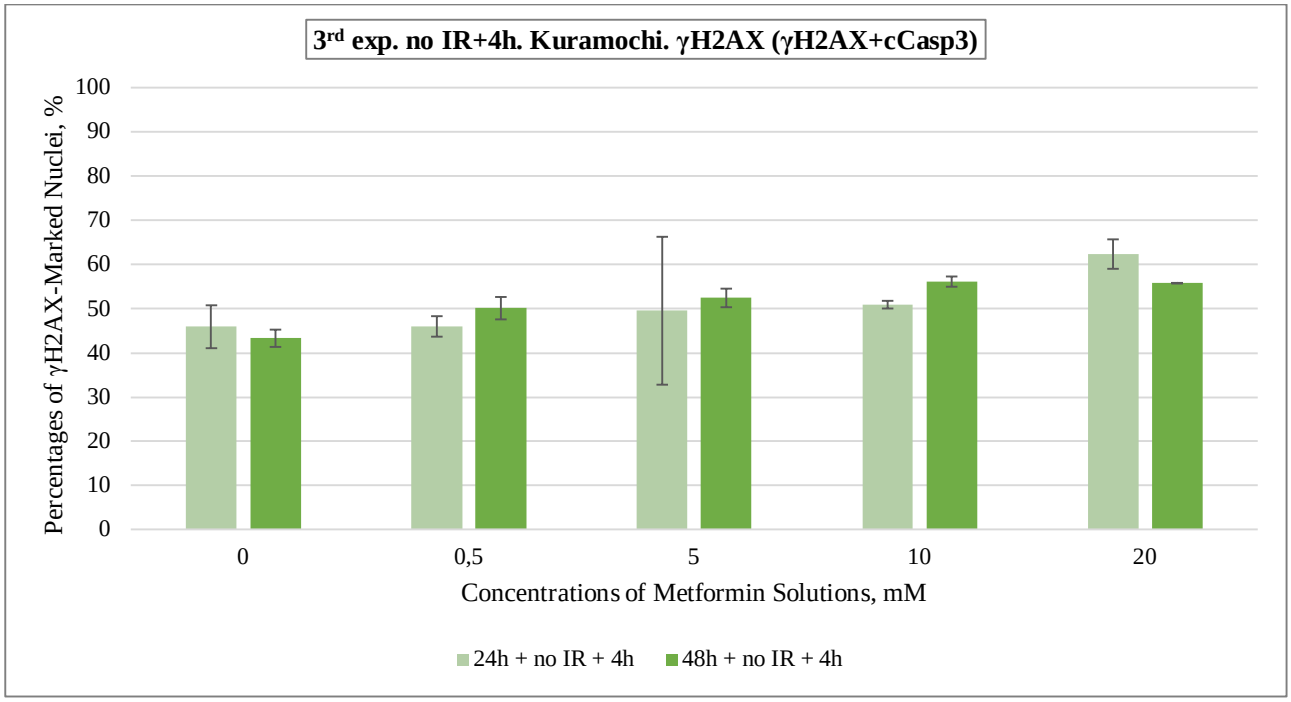

Figure 9. γH2AX results from the γH2AX+Ki67 staining combination used for OVCAR4 cells in the no IR+4h part of the third experiment.

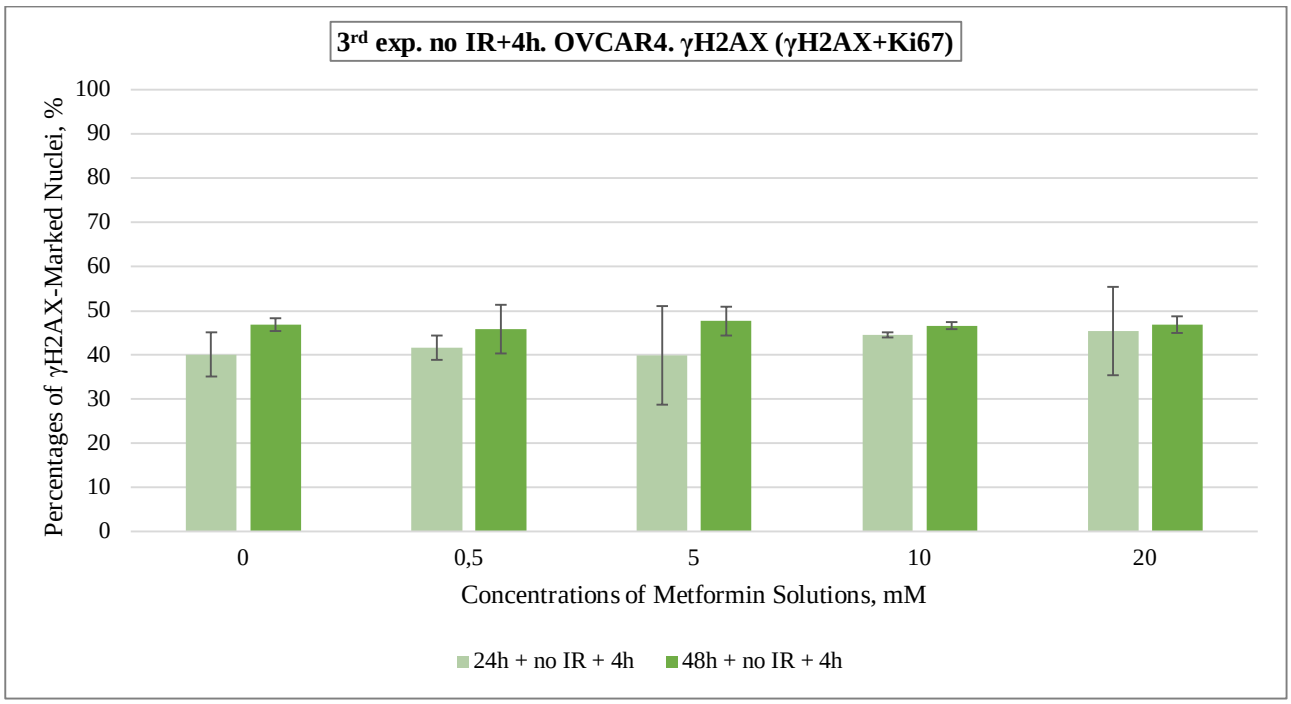

Figure 10. γH2AX results from the γH2AX+cCasp3 staining combination used for OVCAR4 cells in the no IR+4h part of the third experiment.

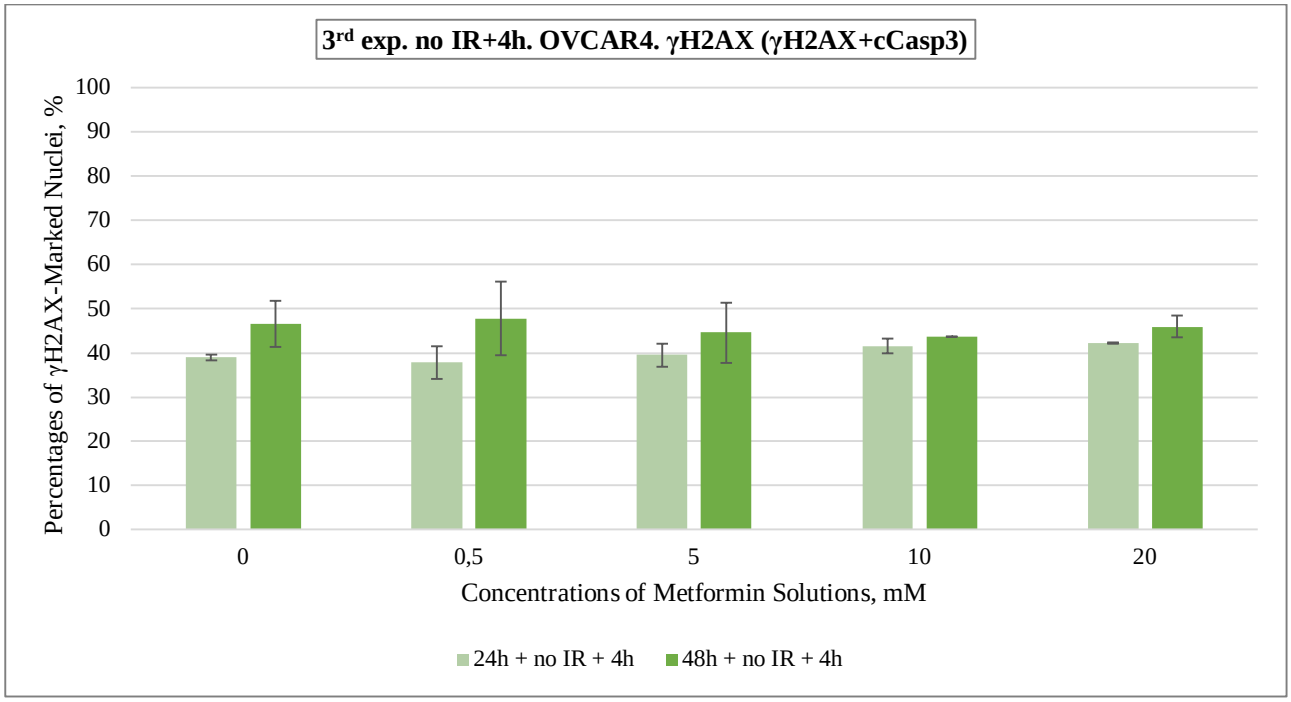

Figure 11. γH2AX results from the γH2AX+Ki67 staining combination used for Kuramochi cells in the no IR+24h part of the third experiment.

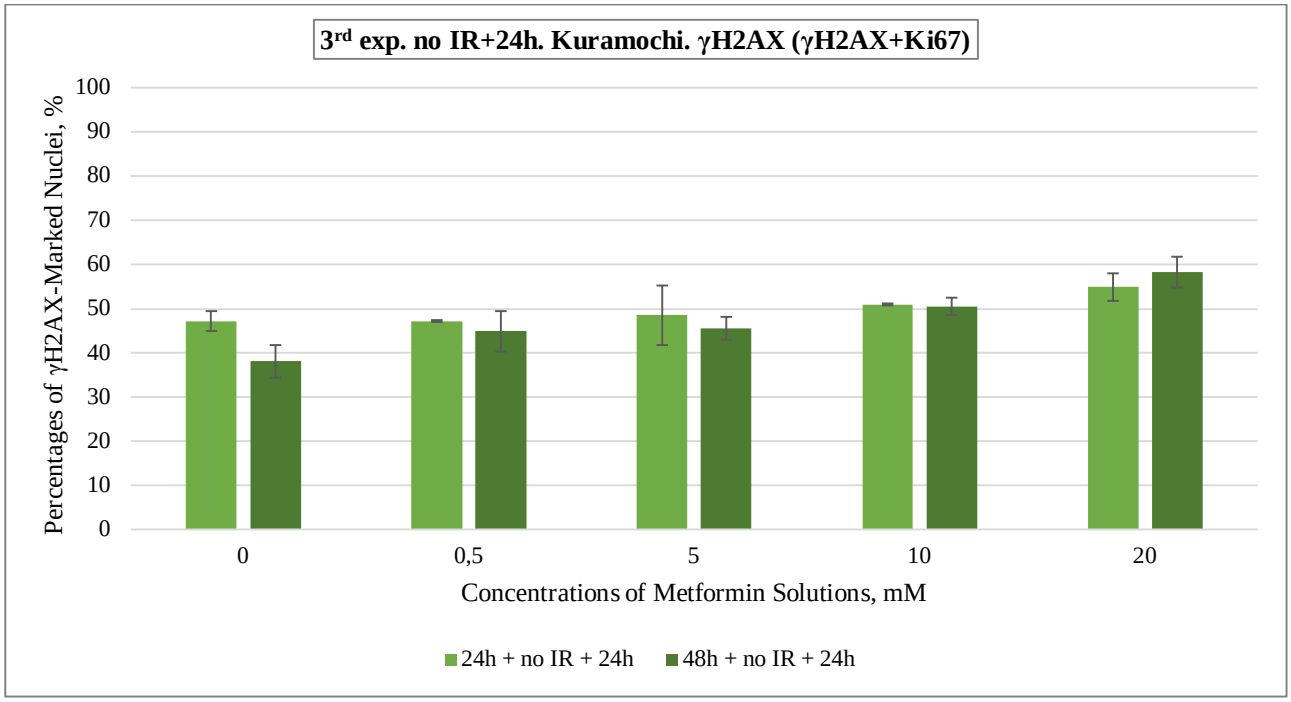

Figure 12. γH2AX results from the γH2AX+cCasp3 staining combination used for Kuramochi cells in the no IR+24h part of the third experiment.

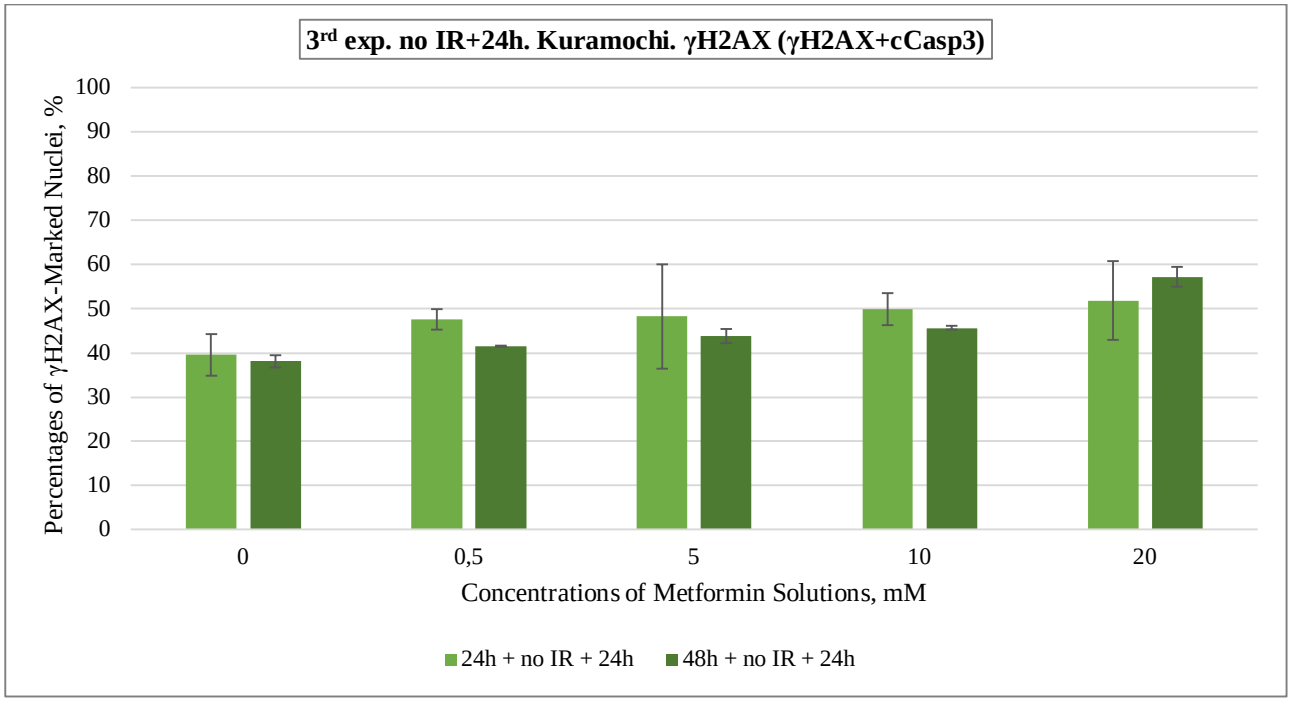

Figure 13. γH2AX results from the γH2AX+Ki67 staining combination used for OVCAR4 cells in the no IR+24h part of the third experiment.

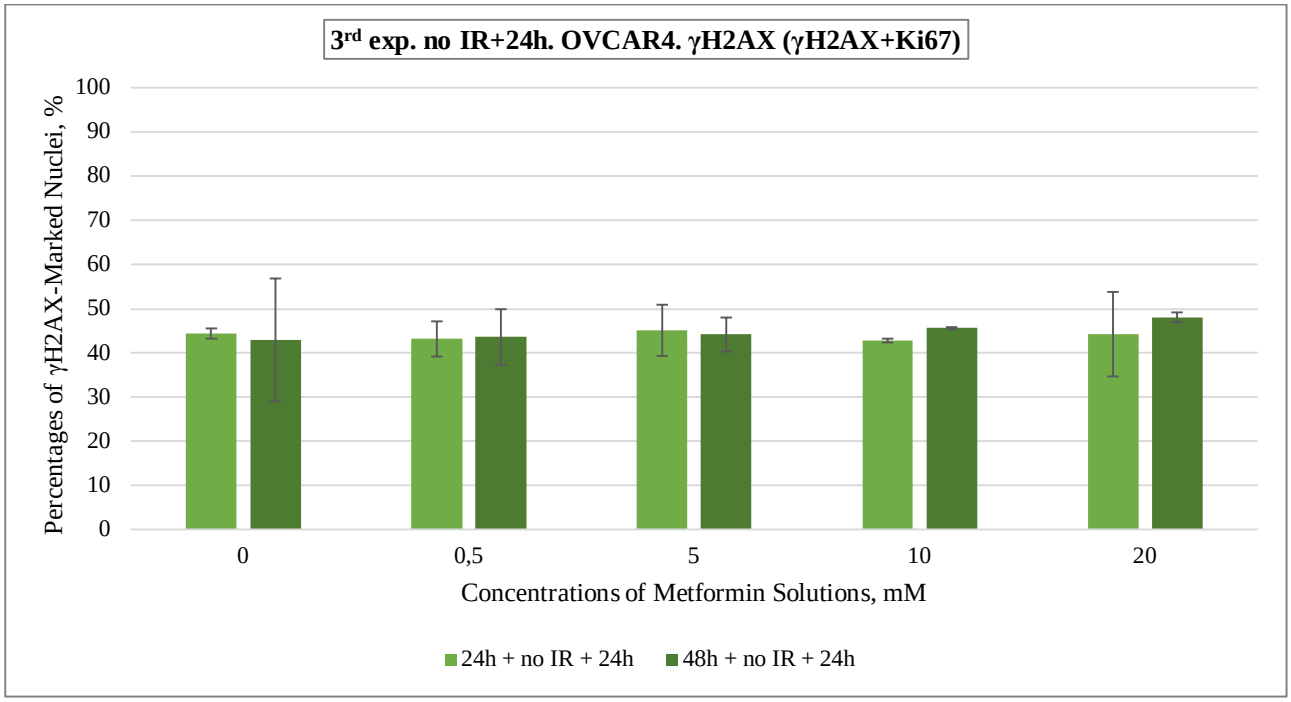

Figure 14. γH2AX results from the γH2AX+cCasp3 staining combination used for OVCAR4 cells in the no IR+24h part of the third experiment.

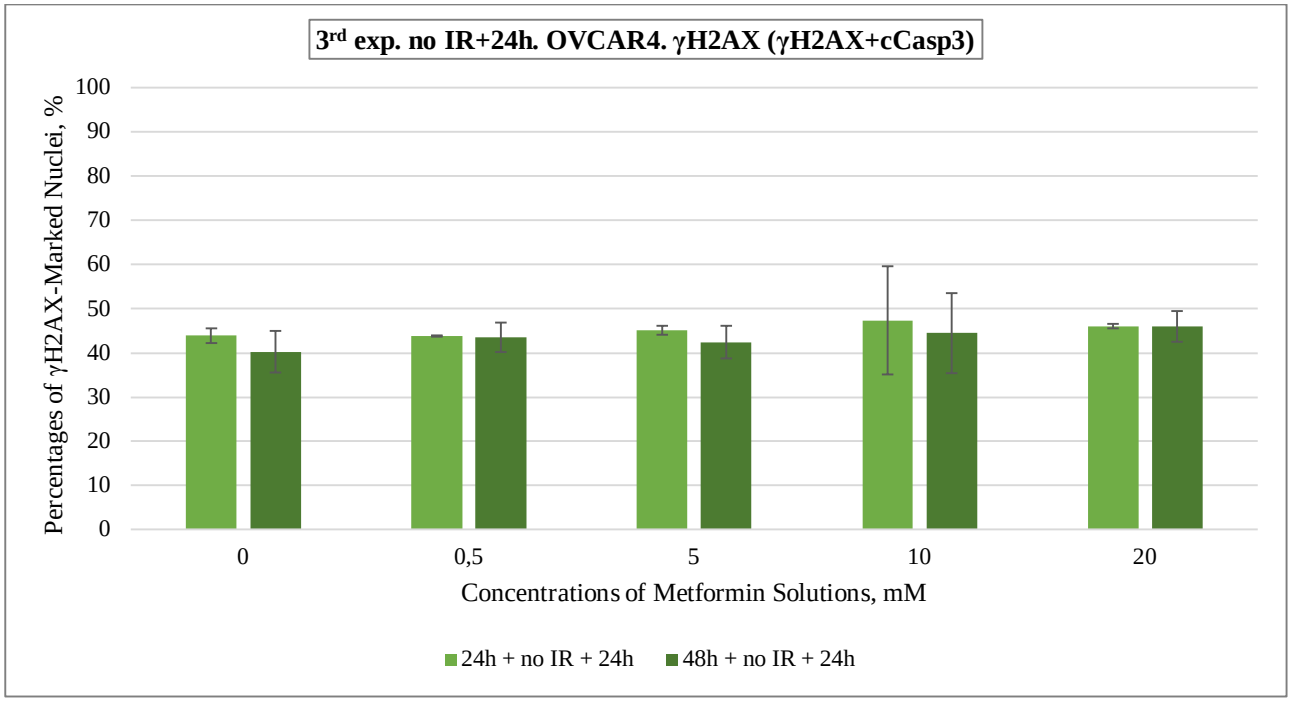

Figure 15. γH2AX results from the γH2AX+Ki67 staining combination used for Kuramochi cells in the IR+4h part of the third experiment.

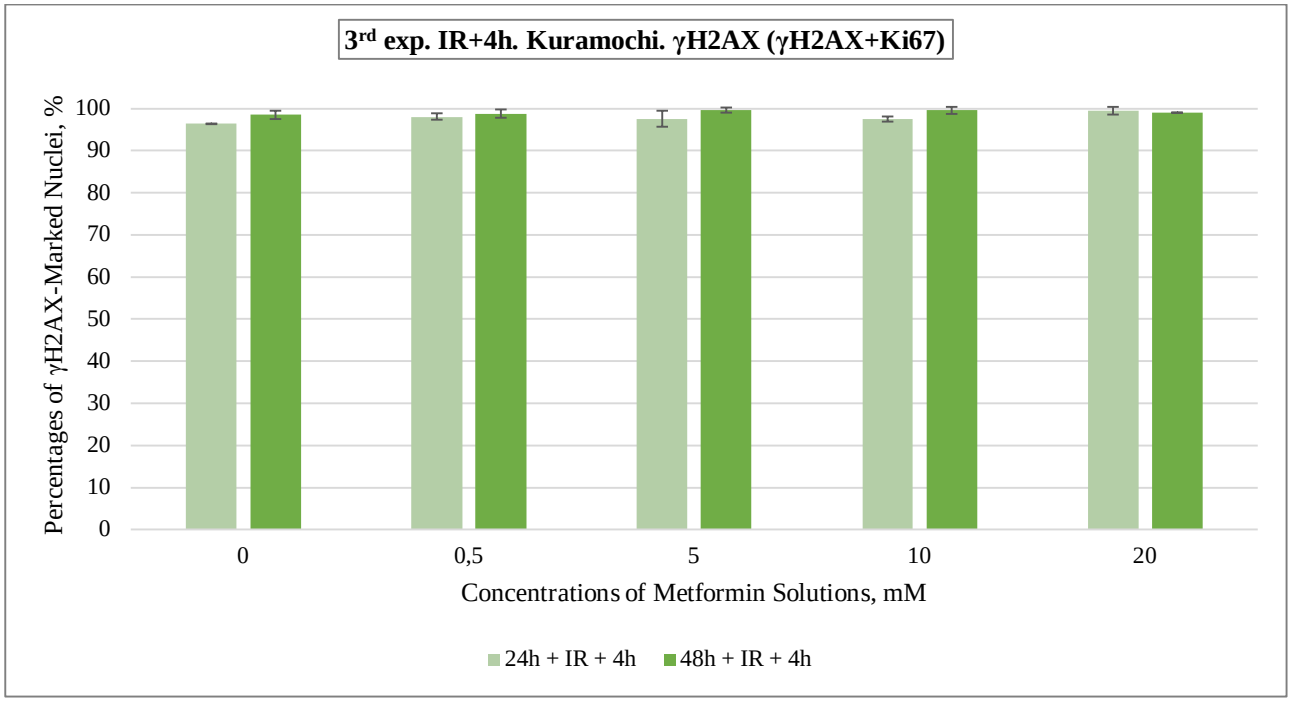

Figure 16. γH2AX results from the γH2AX+cCasp3 staining combination used for Kuramochi cells in the IR+4h part of the third experiment.

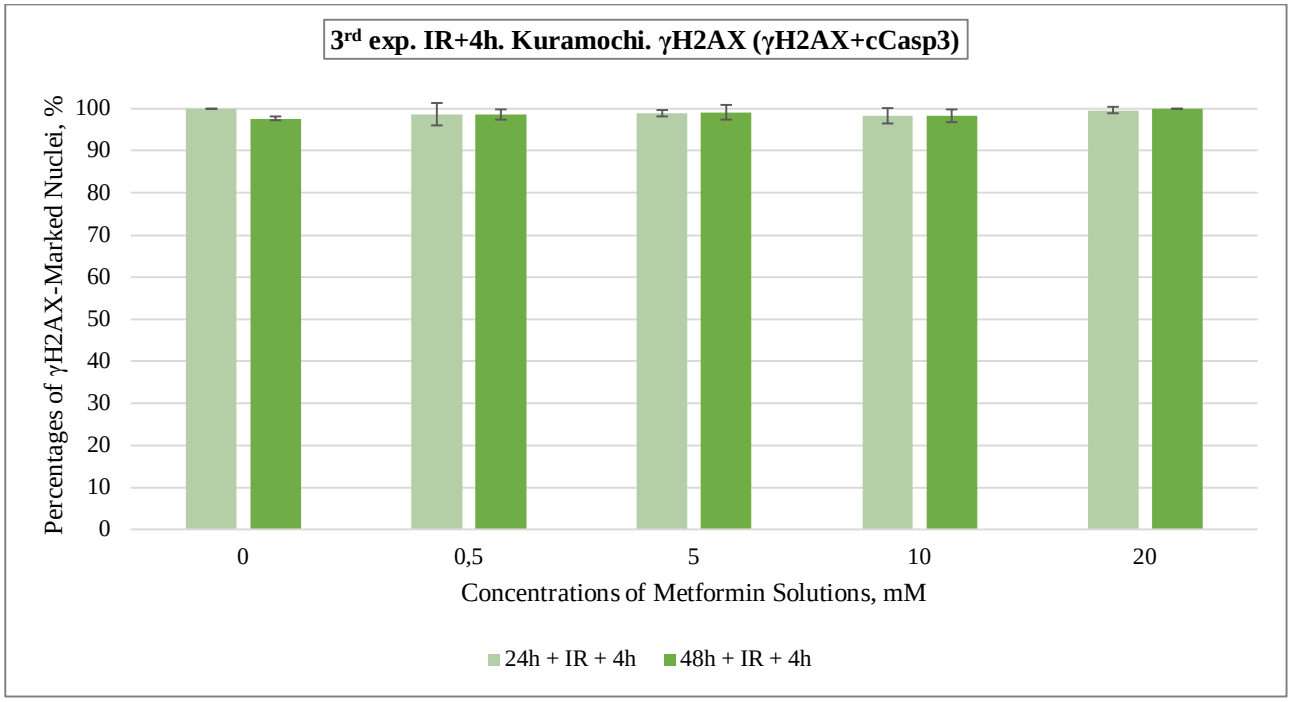

Figure 17. γH2AX results from the γH2AX+Ki67 staining combination used for OVCAR4 cells in the IR+4h part of the third experiment.

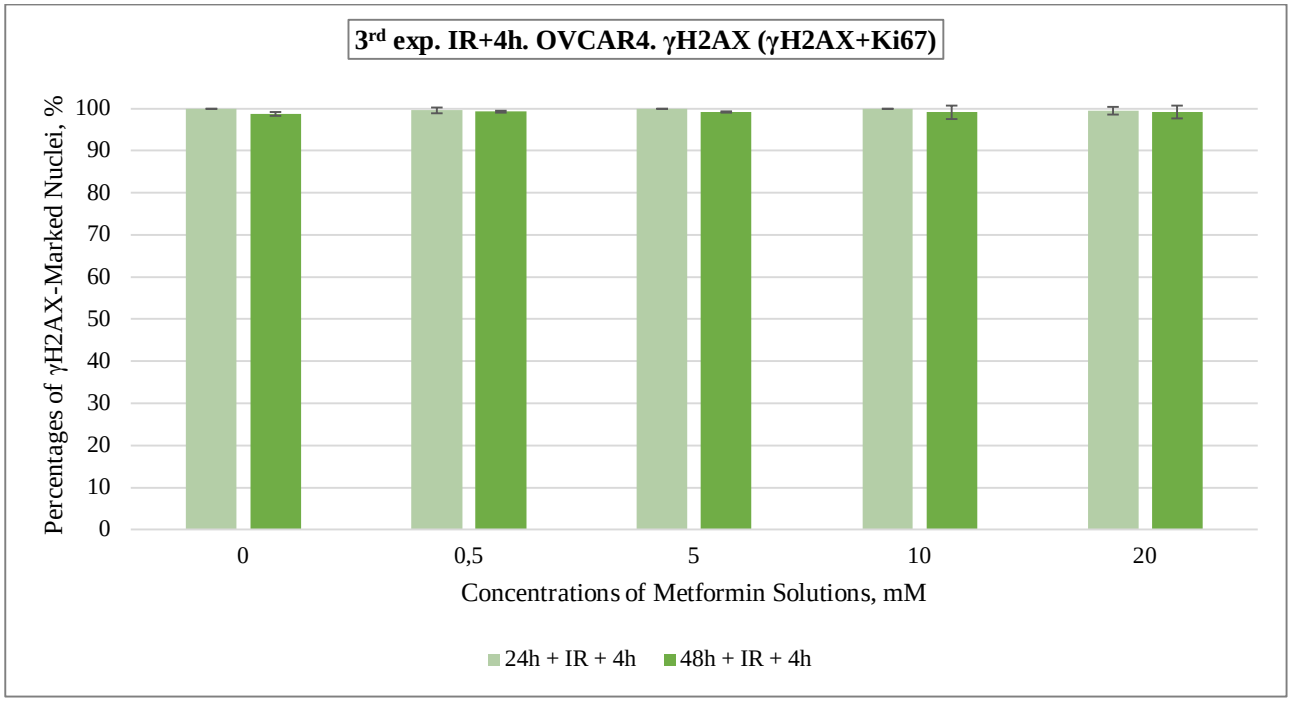

Figure 18. γH2AX results from the γH2AX+cCasp3 staining combination used for OVCAR4 cells in the IR+4h part of the third experiment.

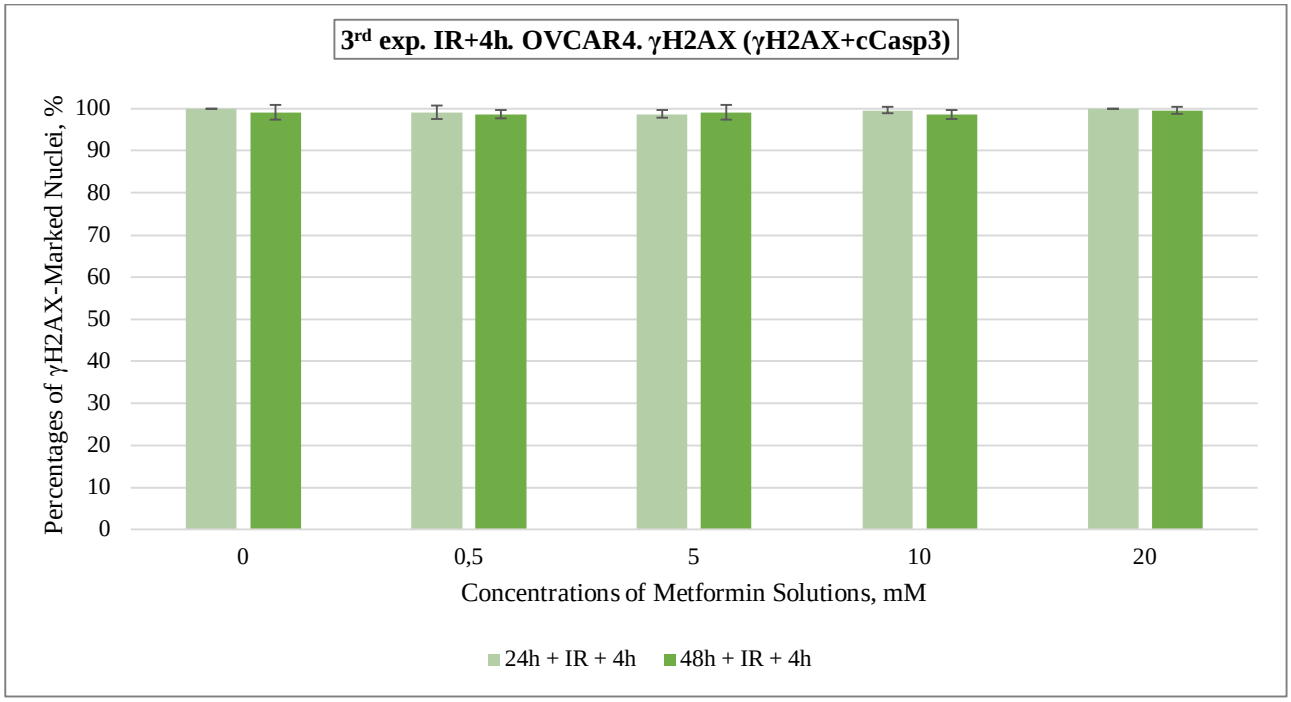

Figure 19. γH2AX results from the γH2AX+Ki67 staining combination used for Kuramochi cells in the IR+24h part of the third experiment.

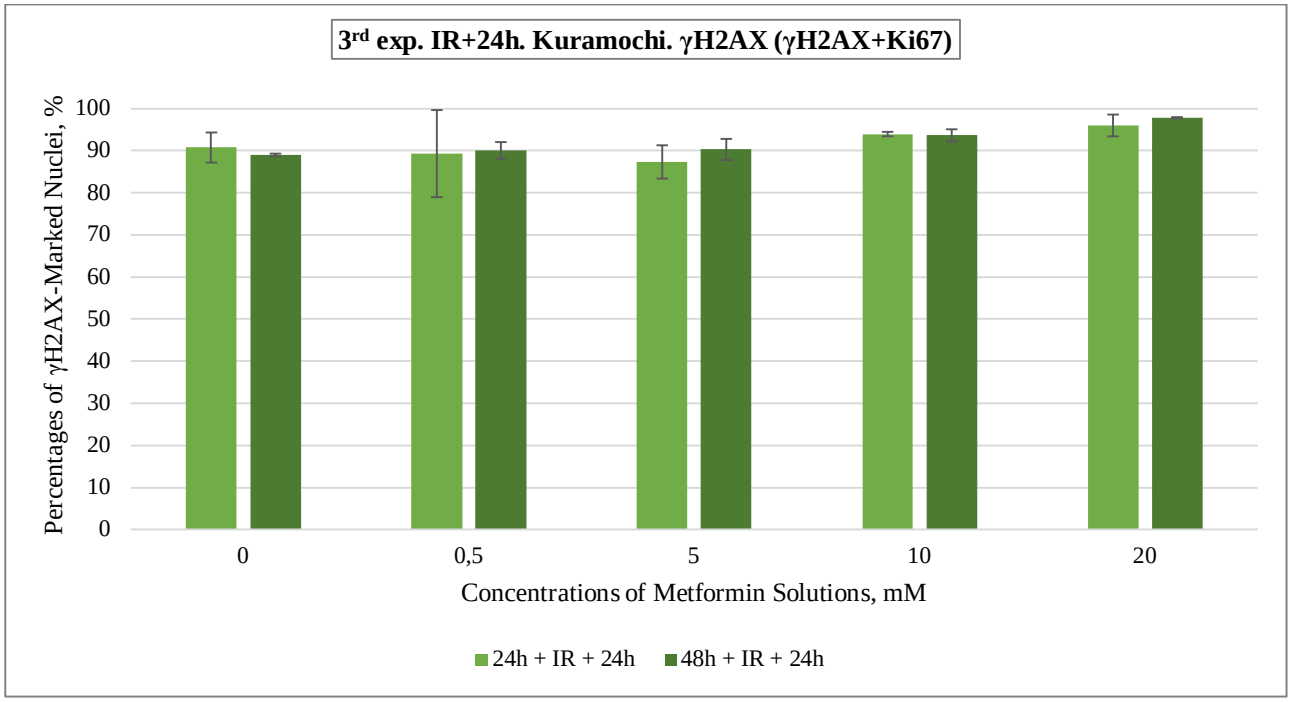

Figure 20. γH2AX results from the γH2AX+cCasp3 staining combination used for Kuramochi cells in the IR+24h part of the third experiment.

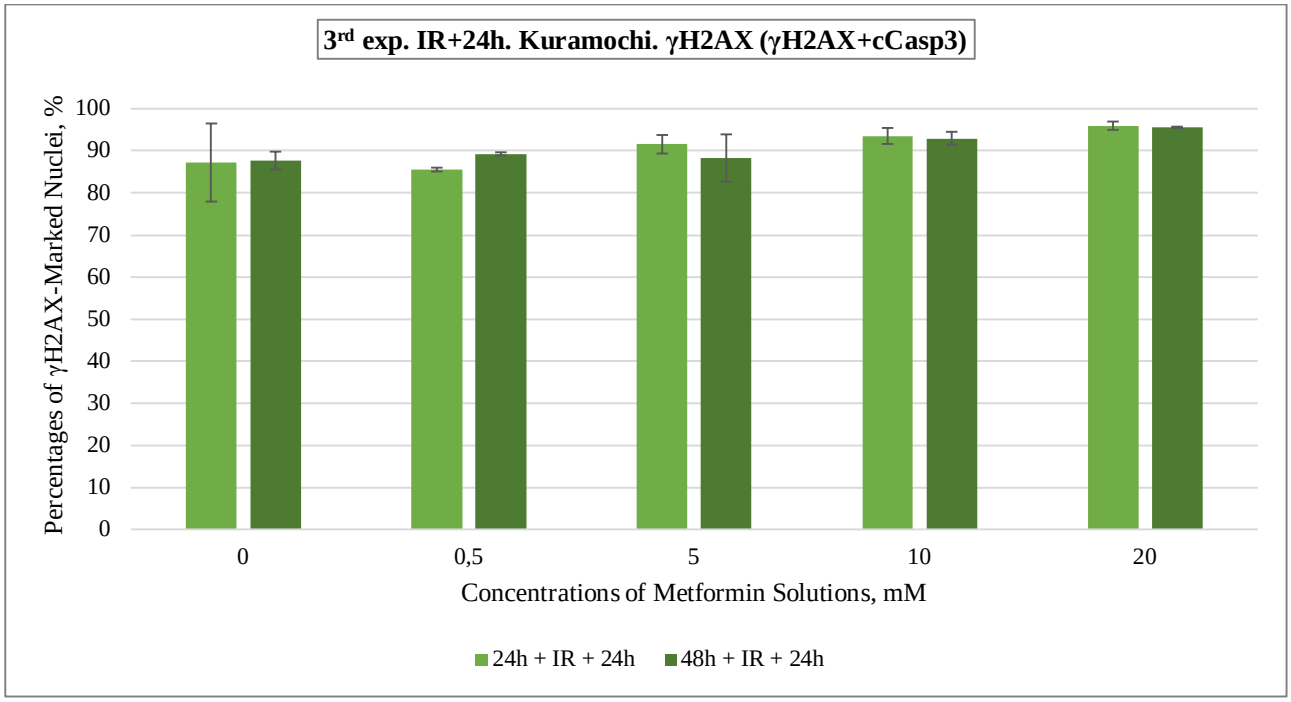

Figure 21. γH2AX results from the γH2AX+Ki67 staining combination used for OVCAR4 cells in the IR+24h part of the third experiment.

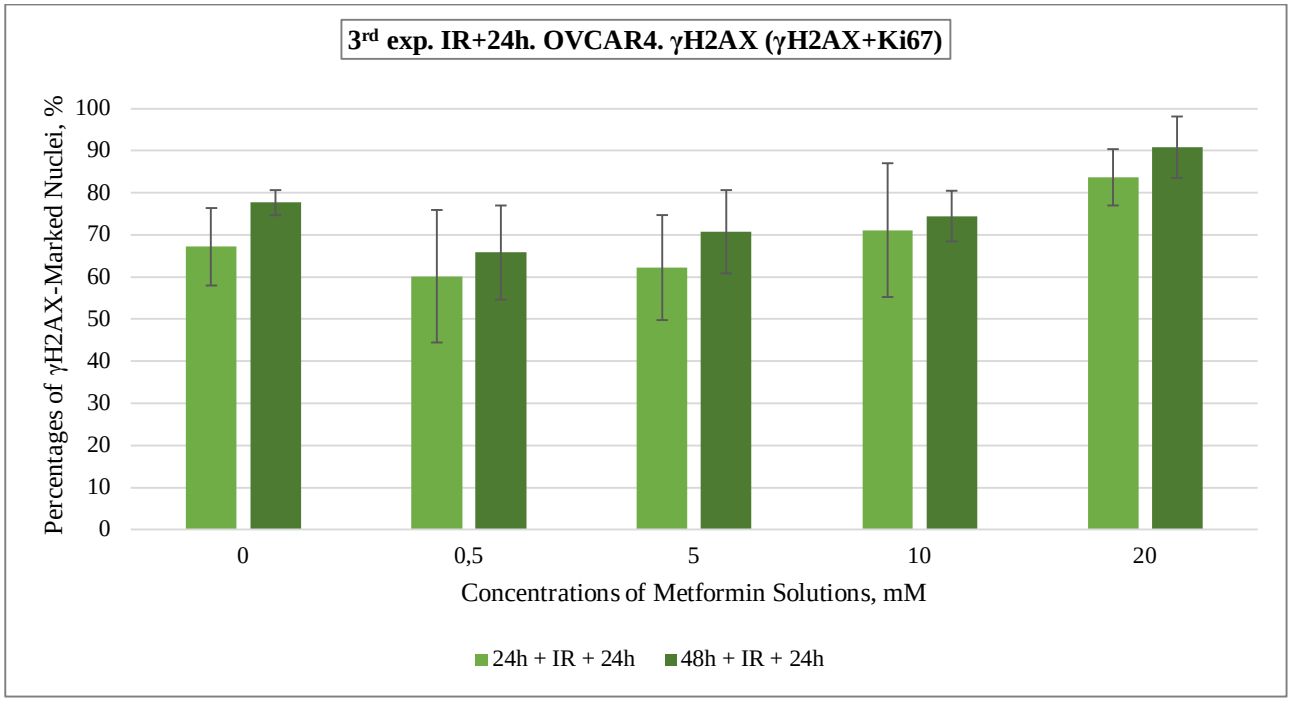

Figure 22. γH2AX results from the γH2AX+cCasp3 staining combination used for OVCAR4 cells in the IR+24h part of the third experiment.

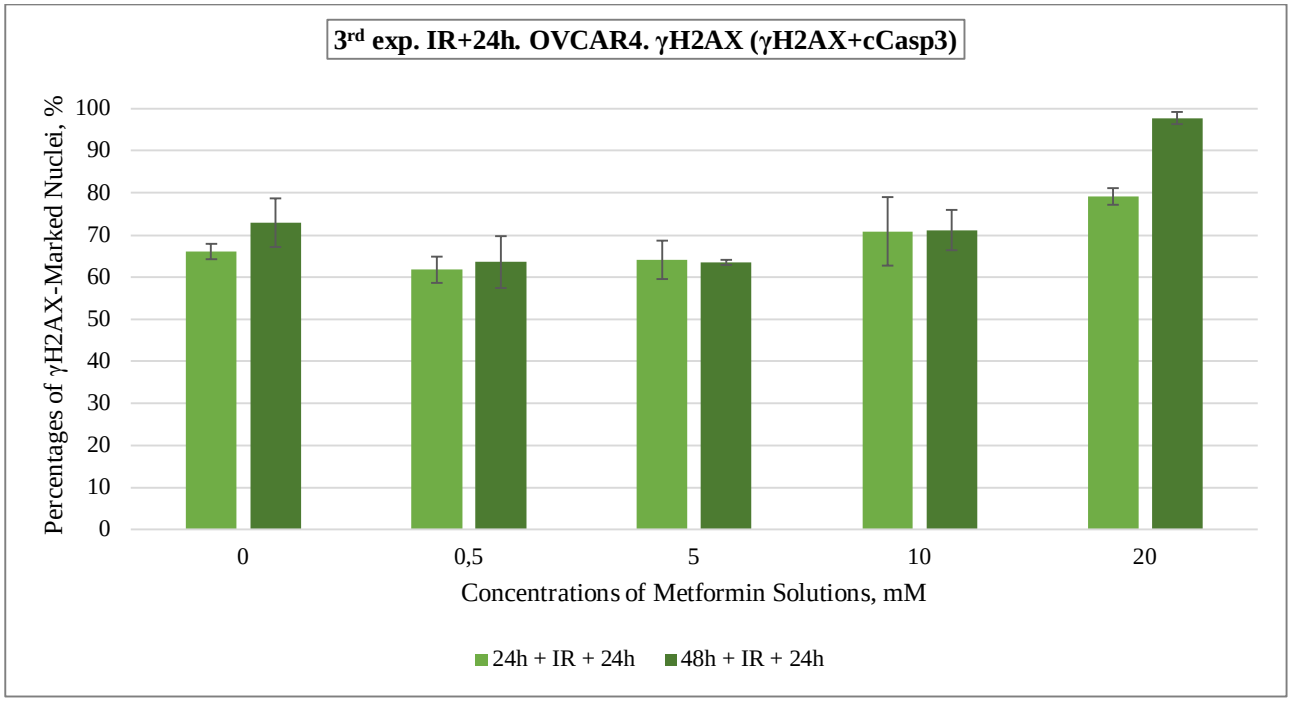

Appendix D: Full Pooled no IR γH2AX and Ki67 Data from All Three Experiments.

Figure 23. Pooled γH2AX results from all non-irradiated Kuramochi cells.

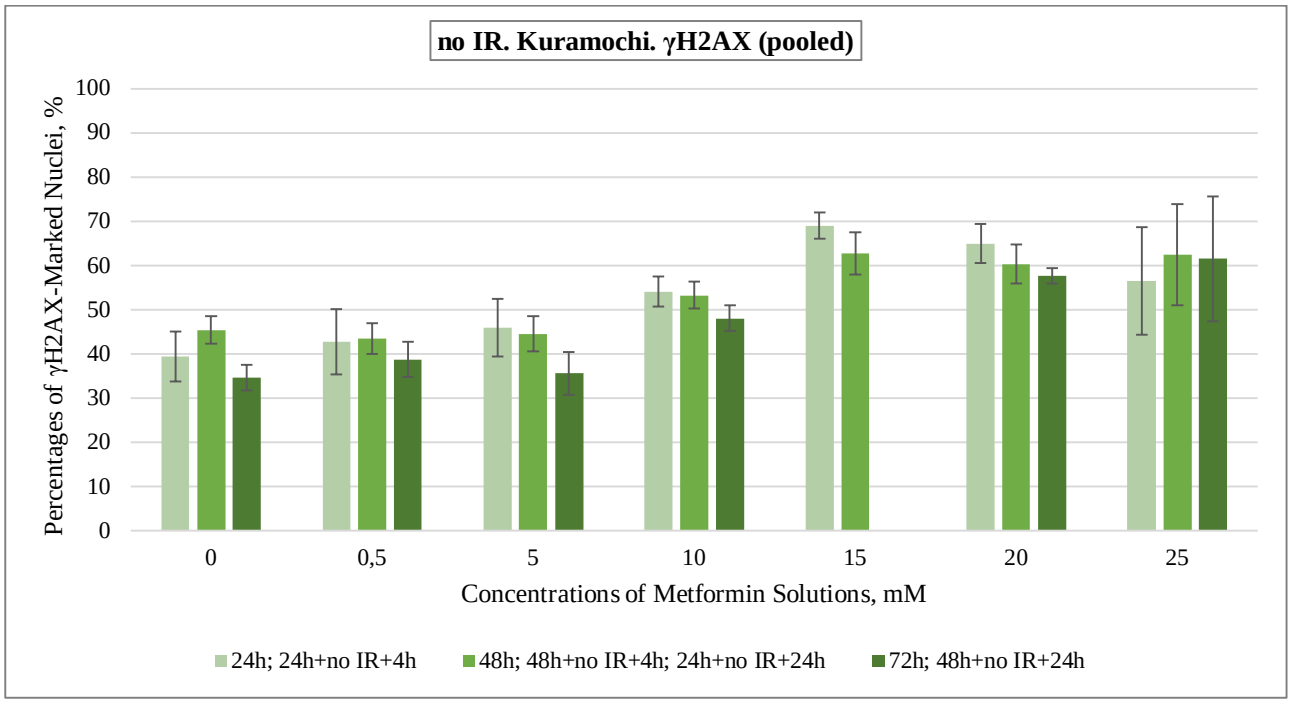

Figure 24. Pooled γH2AX results from all non-irradiated OVCAR4 cells.

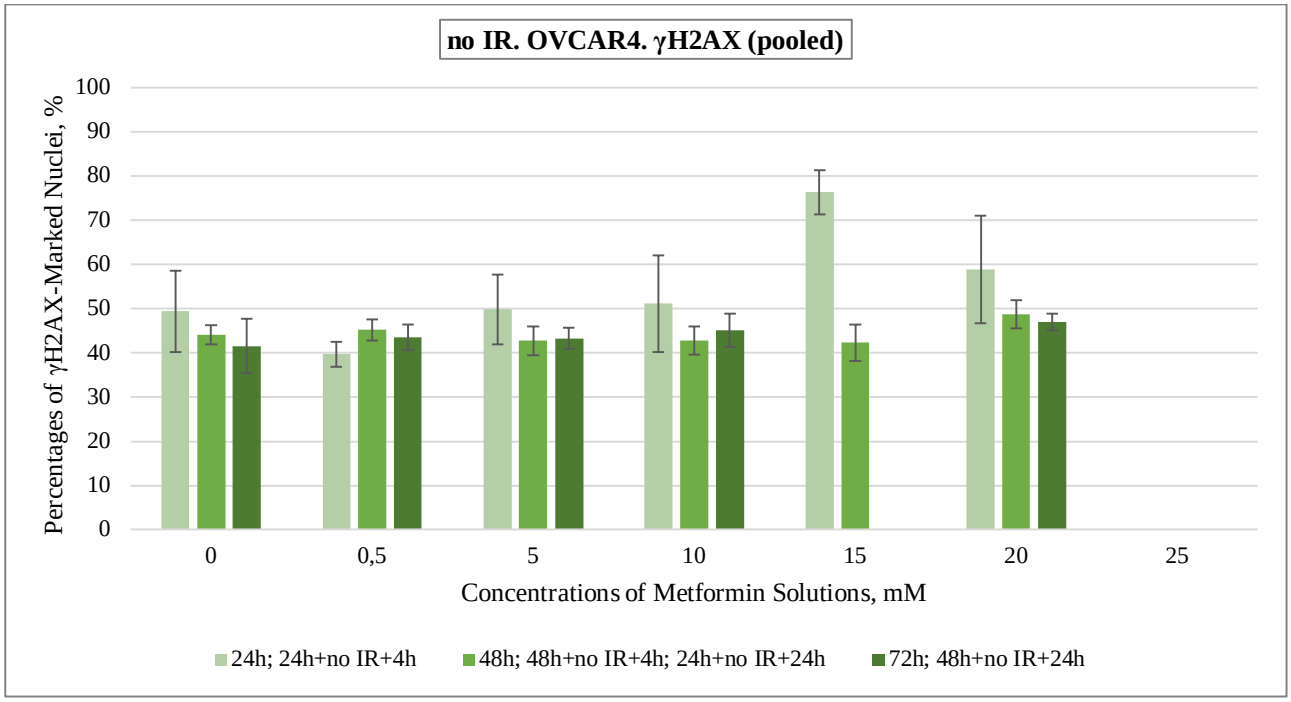

Figure 25. Pooled Ki67 results from all non-irradiated Kuramochi cells.

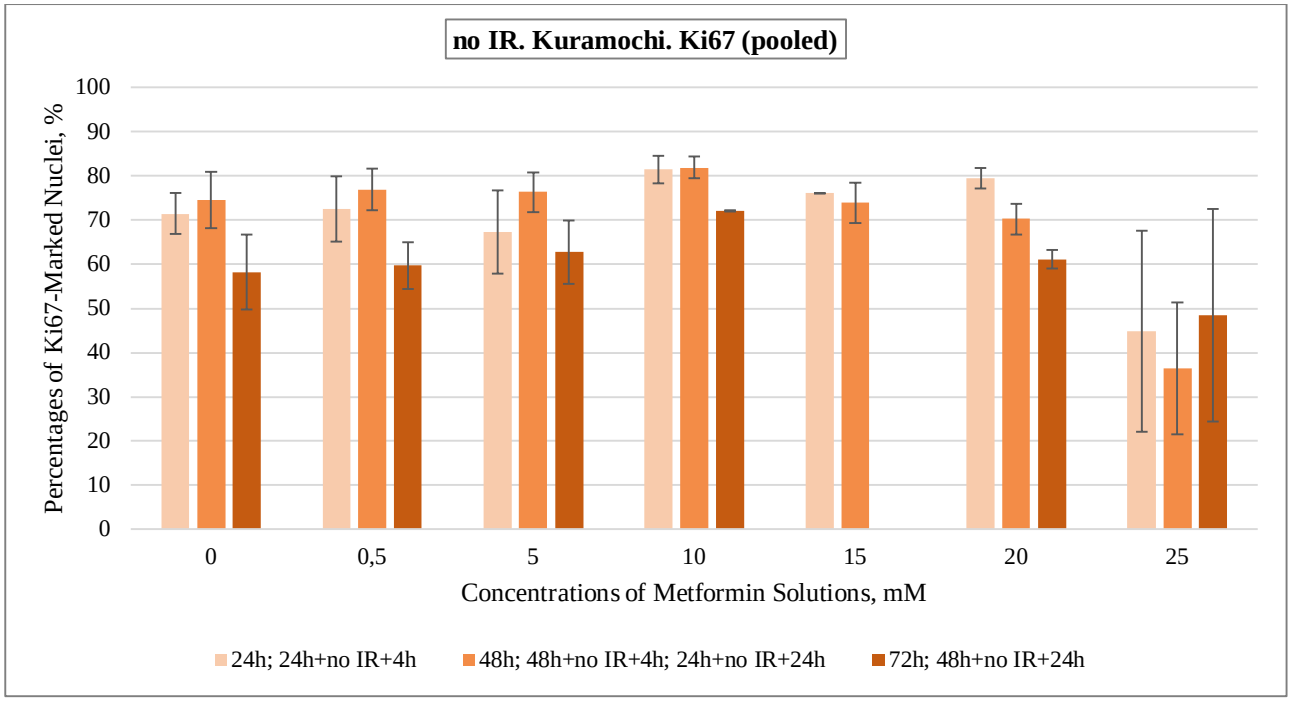

Figure 26. Pooled Ki67 results from all non-irradiated OVCAR4 cells.

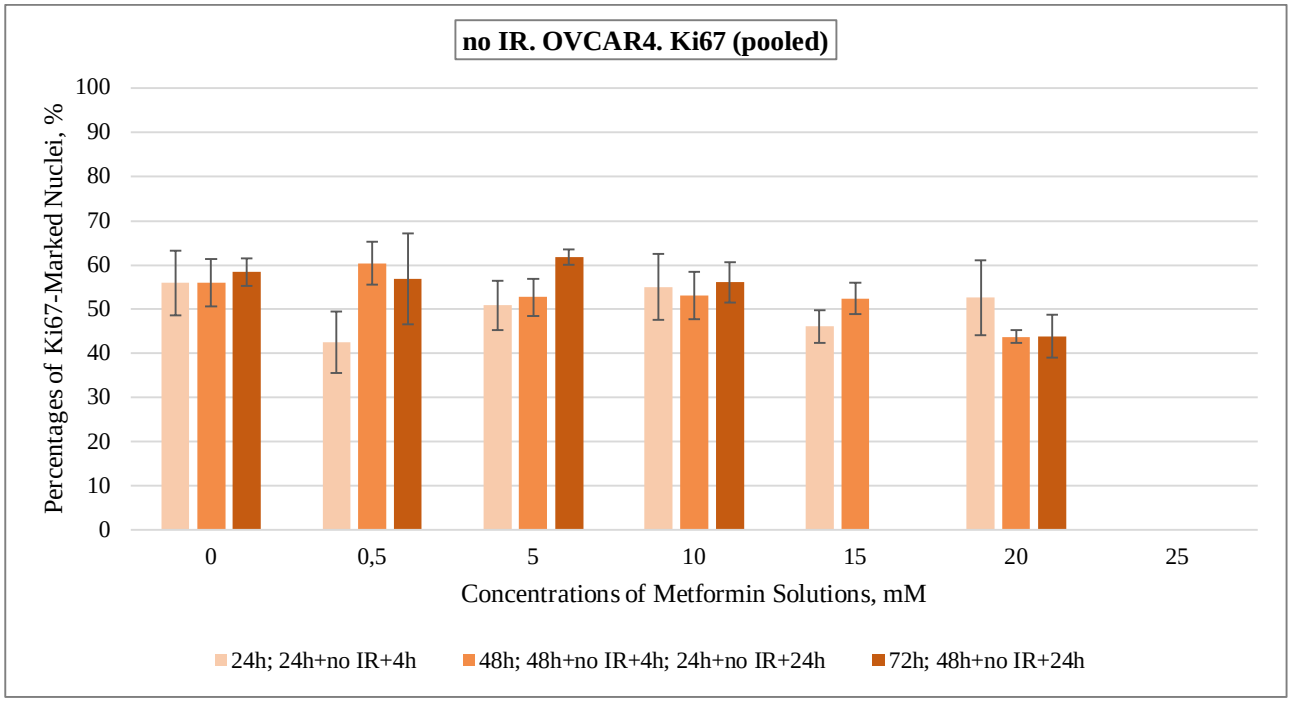

Appendix E: Numbers of Analyzed Nuclei with Numbers of γH2AX-, Ki67-, and cCasp3-Positives in Each Condition Throughout All Three Experiments. Abbreviations: pl. – plate, met. – metformin, K – Kuramochi, O – OVCAR4, (m) – manual scoring, n/a – not available.

Condition	γH2AX-Ki67 staining: γH2AX-positive nuclei / all nuclei	γH2AX-cCasp3 staining: γH2AX-positive nuclei / all nuclei	Combined γH2AX stainings: total number of γH2AX-positive nuclei / total number of nuclei	Ki67-positive nuclei / all nuclei	cCasp3-positive nuclei / all nuclei
The 1st experiment					
24h pl., 0 mM met.	K: 157 / 377 O: n/a	K: 69 / 218 O: n/a	K: 226 / 595 O: n/a	K: 252 / 377 O: n/a	K: 80 / 218 O: n/a
24h pl., 0,5 mM met.	K: 57 / 130 O: n/a	K: 45 / 149 O: n/a	K: 102 / 279 O: n/a	K: 90 / 130 O: n/a	K: 60 / 149 O: n/a
24h pl., 5 mM met.	K: 60 / 143 O: n/a	K: 93 / 273 O: n/a	K: 153 / 416 O: n/a	K: 83 / 143 O: n/a	K: 112 / 273 O: n/a
24h pl., 25 mM met.	K: 36 / 67 O: n/a	K: 87 / 190 O: n/a	K: 123 / 257 O: n/a	K: 21 / 67 O: n/a	K: 112 / 190 O: n/a
48h pl., 0 mM met.	K: 162 / 316 O: n/a	K: 286 / 669 O: n/a	K: 448 / 985 O: n/a	K: 223 / 316 O: n/a	K: 124 / 669 O: n/a
48h pl., 0,5 mM met.	K: 172 / 405 O: n/a	K: 164 / 478 O: n/a	K: 336 / 883 O: n/a	K: 291 / 405 O: n/a	K: 121 / 478 O: n/a
48h pl., 5 mM met.	K: 167 / 352 O: n/a	K: 131 / 462 O: n/a	K: 298 / 814 O: n/a	K: 243 / 352 O: n/a	K: 142 / 462 O: n/a
48h pl., 25 mM met.	K: 31 / 57 O: n/a	K: 21 / 37 O: n/a	K: 52 / 94 O: n/a	K: 21 / 57 O: n/a	K: 35 / 37 O: n/a
72h pl., 0 mM met.	K: 206 / 576 O: n/a	K: 437 / 1297 O: n/a	K: 643 / 1873 O: n/a	K: 338 / 576 O: n/a	K: 100 / 1297 O: n/a
72h pl., 0,5 mM met.	K: 307 / 796 O: n/a	K: 192 / 600 O: n/a	K: 499 / 1396 O: n/a	K: 461 / 796 O: n/a	K: 139 / 600 O: n/a
72h pl., 5 mM met.	K: 155 / 476 O: n/a	K: 192 / 654 O: n/a	K: 347 / 1130 O: n/a	K: 285 / 476 O: n/a	K: 147 / 654 O: n/a
72h pl.,	K: 20 / 33	K: 46 / 92	K: 66 / 125	K: 13 / 33	K: 72 / 92

25 mM met.	O: n/a	O: n/a	O: n/a	O: n/a	O: n/a
The 2nd experiment					
24h pl., 0 mM met.	K: 486 / 935 O: 433 / 710	K: 661 / 1316 O: 618 / 982	K: 1147 / 2251 O: 1051 / 1692	K: 785 / 935 O: 346 / 710	K: n/a O: n/a
24h pl., 5 mM met.	K: 1361 / 2422 O: 930 / 1573	K: 1626 / 2719 O: 620 / 1022	K: 2987 / 5141 O: 1550 / 2595	K: 1853 / 2422 O: 724 / 1573	K: n/a O: n/a
24h pl., 10 mM met.	K: 1642 / 2700 O: 157 / 208	K: 1649 / 3011 O: 371 / 630	K: 3291 / 5711 O: 528 / 838	K: 2115 / 2700 O: 99 / 208	K: n/a O: n/a
24h pl., 15 mM met.	K: 1556 / 2212 O: 678 / 937	K: 1619 / 2415 O: 279 / 363	K: 3175 / 4627 O: 957 / 1300	K: 1682 / 2212 O: 441 / 937	K: n/a O: n/a
24h pl., 20 mM met.	K: 2569 / 3734 O: 863 / 1290	K: 2462 / 3743 O: 668 / 831	K: 5031 / 7477 O: 1531 / 2121	K: 2888 / 3734 O: 583 / 1290	K: n/a O: n/a
48h pl., 0 mM met.	K: 4122 / 10732 O: 1972 / 5359	K: 5120 / 13966 O: 1704 / 4200	K: 9242 / 24698 O: 3676 / 9559	K: 9170 / 10732 O: 2661 / 5359	K: n/a O: n/a
48h pl., 5 mM met.	K: 2395 / 4653 O: 3555 / 10325	K: 5144 / 12964 O: 1756 / 4801	K: 7539 / 17617 O: 5311 / 15126	K: 3921 / 4653 O: 4816 / 10325	K: n/a O: n/a
48h pl., 10 mM met.	K: 3358 / 5621 O: 1500 / 4452	K: 5482 / 12047 O: 3061 / 8065	K: 8940 / 17668 O: 4561 / 12517	K: 4407 / 5621 O: 2149 / 4452	K: n/a O: n/a
48h pl., 15 mM met.	K: 4224 / 6329 O: 3247 / 8255	K: 5631 / 9592 O: 3199 / 7149	K: 9855 / 15921 O: 6446 / 15404	K: 4675 / 6329 O: 4301 / 8255	K: n/a O: n/a
48h pl., 20 mM met.	K: 4354 / 6064 O: 3156 / 6247	K: 6057 / 9154 O: 3411 / 5820	K: 10414 / 15218 O: 6567 / 12067	K: 4192 / 6064 O: 2717 / 6247	K: n/a O: n/a
The 3rd experiment					
24h+no IR+4h pl., 0 mM met.	K: 108 / 233 (m) O: 88 / 219 (m)	K: 141 / 310 (m) O: 81 / 208 (m)	K: 249 / 543 (m) O: 169 / 427 (m)	K: 2216 / 2872 O: 1045 / 1746	K: n/a O: n/a
24h+no IR+4h pl., 0,5 mM met.	K: 109 / 225 (m) O: 91 / 219 (m)	K: 110 / 240 (m) O: 87 / 229 (m)	K: 219 / 465 (m) O: 178 / 448 (m)	K: 3641 / 4231 O: 1237 / 2919	K: n/a O: n/a
24h+no IR+4h pl., 5 mM met.	K: 117 / 215 (m) O: 85 / 215 (m)	K: 110 / 227 (m) O: 79 / 200 (m)	K: 227 / 442 (m) O: 164 / 415 (m)	K: 2246 / 2660 O: 755 / 1337	K: n/a O: n/a
24h+no IR+4h pl., 10 mM met.	K: 126 / 253 (m) O: 102 / 229 (m)	K: 112 / 220 (m) O: 97 / 234 (m)	K: 238 / 473 (m) O: 199 / 463 (m)	K: 3370 / 4010 O: 1677 / 2857	K: n/a O: n/a
24h+no IR+4h pl., 20 mM met.	K: 125 / 205 (m) O: 112 / 250 (m)	K: 124 / 199 (m) O: 105 / 249 (m)	K: 249 / 404 (m) O: 217 / 499 (m)	K: 3297 / 4079 O: 1604 / 2703	K: n/a O: n/a
48h+no IR+4h pl., 0 mM met.	K: 86 / 209 (m) O: 112 / 240 (m)	K: 128 / 298 (m) O: 121 / 260 (m)	K: 214 / 507 (m) O: 233 / 500 (m)	K: 8454 / 11231 O: 1704 / 2752	K: n/a O: n/a
48h+no IR+4h pl., 0,5 mM met.	K: 150 / 315 (m) O: 94 / 204 (m)	K: 116 / 232 (m) O: 99 / 208 (m)	K: 266 / 547 (m) O: 193 / 412 (m)	K: 10526 / 12711 O: 5870 / 9097	K: n/a O: n/a

48h+no IR+4h pl., 5 mM met.	K: 136 / 268 (m) O: 114 / 238 (m)	K: 109 / 208 (m) O: 89 / 204 (m)	K: 245 / 476 (m) O: 203 / 442 (m)	K: 10446 / 13010 O: 4677 / 8065	K: n/a O: n/a
48h+no IR+4h pl., 10 mM met.	K: 167 / 287 (m) O: 112 / 240 (m)	K: 181 / 323 (m) O: 93 / 213 (m)	K: 348 / 610 (m) O: 205 / 453 (m)	K: 6560 / 7819 O: 923 / 1639	K: n/a O: n/a
48h+no IR+4h pl., 20 mM met.	K: 165 / 270 (m) O: 155 / 331 (m)	K: 125 / 224 (m) O: 92 / 200 (m)	K: 290 / 494 (m) O: 247 / 531 (m)	K: 5048 / 7486 O: 1476 / 3472	K: n/a O: n/a
24h+no IR+24h pl., 0 mM met.	K: 109 / 231 (m) O: 94 / 212 (m)	K: 96 / 241 (m) O: 115 / 263 (m)	K: 205 / 472 (m) O: 209 / 475 (m)	K: 3189 / 3838 O: 5655 / 10770	K: n/a O: n/a
24h+no IR+24h pl., 0,5 mM met.	K: 92 / 195 (m) O: 114 / 265 (m)	K: 118 / 248 (m) O: 99 / 226 (m)	K: 210 / 443 (m) O: 213 / 491 (m)	K: 5550 / 6515 O: 4972 / 8864	K: n/a O: n/a
24h+no IR+24h pl., 5 mM met.	K: 116 / 238 (m) O: 105 / 234 (m)	K: 116 / 238 (m) O: 109 / 241 (m)	K: 232 / 476 (m) O: 214 / 475 (m)	K: 4048 / 4734 O: 5595 / 10480	K: n/a O: n/a
24h+no IR+24h pl., 10 mM met.	K: 113 / 222 (m) O: 161 / 376 (m)	K: 109 / 218 (m) O: 128 / 286 (m)	K: 222 / 440 (m) O: 289 / 662 (m)	K: 2872 / 3439 O: 4602 / 9385	K: n/a O: n/a
24h+no IR+24h pl., 20 mM met.	K: 127 / 231 (m) O: 256 / 598 (m)	K: 106 / 206 (m) O: 105 / 228 (m)	K: 233 / 437 (m) O: 361 / 826 (m)	K: 1573 / 2125 O: 2165 / 4829	K: n/a O: n/a
48h+no IR+24h pl., 0 mM met.	K: 80 / 210 (m) O: 114 / 281 (m)	K: 109 / 288 (m) O: 128 / 321 (m)	K: 189 / 498 (m) O: 242 / 602 (m)	K: 13590 / 21163 O: 160 / 274 (m)	K: n/a O: n/a
48h+no IR+24h pl., 0,5 mM met.	K: 118 / 261 (m) O: 97 / 223 (m)	K: 90 / 217 (m) O: 134 / 310 (m)	K: 208 / 478 (m) O: 231 / 533 (m)	K: 15529 / 22754 O: 8888 / 17227	K: n/a O: n/a
48h+no IR+24h pl., 5 mM met.	K: 118 / 258 (m) O: 112 / 255 (m)	K: 90 / 205 (m) O: 148 / 357 (m)	K: 208 / 463 (m) O: 260 / 612 (m)	K: 15069 / 21060 O: 142 / 246 (m)	K: n/a O: n/a
48h+no IR+24h pl., 10 mM met.	K: 101 / 200 (m) O: 120 / 263 (m)	K: 124 / 272 (m) O: 95 / 209 (m)	K: 225 / 472 (m) O: 215 / 472 (m)	K: 12979 / 18013 O: 117 / 209 (m)	K: n/a O: n/a
48h+no IR+24h pl., 20 mM met.	K: 124 / 213 (m) O: 150 / 312 (m)	K: 133 / 233 (m) O: 100 / 217 (m)	K: 257 / 446 (m) O: 250 / 529 (m)	K: 5795 / 9480 O: 2870 / 6624	K: n/a O: n/a
24h+IR+4h pl., 0 mM met.	K: 269 / 279 (m) O: 345 / 345 (m)	K: 395 / 395 (m) O: 227 / 227 (m)	K: 664 / 674 (m) O: 572 / 572 (m)	K: 4461 / 5547 O: 2477 / 5329	K: n/a O: n/a
24h+IR+4h pl., 0,5 mM met.	K: 214 / 218 (m) O: 216 / 217 (m)	K: 244 / 248 (m) O: 247 / 250 (m)	K: 458 / 466 (m) O: 463 / 467 (m)	K: 3866 / 4625 O: 1450 / 4508	K: n/a O: n/a
24h+IR+4h pl., 5 mM met.	K: 255 / 261 (m) O: 242 / 242 (m)	K: 277 / 280 (m) O: 238 / 241 (m)	K: 532 / 541 (m) O: 480 / 483 (m)	K: 1997 / 2487 O: 1140 / 2825	K: n/a O: n/a
24h+IR+4h pl., 10 mM met.	K: 232 / 238 (m) O: 244 / 244 (m)	K: 237 / 241 (m) O: 218 / 219 (m)	K: 469 / 479 (m) O: 462 / 463 (m)	K: 1702 / 2323 O: 2110 / 4537	K: n/a O: n/a
24h+IR+4h pl., 20 mM met.	K: 213 / 214 (m) O: 210 / 211 (m)	K: 263 / 264 (m) O: 212 / 212 (m)	K: 476 / 478 (m) O: 422 / 423 (m)	K: 2764 / 4140 O: 2490 / 5334	K: n/a O: n/a
48h+IR+4h pl.,	K: 212 / 215 (m)	K: 256 / 262 (m)	K: 468 / 477 (m)	K: 4197 / 5296	K: n/a

0 mM met.	O: 239 / 242 (m)	O: 238 / 240 (m)	O: 477 / 482 (m)	O: 171 / 271 (m)	O: n/a
48h+IR+4h pl., 0,5 mM met.	K: 329 / 333 (m) O: 295 / 297 (m)	K: 228 / 231 (m) O: 239 / 242 (m)	K: 557 / 564 (m) O: 534 / 539 (m)	K: 9810 / 11852 O: 7615 / 12917	K: n/a O: n/a
48h+IR+4h pl., 5 mM met.	K: 301 / 302 (m) O: 272 / 274 (m)	K: 225 / 227 (m) O: 250 / 252 (m)	K: 526 / 529 (m) O: 522 / 526 (m)	K: 9049 / 10918 O: 3780 / 7013	K: n/a O: n/a
48h+IR+4h pl., 10 mM met.	K: 262 / 263 (m) O: 262 / 264 (m)	K: 224 / 228 (m) O: 280 / 284 (m)	K: 486 / 491 (m) O: 542 / 548 (m)	K: 4579 / 5446 O: 5948 / 12343	K: n/a O: n/a
48h+IR+4h pl., 20 mM met.	K: 206 / 208 (m) O: 280 / 282 (m)	K: 307 / 307 (m) O: 252 / 253 (m)	K: 513 / 515 (m) O: 532 / 535 (m)	K: 3936 / 5551 O: 4825 / 11318	K: n/a O: n/a
24h+IR+24h pl., 0 mM met.	K: 190 / 209 (m) O: 162 / 241 (m)	K: 188 / 215 (m) O: 140 / 212 (m)	K: 378 / 424 (m) O: 302 / 453 (m)	K: 1692 / 2041 O: 7818 / 12116	K: n/a O: n/a
24h+IR+24h pl., 0,5 mM met.	K: 222 / 248 (m) O: 151 / 249 (m)	K: 248 / 290 (m) O: 129 / 209 (m)	K: 470 / 538 (m) O: 280 / 458 (m)	K: 2646 / 2991 O: 5985 / 8290	K: n/a O: n/a
24h+IR+24h pl., 5 mM met.	K: 228 / 260 (m) O: 173 / 279 (m)	K: 195 / 213 (m) O: 133 / 208 (m)	K: 423 / 473 (m) O: 306 / 487 (m)	K: 2727 / 3236 O: 5446 / 7632	K: n/a O: n/a
24h+IR+24h pl., 10 mM met.	K: 199 / 213 (m) O: 171 / 244 (m)	K: 202 / 216 (m) O: 146 / 207 (m)	K: 401 / 429 (m) O: 317 / 451 (m)	K: 2722 / 3248 O: 2960 / 3956	K: n/a O: n/a
24h+IR+24h pl., 20 mM met.	K: 216 / 225 (m) O: 209 / 251 (m)	K: 211 / 220 (m) O: 206 / 260 (m)	K: 427 / 445 (m) O: 415 / 511 (m)	K: 3132 / 4543 O: 1300 / 2239	K: n/a O: n/a
48h+IR+24h pl., 0 mM met.	K: 219 / 246 (m) O: 177 / 228 (m)	K: 213 / 243 (m) O: 163 / 223 (m)	K: 432 / 489 (m) O: 340 / 451 (m)	K: 8859 / 15169 O: 182 / 233 (m)	K: n/a O: n/a
48h+IR+24h pl., 0,5 mM met.	K: 200 / 222 (m) O: 162 / 250 (m)	K: 198 / 222 (m) O: 131 / 207 (m)	K: 398 / 444 (m) O: 293 / 457 (m)	K: 11085 / 16818 O: 168 / 206 (m)	K: n/a O: n/a
48h+IR+24h pl., 5 mM met.	K: 204 / 216 (m) O: 142 / 201 (m)	K: 191 / 216 (m) O: 130 / 205 (m)	K: 395 / 432 (m) O: 272 / 406 (m)	K: 10878 / 15272 O: 184 / 237 (m)	K: n/a O: n/a
48h+IR+24h pl., 10 mM met.	K: 208 / 222 (m) O: 170 / 227 (m)	K: 198 / 213 (m) O: 174 / 244 (m)	K: 406 / 435 (m) O: 344 / 471 (m)	K: 8642 / 12879 O: 188 / 229 (m)	K: n/a O: n/a
48h+IR+24h pl., 20 mM met.	K: 228 / 233 (m) O: 205 / 226 (m)	K: 217 / 227 (m) O: 226 / 231 (m)	K: 445 / 460 (m) O: 431 / 457 (m)	K: 4832 / 8096 O: 1844 / 4748	K: n/a O: n/a